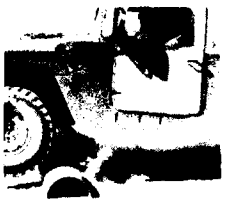

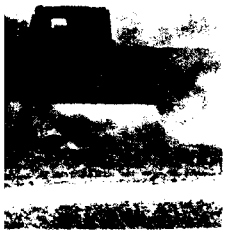

TECHNICAL REPORT GL-92-17

(2)

VALIDATION STUDY OF TWO RIGID BODY DYNAMIC COMPUTER MODELS

by

Randolph Anthony Jones

Geotechnical Laboratory

DEPARTMENT OF THE ARMY
Waterways Experiment Station, Corps of Engineers
3909 Halls Ferry Road, Vicksburg, Mississippi 39180-6199

September 1992
Final Report

Prepared for DEPARTMENT OF THE ARMY
U.S. Army Corps of Engineers
Washington, DC 20314-1000

Under Project No. 1V665810DE65

Destroy this report when no longer needed. Do not return it to the originator.

The findings in this report are not to be construed as an official Department of the Army position unless so designated by other authorized documents.

The contents of this report are not to be used for advertising, publication, or promotional purposes. Citation of trade names does not constitute an official endorsement or approval of the use of such commercial products.

REPORT DOCUMENTATION PAGE

Form Approved
OMB No. 0704-0188

1. AGENCY USE ONLY (Leave blank)	2. REPORT DATE	3. REPORT TYPE AND DATES COVERED
	September 1992	Final Report

4. TITLE AND SUBTITLE
Validation Study of Two Rigid Body Dynamic Computer Models

5. FUNDING NUMBERS
MIPR
No. W56HZW90-EKE

Project No.
1V665810DE65

6. AUTHOR(S)
Randolph Anthony Jones

7. PERFORMING ORGANIZATION NAME(S) AND ADDRESS(ES)
USAE Waterways Experiment Station
Geotechnical Laboratory
3909 Halls Ferry Road
Vicksburg, MS 39180-6199

8. PERFORMING ORGANIZATION REPORT NUMBER
Technical Report
GL-92-17

9. SPONSORING/MONITORING AGENCY NAME(S) AND ADDRESS(ES)
US Army Corps of Engineers
Washington, DC 20314-1000

10. SPONSORING/MONITORING AGENCY REPORT NUMBER

11. SUPPLEMENTARY NOTES
This report is available from the National Technical Information Service, 5285 Port Royal Road, Springfield, VA 22161

12a. DISTRIBUTION/AVAILABILITY STATEMENT
Approved for public release; distribution unlimited.

12b. DISTRIBUTION CODE

13. ABSTRACT *(Maximum 200 words)*

The following validation study analyzes rigid muiltibody dynamic models for the US Army's High Mobility Multipurpose Wheeled Vehicle (HMMWV) using the Dynamic Analysis and Design System (DADS) computer code and the US Army's Vehicle Dynamics Module (VEHDYN) computer code. Simulated testing of the two vehicle models was conducted over non-deformable discrete obstacles and non-deformable continuous undulating terrains. Results from the model simulations (vertical acceleration time histories, frequency distributions, and absorbed power calculations) were compared with dynamic responses of the HMMWV during field tests conducted by the US Army Engineer Waterways Experiment Station (WES).

14. SUBJECT TERMS
Dynamic Analysis & Design System (DADS)
Frequency distributions (FFT)
HMMWV
Time histories
Vertical acceleration
Vehicle ride dynamics

15. NUMBER OF PAGES
170

16. PRICE CODE

17. SECURITY CLASSIFICATION OF REPORT	18. SECURITY CLASSIFICATION OF THIS PAGE	19. SECURITY CLASSIFICATION OF ABSTRACT	20. LIMITATION OF ABSTRACT
Unclassified	Unclassified		

PREFACE

The research described in this report is the result of studies conducted at the University of Iowa under the Secretary of the Army Research and Study Fellowships program during August 1989-1990, under training No. E27891215. Field test results presented in this report were supplied by the US Army Engineer Waterways Experiment Station (WES) from tests conducted during September-March 1991 for the Program Executive Office, Combat Support, US Army Tank Automotive Command (TACOM), under Military Interdepartmental Purchase Request No. W56HZW90-EKE and Project No. 1V665810DE65.

The field test study was conducted under the general supervision of Dr. W. F. Marcuson III, Director, Geotechnical Laboratory (GL), and under the direct supervision of N. R. Murphy, Jr., Chief, Mobility Systems Division (MSD), GL, and R. H. Gillespie, Chief, Mobility Investigations Branch, MSD. The field test program was conducted by R. A. Jones, and R. H. Johnson, MSD. Field test support was provided by D. E. McClurg, A. C. Roberson, D. E. Strong, R. N. Tennant, T. J. McCaffrey, J. Priddy, MSD; R. L. Coffing, Jr., Pavement Syetems Division; R. Lackey, Hilton Systems, Inc.; L. B. Naron, and W. C. Fryer, Instrumentations Service Division.

This report was prepared by Mr. Jones as partial fulfillment of the requirements for the Master of Science degree in Mechanical Engineering in the Graduate College of the University of Iowa.

At the time of publication of this report, Director of WES was Dr. Robert W. Whalin. Commander and Deputy Director was COL Leonard G. Hassell, EN.

To LCDR Roy Livingston Jones USN
(1924 - 1991)
My father, teacher and friend

ACKNOWLEDGMENTS

The author is grateful to the US Army Engineer Waterways Experiment Station for their dedication in supporting educational fellowships for their employees. In addition, the author extends his gratitude to his faculty advisor, Dr. Sang Sup Kim, whose counsel and guidance during this study was invaluable. The author would also like to extend his thanks to his brother Ken, whose encouragement was greatly appreciated during this study. Special acknowledgment is extended to Mr. Jody Priddy for his help in preparing the figures for this thesis. Also, the support and patience extended by Mr. David Venem, of CADSi, and Mr. Daniel Creighton, of WES, was indispensable.

R. A. J.

Vicksburg, MS
May 1992

ABSTRACT

The following validation study analyzes rigid multibody dynamic models for the US Army's High Mobility Multipurpose Wheeled Vehicle (HMMWV) using the Dynamic Analysis and Design System (DADS) computer code and the US Army's Vehicle Dynamics Module (VEHDYN) computer code. Simulated testing of the two vehicle models was conducted over non-deformable discrete obstacles and non-deformable continuous undulating terrains. Results from the model simulations (vertical acceleration time histories, frequency distributions, and absorbed power calculations) were compared with dynamic responses of the HMMWV during field tests conducted by the US Army Engineer Waterways Experiment Station (WES).

TABLE OF CONTENTS

LIST OF TABLES

LIST OF FIGURES

CHAPTER 1

INTRODUCTION

1.1 Background

Since the introduction of economically priced computers, scientists and engineers have been employing computer simulations to answer complex questions in a variety of areas, such as structural analysis, weather predictions, groundwater movement and tidal fluctuations. As new ideas in science and engineering are implemented so are their computer codes, which has placed the computer at a focal point in the scientific and engineering community. One area in which improvements have come rapidly is the implementation of advanced dynamic formulations. The implementation of new dynamic codes has allowed the design engineer to mathematically create prototype mechanical systems and resolve many basic design problems prior to construction and testing of the system. As the mechanism evolves to a realized construction, the initial simulation model matures to an applicable evaluation tool. Past standard practices in mechanical engineering have followed the road of "design, construct, test, modify, test, modify ..etc." With digital computing power now available to so many scientists and engineers, it is only natural that

certain standard practices be challenged by, or improved through computer simulations.

1.2 Objective and Scope

The objective of this thesis is to apply two different dynamic formulation methods to the area of vehicle dynamic studies, specifically in the area of vertical acceleration predictions, and determine the accuracy of the resultant models. The two modeling programs used for this study were selected not only to determine their accuracy in vehicle dynamic predictions, but also to define how each model can best be utilized for detailed dynamic studies.

Two dynamic vehicle models were developed and their simulated test results were compared to the measured vehicle dynamic test results. The Dynamic Analysis and Design System (DADS) computer code was used to generate a three dimensional rigid multibody vehicle model and the Vehicle Dynamics Module (VEHDYN) was used to generate a two dimensional rigid multibody vehicle model. These models were generated to simulate the dynamic responses of the US Army's High Mobility Multipurpose Wheeled Vehicle (HMMWV). The dynamic models were used to simulate testing conducted with the HMMWV. The results of the models and field tests were analyzed and compared using standard vehicle dynamics analysis techniques involving vertical acceleration time histories, peak vertical accelerations, pitch rates,

vertical absorbed powers (AP_{vt}), frequency distributions, and root-mean-square (rms) of time histories. Also, several computer programs were written to achieve a non-biased data comparison.

1.3 Literature Review

In the design of mechanical systems, all available engineering tools should be used to gain a basic understanding of the task at hand. To accomplish this goal, analytical computer programs are used to gain an understanding of the problem in the shortest time period possible. In the area of vehicle dynamics, programs are often written and structured for the specific vehicle under study, which can require more time than allowed by the study phase. This being the case, many engineers and scientists turn to available packaged software that allows enough design flexibility to accomplish the same task. The DADS and VEHDYN dynamic codes are examples of such software products.

Navistar International Transportation Corporation currently uses DADS to conduct steering and suspension analysis on heavy transportation trucks (Grohnke, 1991). Penske Racing of the United Kingdom also uses DADS to perform dynamic analysis on race car suspension components and on the roll, pitch and yaw of the race car's chassis (Beckert, 1991). The US Army Tank Automotive Command uses

both the DADS and VEHDYN programs (Beck, 1992 and Murphy, 1981) to perform vehicle dynamics research. Caterpillar Corporation uses VEHDYN to conduct dynamic analysis on new suspension designs for light weight bull dozers. The US Army Engineer Waterways Experiment Station (WES) currently uses the VEHDYN (Creighton 1986) to make vehicle dynamics predictions, and has released a new VEHDYN version. The latest VEHDYN release uses the same methodology as the older version, but has incorporated a larger variety of suspension designs for tracked vehicle models. (The newest VEHDYN release was used for model predictions in this study.) The literature review also revealed that some of the currently used DADS and VEHDYN vehicle models were validated for displacements and velocities, but not for vertical accelerations. It was also determined that the DADS and VEHDYN vehicle models were used to make predictions of the vehicle's dynamics which were used in assessing the need for design modifications of existing and future vehicle systems. Also, VEHDYN vehicle models were used to make vertical acceleration predictions for the NATO Reference Mobility Model (McGill University, 1982), which is used to predict the off-road performance of military vehicles.

The literature review led to the area of acceptable methods of vehicle model validation (Murphy, 1987). Most often, models are validated in the area of intended use. That is, if a model is used for predicting motion, or the

rate at which motion occurs, it should be validated using results from tests which were conducted with the vehicle going through its intended motion. The method of model validation for this study was based on the intended use of the two models. Since predictions in the area of vertical accelerations were needed, a vehicle was selected that had been tested in that area of interest (Jones, 1992).

In order to analyze each data base using the same techniques, a literature review was conducted to determine suitable techniques for filtering vertical accelerations, and calculating absorbed power and instantaneous peak vertical accelerations (Lins, 1972 and Murphy, 1981).

CHAPTER 2

DEVELOPMENT OF DYNAMIC EQUATIONS OF MOTION

2.1 Introduction

The DADS and VEHDYN dynamic codes were developed by means of conventional Newtonian mechanics. Whereas VEHDYN was developed by applying equations of motion which represent standard planar vehicle components, DADS is an "all encompassing" versatile dynamics package in which a mechanism can be constructed in a spatial environment. Since VEHDYN models a planar environment, its resulting equations of motion are much easier to develop and solve. The resulting equations of motion generated in a DADS spatial environment would be virtually impossible to solve without the aid of a digital computer.

2.2 Spatial Dynamic Equations of Motion

To develop the equations of motion for a spatial system, the methodology used by DADS will be presented. To develop Newton's equation of motion of a rigid body, let vector **r** locate a set of generalized coordinates that define the orientation of the x'-y'-z' body-fixed frame, relative to an inertial x-y-z reference frame, and let body vector $\mathbf{s}'^{P}$ locate a differential mass $dm(P)$ at a typical point P on

the rigid body where, $\mathbf{s'}^{P}$ is constant (Haug, 1989). As a model of a rigid body let each differential element in the rigid body be fixed and let an external force $\mathbf{F}(P)$ per unit of mass act on a differential element of mass at point P. Also consider the internal force $\mathbf{f}(P,R)$ per unit mass acting at points P and R, which are only due to gravitational interaction and distance constraints which fix each element.

$$\ddot{\mathbf{r}}^{P} dm(P) - \mathbf{F}(P)\, dm(P) - \int_{m} \mathbf{f}(P,R)\, dm(R)\, dm(P) = 0 \qquad (2.1)$$

Let $\delta\mathbf{r}^{P}$ denote a virtual displacement of point P. Multiplying both sides of equation 2.1 by $\delta\mathbf{r}^{PT}$ and integrating over the total mass of the body yields

$$\int_{m} \delta\mathbf{r}^{PT}\ddot{\mathbf{r}}^{P} dm(p) - \int_{m} \delta\mathbf{r}^{PT}\mathbf{F}(P)\, dm(P) - \int_{m}\int_{m} \delta\mathbf{r}^{PT}\mathbf{f}(P,R)\, dm(R)\, dm(P) = 0 \qquad (2.2)$$

Manipulating the double integral yields

$$\int_{m}\int_{m} \delta\mathbf{r}^{PT}\mathbf{f}(P,R)\, dm(R)\, dm(P) =$$

$$\frac{1}{2}\int_{m}\int_{m} \delta\mathbf{r}^{PT}\mathbf{f}(P,R)\, dm(R)\, dm(P)$$

$$+\frac{1}{2}\int_{m}\int_{m} \delta\mathbf{r}^{RT}\mathbf{f}(R,P)\, dm(P)\, dm(R) =$$

$$\frac{1}{2}\int_{m}\int_{m} (\delta\mathbf{r}^{P}-\delta\mathbf{r}^{R})^{T}\mathbf{f}(P,R)\, dm(P)\, dm(R) \qquad (2.3)$$

The second equality follows from interchanging the order of integration where $\mathbf{f}(P,R)\,dm(P)\,dm(R) = -\mathbf{f}(R,P)\,dm(R)\,dm(P)$ which uses Newton's third law of action and reaction.

For a rigid body, with fixed distances between all point masses, $(\mathbf{r}^P-\mathbf{r}^R)^T(\mathbf{r}^P-\mathbf{r}^R) = C$, and by taking the differential of both sides yields

$$(\delta\boldsymbol{r}^P-\delta\boldsymbol{r}^R)^T(\boldsymbol{r}^P-\boldsymbol{r}^R) = 0 \qquad (2.4)$$

Since the internal force only acts between points P and R then

$$\boldsymbol{f}(P,R) = k(\boldsymbol{r}^P-\boldsymbol{r}^R) \qquad (2.5)$$

where k is a constant, therefore the right side of equation 2.3 equals zero. It should be noted that the internal forces are workless for the development of the equations of motion for rigid bodies. Substituting equations 2.4 and 2.5 into equation 2.3 yields

$$\int_m \int_m \delta\boldsymbol{r}^{PT}\boldsymbol{f}(P,R)\,dm(P)\,dm(R) = 0 \qquad (2.6)$$

Therefore equation 2.2 can be written as

$$\int_m \delta\boldsymbol{r}^{PT}\ddot{\boldsymbol{r}}^P dm(P) - \int_m \delta\boldsymbol{r}^{PT}\boldsymbol{F}(P)\,dm(P) = 0 \qquad (2.7)$$

and must hold true for all virtual displacements $\delta\mathbf{r}^P$ which act consistent with the constraints on the body.

To take full advantage of the virtual displacement of point P, equation 2.7 may be written in terms of a virtual displacement of the origin of the x'-y'-z' frame and a

virtual rotation of the body. Let equation 2.8 represent a virtual displacement of point P

$$\delta \boldsymbol{r}^P = \delta \boldsymbol{r} - \boldsymbol{A}\tilde{\boldsymbol{s}}'^{P}\delta\pi' \tag{2.8}$$

where

$\boldsymbol{A}$ = Transformation matrix

$\tilde{\ }$ = Indicates a skew-symmetric matrix

$\delta\boldsymbol{\pi}$ = Virtual rotation

with the acceleration of point P written as

$$\begin{aligned} \ddot{\boldsymbol{r}}^P &= \ddot{\boldsymbol{r}} + \ddot{\boldsymbol{A}}\boldsymbol{s}'^{P} \\ &= \ddot{\boldsymbol{r}} + \boldsymbol{A}\dot{\tilde{\omega}}'\boldsymbol{s}'^{P} + \boldsymbol{A}\tilde{\omega}'\,\tilde{\omega}'\boldsymbol{s}'^{P} \end{aligned} \tag{2.9}$$

where

ω = Angular velocity vector

Substituting equations 2.8 and 2.9 into equation 2.7 yields

$$\int_m (\delta \boldsymbol{r}^T + \delta\pi'^T\tilde{\boldsymbol{s}}'^{P}\boldsymbol{A}^T)\,(\ddot{\boldsymbol{r}} + \boldsymbol{A}\dot{\tilde{\omega}}'\boldsymbol{s}'^{P} + \boldsymbol{A}\tilde{\omega}'\tilde{\omega}'\boldsymbol{s}'^{P})\,dm(P)$$

$$-\int_m (\delta \boldsymbol{r}^T + \delta\pi'^T\,\tilde{\boldsymbol{s}}'^{P}\boldsymbol{A}^T)\,\boldsymbol{F}(P)\,dm(P) = 0 \tag{2.10}$$

for all $\delta\boldsymbol{r}$ and $\delta\boldsymbol{\pi}'$ that are consistent with fixed constraints.

Expanding the integrals of equation 2.10 yields

$$\delta \mathbf{r}^T \ddot{\mathbf{r}} \int_m dm(P) + \delta \mathbf{r}^T (\mathbf{A}\tilde{\dot{\omega}}' + \mathbf{A}\tilde{\omega}'\tilde{\omega}') \int_m \mathbf{s}'^P dm(P)$$

$$+ \delta \pi'^T \int_m \mathbf{s}'^P dm(P)\, \mathbf{A}^T \ddot{\mathbf{r}} + \delta \pi'^T \int_m \tilde{\mathbf{s}}'^P \tilde{\dot{\omega}}' \mathbf{s}'^P dm(P)$$

$$+ \delta \pi'^T \int_m \tilde{\mathbf{s}}'^P \tilde{\omega}' \tilde{\omega}' \mathbf{s}'^P dm(P) - \delta \mathbf{r}^T \int_m \mathbf{F}(P)\, dm(P)$$

$$- \delta \pi'^T \int_m \tilde{\mathbf{s}}'^P \mathbf{F}'(P)\, dm(P) = 0 \qquad (2.11)$$

for all $\delta \mathbf{r}$ and $\delta \pi'$ that are consistent with fixed constraints.

To develop the equations of motion for a rigid body located in space by a vector $\mathbf{r}$ to the origin of the body-fixed x'-y'-z' which resides at the rigid body's center of mass, let total mass m equal

$$m \equiv \int_m dm(P) \qquad (2.12)$$

and, by definition of the centroidal body-fixed frame,

$$\int_m \mathbf{s}'^P dm(P) = 0 \qquad (2.13)$$

The total external force acting on the body is

$$\mathbf{F} \equiv \int_m \mathbf{F}(P)\, dm(P) \qquad (2.14)$$

and the applied torque with respect to the origin of the x'-y'-z' frame is

$$\mathbf{n}' \equiv \int_m \tilde{\mathbf{s}}'^P \mathbf{F}'(P)\, dm(P) \qquad (2.15)$$

and the inertia matrix with respect to the x'-y'-z' centroidal frame is

$$\boldsymbol{J}' = -\int_m \tilde{\boldsymbol{s}}'^{P}\,\tilde{\boldsymbol{s}}'^{P} dm(P) \tag{2.16}$$

Expanding the fifth integral of equation 2.11 yields

$$\begin{aligned}\tilde{\boldsymbol{s}}'^{P}\tilde{\omega}'\tilde{\omega}'\boldsymbol{s}'^{P} &= -\tilde{\boldsymbol{s}}'^{P}\tilde{\omega}'\tilde{\boldsymbol{s}}'^{P}\omega' \\ &= -\tilde{\omega}'\tilde{\boldsymbol{s}}'^{P}\tilde{\boldsymbol{s}}'^{P}\omega' - \omega'\boldsymbol{s}'^{PT}\tilde{\boldsymbol{s}}'^{P}\omega' - \boldsymbol{s}'^{P}\omega'^{T}\tilde{\omega}'\boldsymbol{s}'^{P} \\ &= -\tilde{\omega}'\tilde{\boldsymbol{s}}'^{P}\tilde{\boldsymbol{s}}'^{P}\omega'\end{aligned} \tag{2.17}$$

Integrating both sides over the mass of the body yields

$$\begin{aligned}\int_m \tilde{\boldsymbol{s}}'^{P}\tilde{\omega}'\tilde{\omega}'\boldsymbol{s}'^{P} dm(P) &= \tilde{\omega}'\left(-\int_m \tilde{\boldsymbol{s}}'^{P}\tilde{\boldsymbol{s}}'^{P} dm(P)\right)\omega' \\ &= \tilde{\omega}'\boldsymbol{J}'\omega'\end{aligned} \tag{2.18}$$

The variational Newton-Euler equations of motion are obtained by substituting equations 2.12 to 2.18 into equation 2.11, with the results shown by equation 2.19.

$$\delta\boldsymbol{r}^{T}[m\ddot{\boldsymbol{r}} - \boldsymbol{F}] + \delta\pi'^{T}[\boldsymbol{J}'\dot{\omega}' + \tilde{\omega}'\boldsymbol{J}'\omega' - \boldsymbol{n}'] = 0 \tag{2.19}$$

Equation 2.19 must hold for all virtual displacements $\delta\boldsymbol{r}$ and virtual rotations $\delta\boldsymbol{\pi}'$ of the centroidal x'-y'-z' body frame that are consistent with constraints that act on the body.

If no external constraints are imposed on a body, then $\delta\boldsymbol{r}$ and $\delta\boldsymbol{\pi}'$ are arbitrary and their coefficients equal zero.

Therefore, the resultant Newton-Euler equations of motion for an unconstrained body would be

$$m\ddot{\boldsymbol{r}} = \boldsymbol{F}$$
$$\boldsymbol{J}'\dot{\omega}' = \boldsymbol{n}' - \tilde{\omega}'\boldsymbol{J}'\omega' \qquad (2.20)$$

Integration of equation 2.20 for body orientation is possible, but first a set of orientational generalized coordinates must be introduced into the equation. This is necessary to allow for the direct integration of ω.

By combining the equation of motion of each body and constraint equations between bodies and using a set of orientational generalized coordinates, equation 2.19 can be written as

$$\delta\boldsymbol{q}^T[\ \boldsymbol{M}^*\ddot{\boldsymbol{q}} - \boldsymbol{Q}^*\ ] = 0 \qquad (2.21)$$

where

$$\delta\boldsymbol{q} = [\ \delta\boldsymbol{q}_1^T, \delta\boldsymbol{q}_2^T, \ldots, \delta\boldsymbol{q}_{nb}^T\ ]^T$$
$$\ddot{\boldsymbol{q}} = [\ \ddot{\boldsymbol{q}}_1^T, \ddot{\boldsymbol{q}}_1^T, \ldots, \ddot{\boldsymbol{q}}_{nb}^T\ ]$$
$$\boldsymbol{M}^* = diag[\ \boldsymbol{M}_1, \boldsymbol{M}_2, \ldots, \boldsymbol{M}_{nb}\ ]$$
$$\boldsymbol{Q}^* = [\ \boldsymbol{Q}_1^T, \boldsymbol{Q}_2^T, \ldots, \boldsymbol{Q}_{nb}^T\ ]$$

and **M** is the generalized mass matrix, **Q** is the generalized force vector applied externally on the system, nb denotes the total number of bodies in the constrained system, and

$$Q_j^* = Q_j - S_j \,, \qquad j = 1,\ldots,nb$$

$$\delta q_j^T = \{\, \delta r_j^T, \delta \pi_j^T \,\}, \qquad j = 1,\ldots,nb$$

$$\ddot{q}_j^T = \{\, \ddot{r}_j^T, \dot{\omega}_j^T \,\}, \qquad j = 1,\ldots,nb$$

S_j contains terms that are quadratic in velocity.

Kinematic constraints between bodies can be formulated as a set of nonlinear algebraic equations that describe the kinematic relations among bodies. These equations can be written as

$$\Phi(q, t) = 0 \tag{2.22}$$

Variations dq in the system generalized coordinates q must satisfy

$$\Phi_q \, \delta q = 0 \tag{2.23}$$

The system equations of motion of the constrained mechanical system can be formulated by incorporating multiplier vector λ as follows:

$$\begin{bmatrix} M^* & \Phi_q^T \\ \Phi_q & 0 \end{bmatrix} \begin{bmatrix} \ddot{q} \\ \lambda \end{bmatrix} = \begin{bmatrix} Q^* \\ \gamma \end{bmatrix} \tag{2.24}$$

for arbitrary dq, where γ is defined in the constraint acceleration equation as

$$\Phi_q \ddot{q} = -(\, \Phi_q \dot{q} \,)_q \dot{q} - 2\Phi_{qt}\dot{q} - \Phi_{tt} \equiv \gamma \tag{2.25}$$

This system of equations, taken with the kinematic constraints and the associated velocity equations, comprises

the mixed differential-algebraic equations of motion of the system. Supplying initial conditions for the system, equation 2.24 may be integrated and the system of equations resolved.

2.3 Planar Dynamic Equations of Motion

To develop a planar system of dynamic equations, the methodology used in VEHDYN will be presented (Murphy, 1976). The dynamic equations of motion for a planar vehicle system require the implementation of at least three sets of dynamic equations. The number of equations depends on the complexity of the vehicle's suspension system. The system of equations presented represents those for a vehicle with an independent suspension system. The first two sets of equations are for the sprung mass, and the third for unsprung.

The vertical motion of the sprung mass' center of gravity (cg) can be written as

$$F_z^T = m_c \ddot{Z}_c \qquad (2.26)$$

where

F^T_z = Total vertical force acting on mass

m_c = Sprung mass

Z_c = Vertical acceleration of mass

The vertical forces acting on the sprung mass are determined through the summation of all contributing vertical forces acting on the system and are defined as

$$m_c \ddot{Z}_c = \sum_{i=1}^{N} \left[F_z^s + F_z^d \right] - F_z^g \qquad (2.27)$$

where

F_z^s = Vertical spring forces

F_z^d = Vertical damping forces

F_z^g = Gravitational force

N = Number of vertical force elements

Therefore, the vertical forces acting on the vehicle's frame consist of each suspension's spring and damper force minus the gravitational force acting on the sprung mass.

The pitch of the sprung mass about its cg is defined as

$$I_c \ddot{\theta} = \sum_{i=1}^{N} \left[F_z^s \, r_{cg}^s + F_z^d \, r_{cg}^d \right] \cos\theta \qquad (2.28)$$

where

I_c = Mass moment of inertia of the sprung mass

θ = Angular rotation with respect to horizontal

r_{cg}^s = Vector from cg to spring

r_{cg}^d = Vector from cg to damper

and is the result of the rotational forces generated from the spring and damper forces times their horizontal distances from the cg.

The vertical forces acting on each unsprung mass are defined as

$$\sum_{i=1}^{N} m_i^w \ddot{Z}_i = \left[-F_z^s - F_z^d + \sum_{i=1}^{N} F_z^t - \sum_{i=1}^{N} m_i^w g \right] \qquad (2.29)$$

where

m_i = Mass of each wheel assembly

F_z^t = Vertical force from each tire element

N = Total number of wheel assemblies

and is the result of each suspension's spring, damper and tire force along with the gravitational force acting on each suspension assembly.

Supplying initial conditions for the system, equations 2.26 through 2.29 may be integrated and the system of equations resolved.

CHAPTER 3

HMMWV DYNAMIC MODELS

3.1 HMMWV Description

The vehicle characteristics of the M998 series of the HMMWV were used to generate the dynamic models. The M998, shown in Figure 3.1, is the US Army's basic HMMWV utility truck. The M998 vehicle characteristics are presented in Table 3.1.

Table 3.1. M998 Utility Truck Characteristics

Vehicle chassis weight	4,573	lb
Total suspension weight	573	lb
Total vehicle weight	5,146	lb
Lateral center of gravity measured from the center line (port)	1.2	in
Longitudinal center of gravity measured from the front axle	57.7	in
Vertical center of gravity measured from the ground	29.9	in
Chassis X moment of inertia (pitch)	41300	$lb\text{-}in^2$
Chassis Y moment of inertia (roll)	13900	$lb\text{-}in^2$
Chassis Z moment of inertia (yaw)	52300	$lb\text{-}in^2$

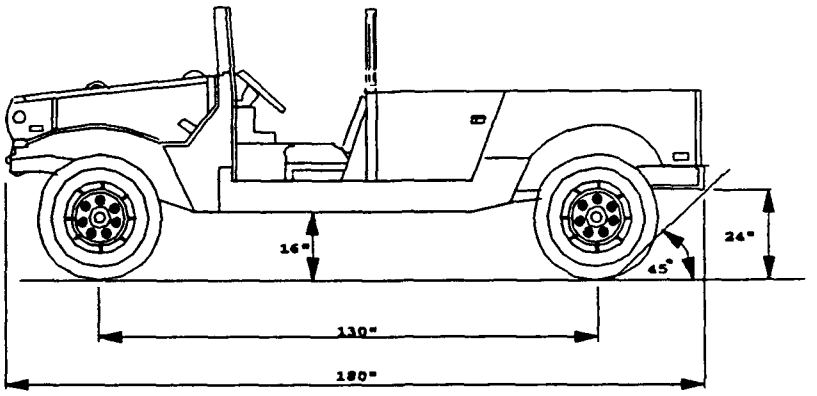

a. Profile view of the M998 Utility Truck

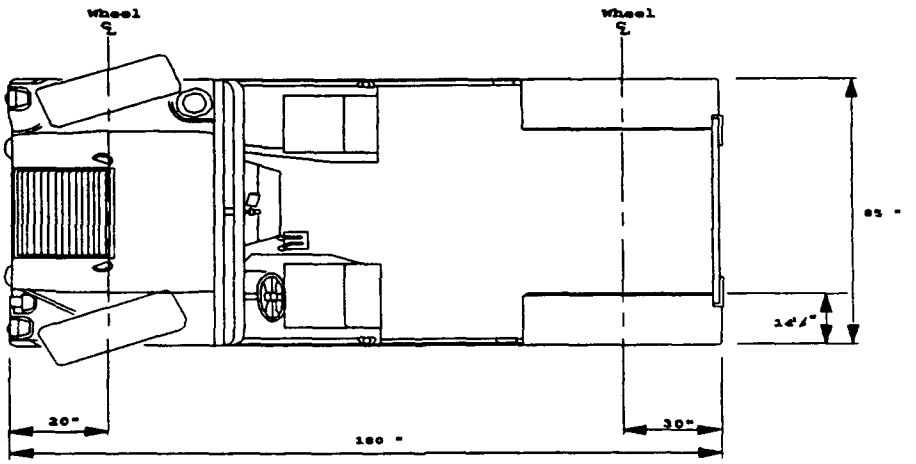

b. Top view of the M998 Utility Truck

Figure 3.1. Profile and top view of the M998 Utility Truck

Figure 3.2 shows the front vehicle suspension as a "double wishbone" type. Each suspension on the vehicle has the same design and dimensions. The only difference between the front and rear suspension is the front suspension's extra rotational degree of freedom (DOF) for steering the wheels. The rear wheels are prevented from turning by a tie-rod attached between the wheel and chassis. Each suspension consists of an upper and lower control arm. Each control arm is attached to the chassis by a front and rear pinned bushing joint. A ball joint is used to attach each control arm to a wheel. Each suspension incorporated a spring and damper. The damper on each suspension is attached between the lower control arm and chassis by a pinned bushing joint at each end. The coil spring surrounded the damper and is held in place at the top by a plate attached to the damper and at the bottom by the lower control arm.

The HMMWV's independent suspension design gave each suspension a rotational DOF about the chassis. The jounce and the rebound bump stops in the damper limited the amount of rotation. The suspension is prevented from moving longitudinally by the double pin attachment to the chassis of each control arm. The ball joints, which attached the control arms and wheels, gave each wheel a small amount of twist as the suspension rotated but is insignificant when compared to the total displacement of the wheel.

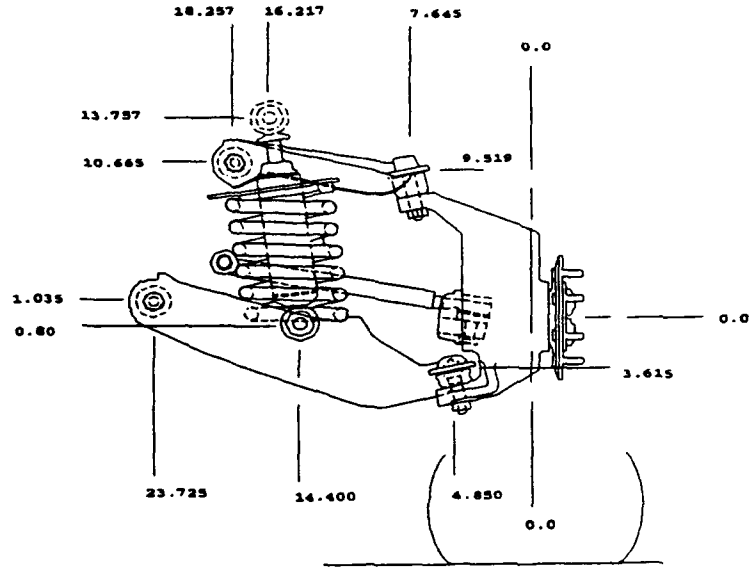

a. Profile of front left suspension

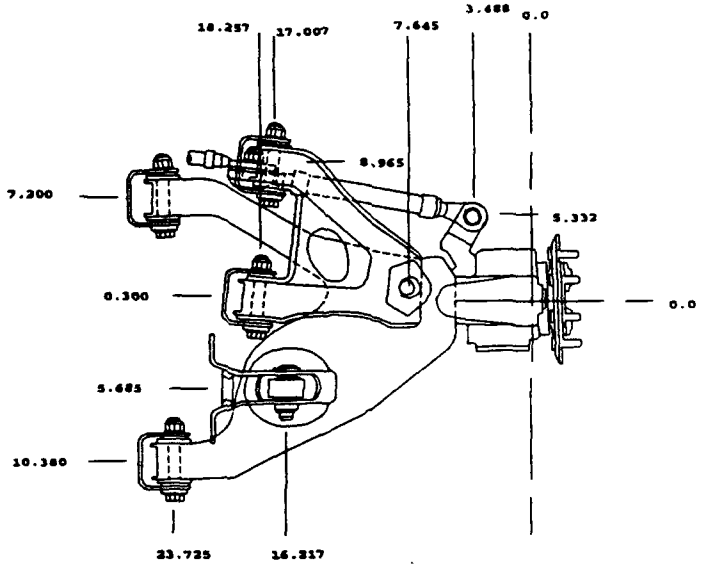

b. Top view of front left suspension

Figure 3.2. Independent suspension design

3.2 Introduction to DADS Methodology

Developed at The University of Iowa, DADS is a large-scale rigid or flexible multibody kinematic and dynamic computer code (Haug, 1989), which implements both planar and spatial dynamic formulations. DADS uses a Cartesian coordinate system to construct the equations of motion which represent the constrained multibody system. In order to construct a system in the DADS environment the user must first decide how to represent the system mathematically. A library of constraining equations is available to the user called "constraining joints." Each kinematic joint available in DADS represents a physical component that could be employed to construct the mechanism. Sample joint selections in the DADS library include: revolute joints which allow 1 rotational DOF, translational joints which allow 1 translational DOF, and spherical joints which allow 3 rotational DOF. Using selections from the library of constraining joints, the user is able to build a mathematical model and simulate the motion of the mechanical system. DADS also offers a library of representative force elements. These model components such as bushings, leaf springs, coil springs, and tires. Once the user has determined how to best represent a model mathematically, accurate Cartesian coordinate locations for placement of each joint and force element are required. This can be an arduous task requiring detailed drawings of the intended

system. Once the system of joints and elements is selected and locational placement is known, DADS allows the user to assemble these through the creation of attachment bodies. These bodies represent distances and masses that exist in the real mechanism. After the assembly process is complete, DADS implements the operations required to solve for the equations of motion and performs the task of bookkeeping for each time step required for reaching numerical solutions.

3.3 DADS Geometry Model

The HMMWV model was constructed in a three dimensional rigid multibody DADS environment using the geometries presented in Table 3.1 and Figures 3.1 and 3.2. The resulting design used for the model is shown in Figure 3.3. A global coordinate system was selected for the model based on available chassis drawings of the vehicle. The coordinate system was placed with the X axis representing the width of the vehicle, the Y axis representing the length of the vehicle, and the Z axis representing the height of the vehicle. Each element and joint was located using the global coordinate system. Since, the style of field testing represented a planar environment, only the components necessary to simulate the field tests were created in the DADS spatial model.

The vehicle's suspension was modeled based on the design. The design called for an independent suspension

with an upper and lower control arm which gave the suspension 1 rotational DOF about the Y axis. Each modeled suspension consisted of three bodies and force elements: an upper and lower control arm, wheel, spring, damper, and tire element. Each body represented the mass and inertia of each component in the actual suspension.

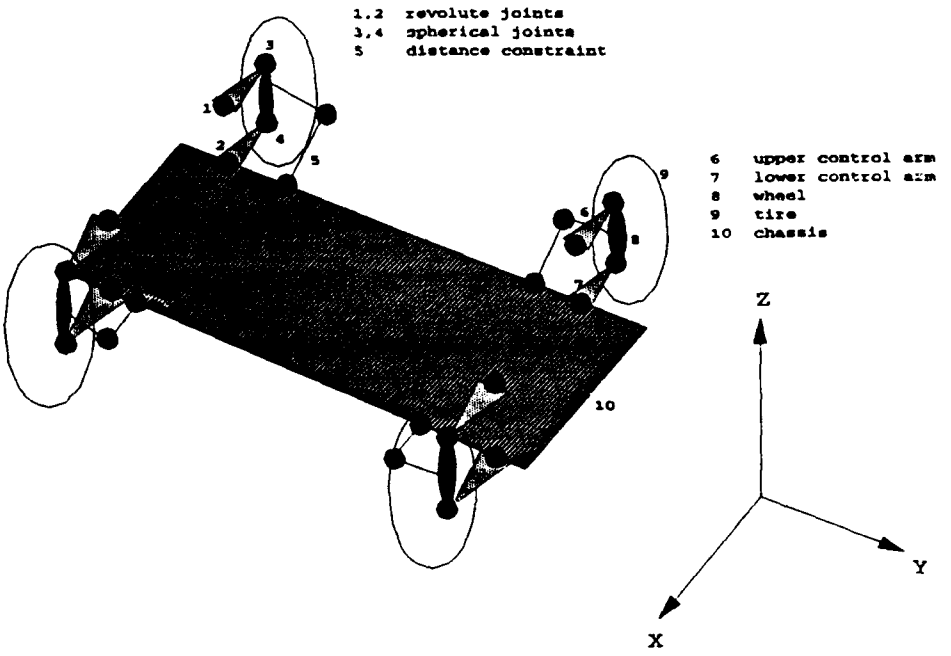

Figure 3.3. Schematic of DADS model

To assemble the suspension bodies, eight revolute joints, eight spherical joints and four distance constraints were used to attach each control arm to the chassis and wheel. By employing revolute joints, each control arm in the model had the same rotational DOF as the actual suspension. Due to the mathematical constraints imposed by

each revolute joint, only one revolute joint per control arm was necessary. The revolute joint allowed each control arm only 1 rotational DOF, and prevented all other rotations or linear displacements. Each revolute joint was attached between the control arm and chassis at a point half way between the two pinned bushing joints used in the actual suspension. One spherical joint was used to attach each control arm to a wheel. Each spherical joint has 3 DOF, but by attaching the upper and lower control arms to a common body with spherical joints results in only 1 rotational DOF about the vertical axis between the pair of joints. This is the same basic design found in the actual suspension. Except for the steering linkage, the actual suspension prevents the rotation about the kingpin axis between the two ball joints by attaching a tie rod between the wheel and chassis. The front suspension is allowed a limited amount of rotation through a rack and pinion linkage which is controlled by the driver. Since only a straight forward line of advancement of the vehicle was needed during simulations, one distance constraint between each wheel and chassis was used to prevent the wheels from steering. Each distance constraint was placed at the same location as the tie rods on the actual suspension. As shown in Table 3.2, the model design yielded the same DOF found in the actual vehicle system. This equated to 6 DOF for the chassis and 1 DOF for each suspension.

Table 3.2. Model Design and Resultant Degrees of Freedom

Bodies		
Chassis		1
Upper control arms		4
Lower control arms		4
Wheels		4
Number of bodies (nb) =		13
Number of generalized coordinates (nc) = nb X 7 =		91
Constraints		
8 Revolute joints		
(5 constraints X 8 joints)	=	40
8 Spherical joints		
(3 constraints X 8 joints)	=	24
4 Distance constraints		
(1 constraint X 4 locations)	=	4
Euler parameter normalization constraint		13
Number of holonomic constraints (nh) =		81
Degrees of freedom = nc - nh = 91 - 81 = 10		

The moments of inertias for the vehicle's chassis, presented in Table 3.1, were obtained from tests conducted by The University of Michigan's Transportation Research Institute. The DADS HMMWV input file is presented in the Appendix.

3.4 DADS Spring and Damper Force Elements

Two force elements were used in each suspension to represent springs and dampers and were attached using the same design parameters found in the actual system. For each suspension, both force elements were attached between the lower control arm and chassis. During model simulations, the DADS model calculates the relative displacements for

springs and relative velocities for dampers. The model then uses either a constant spring or damper rate, or a force/displacement or force/velocity look up table to determine the amount of force to apply to the attachment bodies. The DADS model uses a negative force value to represent jounce and a positive for rebound. The force/deflection curves used in the DADS model are presented in Table 3.3.

Table 3.3. DADS Spring Force/Displacement Data

Displacement* in	Force lb
Front Spring Data	
-6.24	-12000
-5.24 (jounce bump stop)	- 7000
-1.56 (rebound bump stop)	- 1488
-1.559	1488
-0.559	2988
Rear Spring Data	
-5.350	-12516
-4.350 (jounce bump stop)	- 7516
-0.510 (rebound bump stop)	- 881
-0.509	881
0.491	2381

*Measured from vehicle equilibrium

These curves were obtained from suspension tests conducted by WES. In order to simulate damper bump stops, bump stops were imposed in the force/displacement spring curves shown in Figure 3.4. This allowed the modeled suspension the same range of displacement as the actual suspension. The step function rebound bump stop prevented the model from suddenly applying a tension force larger than the last applied compression force. Since the suspension's spring is always in a compressed state, the step function held the maximum displacement of the spring constant.

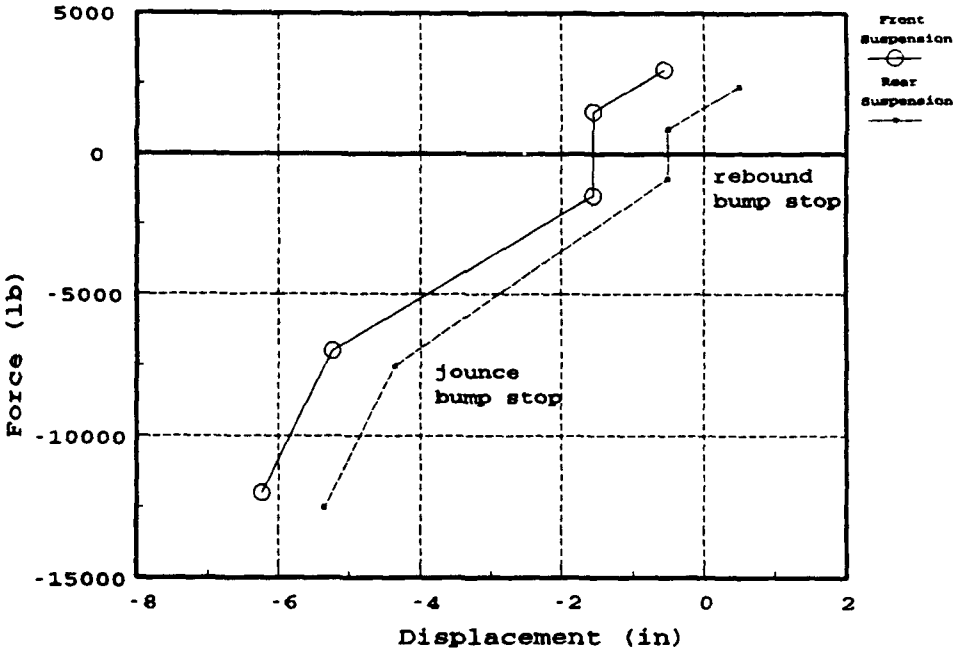

Figure 3.4. DADS spring force/displacement data

Also, the step function held the suspension at the imposed bump stop with only minor oscillations. A steep linear

rebound bump stop causes the model to apply a large tension force on the system after the bump stop is encountered. This causes the model to oscillate between large displacements trying to reach a steady state. The jounce bump stop, shown in Figure 3.4, on the actual suspension dictates the use of a steep linear bump stop. This stops the downward displacement of the chassis once the jounce bump stop is encountered. Bump stop locations for the suspension were supplied by AM General Inc. (manufacturers of the HMMWV).

The force/velocity curves used to represent the front and rear dampers, Table 3.4 and Figure 3.5, were obtained by modifying force/velocity data supplied by AM General Inc. The test results used to validate the dynamic models came from tests conducted in the latter stages of WES's dynamic study (see Chapter 4). Since several hundred dynamic tests had been conducted prior to the test results selected for validation, it was suspected that the dampers had experienced a certain amount of wear. The amount of operational wear in each damper was not measured; therefore, to approximate the force/velocity relationship present in each damper during testing, one field test sequence was selected to represent the force/velocity parameters to be used in the models.

Table 3.4. DADS Damper Force/Velocity Data

Velocity in/sec	Original Force lb	Modified Force lb
	Front Damper Data	
-13.352	-861	-430
- 6.676	-425	-212
- 2.356	- 92	- 46
0.0	0	0
2.356	184	184
6.676	788	400
13.352	1552	900
	Rear Damper Data	
-13.352	-952	-576
- 6.676	-496	-248
- 2.356	-127	- 62
0.0	0	0
2.356	456	228
6.676	1268	634
13.352	2086	1142

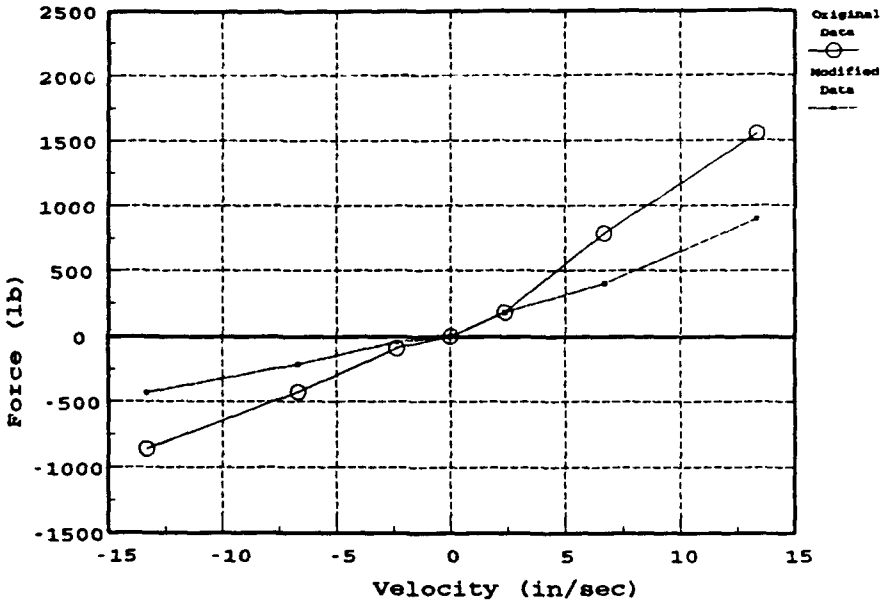

a. Front suspension damper data

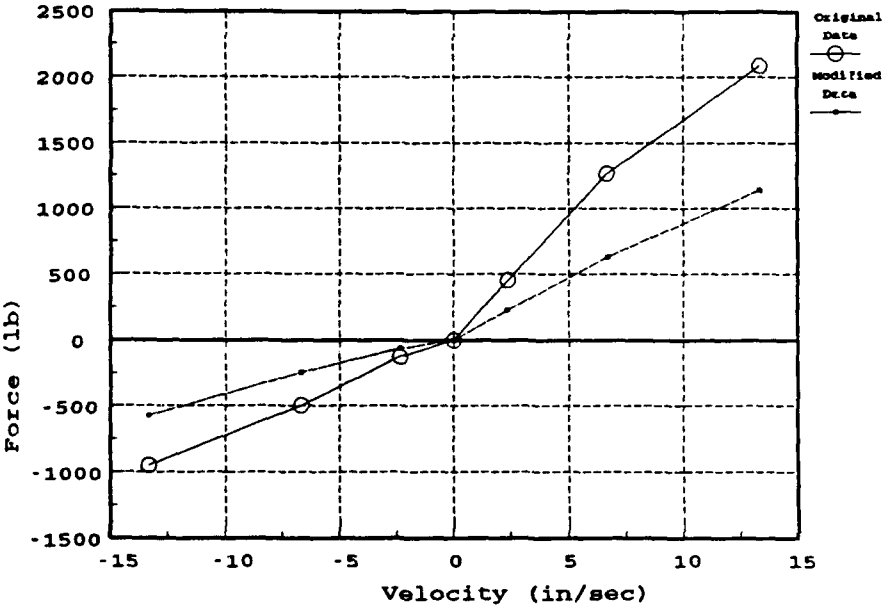

b. Rear suspension damper data

Figure 3.5. Original and modified damper data

The force/velocity relationship from this test was obtained by performing several DADS model iterations. Starting with damper force values that were half of the original values, and keeping modified damper forces within realistic values, model iterations were conducted until the model's vertical acceleration time history results closely matched those from the selected field tests. The resultant force/velocity data from these iterations were then used to complete the validation study.

3.5 DADS Tire Force Element

The tire element in the DADS code uses a radial spring design to represent the dynamics of a tire and is depicted in Figure 3.6. As shown, the tire has an initial deflection caused by the weight of the vehicle.

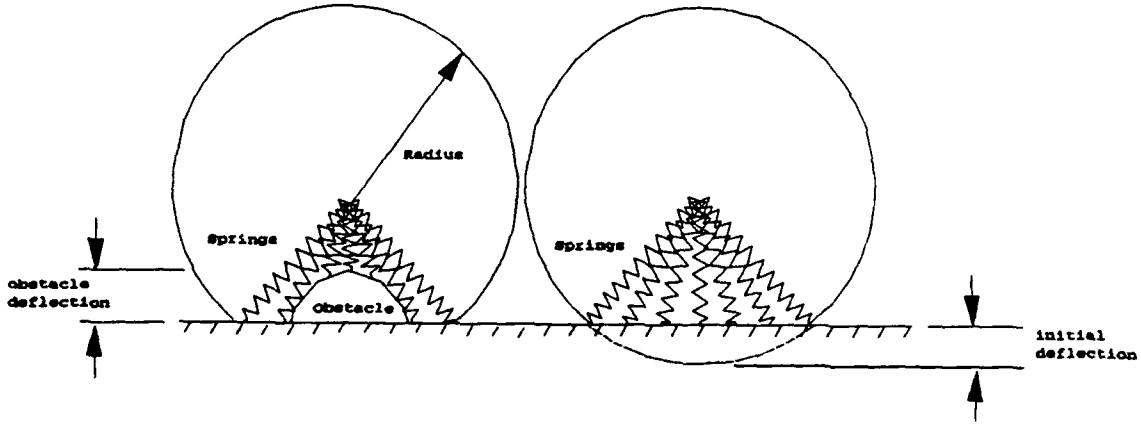

Figure 3.6. Radial spring tire model

As the tire encounters an obstacle, the radial springs deflect to a level which either conforms to the shape of the obstacle, or the amount of force developed by the tire's deflection equals the opposing force applied by the suspension.

There are three levels of tire sophistication offered in the DADS tire element (CADSi, 1991). The intermediate level was selected to best represent the actual tires. The force/deflection tire data used in the tire element were obtained from tests conducted by WES. The force/deflection tire tests were conducted at tire inflation pressures used during field testing.

3.6 DADS Road Element

The road element in DADS permits the user to specify the ground elevation profile as a function of the longitudinal displacement. The road element determines the current ground elevation to be passed to the tire element through the implementation of either a point-to-point linear or spline interpolation of the profile data. The road profile data for obstacle simulations were calculated every 0.1-in. and every 1.0 ft for the ride courses. Therefore, the ground elevations for each model time step were calculated using a linear interpolation between profile points.

3.7 DADS Velocity Control Element

To keep the forward motion of the DADS model realistic, as the tire element impacted ground obstacles, a velocity feedback control system was implemented using DADS control elements. The desired forward chassis velocity was placed in a reference element. At each simulation time step the current velocity was compared to the reference velocity through a feedback element. The difference between the two velocities was determined and a constant gain factor was multiplied by the difference of the velocities. The resultant product was then applied to the chassis' cg as a horizontal force. The direction of the applied force depended on the sign of the velocity differences. This allowed the model to speed up or slow down depending on the resultant horizontal force generated by the tire element. The resultant speed variations, when compared to a constant velocity driver, represented a more realistic speed profile.

3.8 Introduction to VEHDYN Methodology

VEHDYN is a rigid multibody planar dynamic computer code which was developed in 1974 (Murphy, 1976) to provide the US Army with an analytical tool that would predict dynamic vehicle responses. VEHDYN uses a Cartesian coordinate system to construct the equations of motion which represent the constrained multibody system (Creighton, 1986). VEHDYN was programmed with a library of pre-designed

"off-the-shelf" vehicle suspensions available to the user. Each suspension design available in the VEHDYN library represents a standard suspension design used in the manufacture of vehicle systems. Sample suspension selections available in VEHDYN include: independent, unsprung, walking beam, and bogie. Suspension selection is based on the actual design of the system to be modeled. Once a suspension has been selected, VEHDYN only needs the user to adjust the dimensions of the library's design to a more suitable representation of the actual suspension. VEHDYN also offers a library of force elements. These represent vertical and rotational springs and dampers found on most vehicle systems. Once the user has determined how to best model the vehicle's suspension, accurate two dimensional Cartesian coordinate locations for placement of each suspension and force element are required. This, like DADS, can be a very difficult task, since VEHDYN is a two dimensional representation of a three dimensional system, the user must transform the actual system into a two dimensional environment. After locational placement of the chassis, suspension, and force elements, VEHDYN will solve the generated equations of motion for each user-supplied time step.

3.9 VEHDYN Geometry Model

VEHDYN uses the "Y-Z" Cartesian axis convention with the Y axis representing the length of the vehicle and Z axis representing the height. The HMMWV's suspension was modeled using the VEHDYN independent suspension design. The required chassis and suspension dimensions and characteristics were defined using a two dimensional mapping of the vehicle's geometry presented in Table 3.1 and Figures 3.1 and 3.2. The resultant VEHDYN vehicle model, shown in Figure 3.7, was generated using a model body for the chassis and each pair of wheels, a spring and damper force element for each pair of suspensions, and a tire element for each pair of tires.

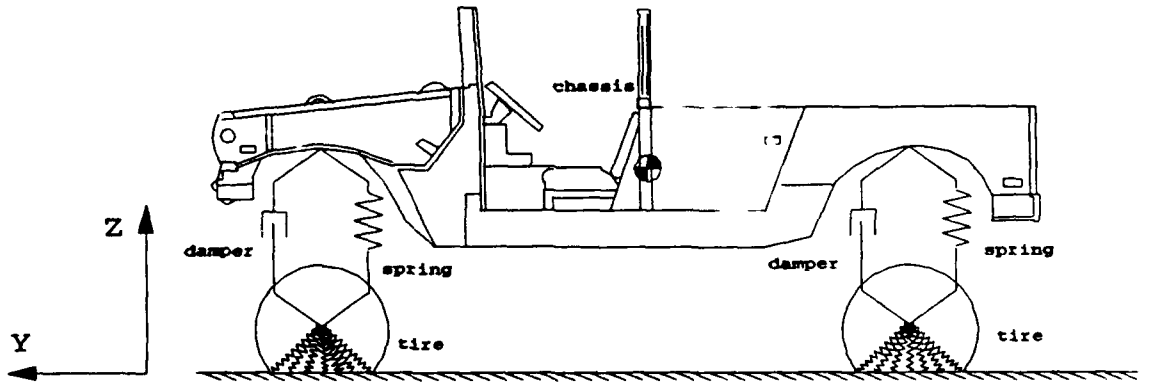

Figure 3.7. Schematic of VEHDYN model

The VEHDYN suspension elements used to model the front and rear suspensions yielded 1 DOF in the vertical direction for each suspension. Using a planar mapping of each

suspension transformed the rotational DOF to a vertical DOF in the Z direction. VEHDYN uses a constant velocity driver which confines the chassis to only 2 DOF, one of which is in the vertical, Z, direction and the other is a rotational DOF in the Y-Z plane. This equates to a total of 4 DOF; 2 DOF for the chassis, and 1 DOF for each suspension. The VEHDYN model is presented in the Appendix.

3.10 VEHDYN Spring and Damper Force Elements

Planar transformation of the HMMWV's bump stops and force elements was accomplished by modifying the information used in the DADS model. This was accomplished through spatial vector calculations. Also, VEHDYN represents a jounce force as positive and a rebound as negative. This is the opposite of how DADS interprets the force data.

For planar transformation of the spatial components let vector $\mathbf{r}_1$ represent the distance from the chassis, along the lower control arm, to the attachment point of the spring. Let vector $\mathbf{r}_2$ represents the distance from the chassis, starting at the lower control arm's attachment point, to the center of the wheel. The rotational displacement of the wheel with respect to the rotational displacement of the spring is derived by equation 3.1. By employing equation 3.1 the suspension bump stops were transformed to a planar environment.

$$d_1 = |r_1|\ \theta$$

$$d_2 = |r_2|\ \theta$$

$$\theta = \frac{d_1}{|r_1|}$$

$$\therefore\ d_2 = \frac{|r_2|}{|r_1|}\ d_1 \qquad (3.1)$$

where

θ = Rotation of suspension

d_1 = Spring displacement

d_2 = Tire displacement

Similar transformations were made on the force curves as shown by equation 3.2.

$$f_1 = |r_1|\ \theta\ f_{s_1}$$

$$f_2 = |r_2|\ \theta\ f_{s_2}$$

By summing vertical forces about the chassis,

$$f_2 = f_1\ \frac{|r_1|}{|r_2|}$$

$$f_1\ \frac{|r_1|}{|r_2|} = |r_2|\ \theta\ f_{s_2}$$

$$f_1 = \frac{|r_2|^2}{|r_1|}\ \theta\ f_{s_2}$$

$$|r_1|\ \theta\ f_{s_1} = \frac{|r_2|^2}{|r_1|}\ \theta\ f_{s_2}$$

$$\therefore \quad f_{s_2} = \frac{|r_1|^2}{|r_2|^2} f_{s_1} \qquad (3.2)$$

where

f_1 = Resultant force at 3-D spring

f_2 = Equivalent force at wheel

f_{s1} = Spring constant for 3-D system

f_{s2} = Equivalent spring constant at wheel

The resultant planar force data are presented in Tables 3.5 and 3.6 and Figure 3.8.

Table 3.5. VEHDYN Spring Force/Displacement Data

Displacement* in		Force lb
	Front Spring Data	
-15.00		-5016
2.53		- 633
2.54	(rebound bump stop)	633
11.12	(jounce bump stop)	2778
21.78		70800
	Rear Spring Data	
-15.00		-6100
1.15		- 406
1.16	(rebound bump stop)	406
10.10	(jounce bump stop)	3535
21.78		71928

*Measured from vehicle equilibrium

Table 3.6. VEHDYN Damper Force/Velocity Data

Velocity in/sec		Force lb
	Front Damper Data	
-31		-383
-16		-177
- 6		- 85
0		0
6		21
16		91
31		180
	Rear Damper Data	
-31		-487
-16		-278
- 6		-106
0		0
6		29
16		108
31		243

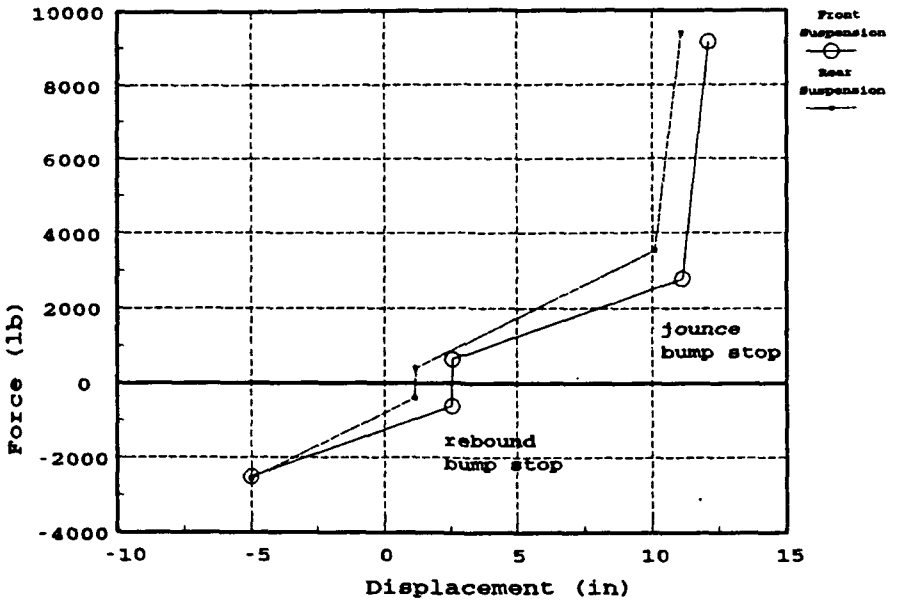

a. Spring force/displacement data

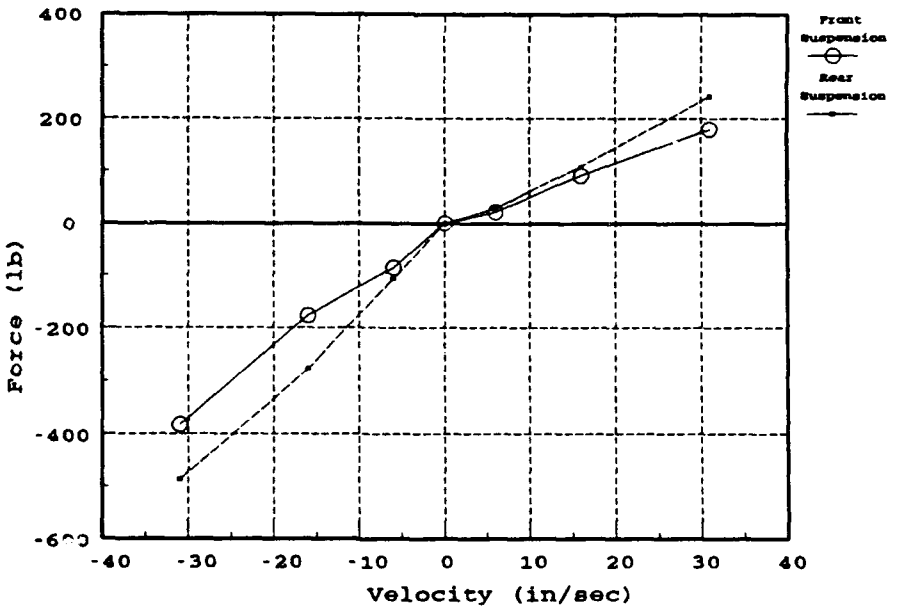

b. Damper force/velocity data

Figure 3.8. VEHDYN spring and damper force curves

3.11 VEHDYN Tire Element

To represent tire dynamics, the tire element in the VEHDYN code uses a continuous ring of radial springs, as shown in Figure 3.6. The VEHDYN tire model was developed through laboratory tests conducted at WES in 1968, (Lessem, 1968). The tire force/deflection data used in the VEHDYN tire model were the same as used in the DADS tire model.

3.12 VEHDYN Road Element

The road element in VEHDYN operates like the DADS road element. The user specifies the ground elevation profile as a function of the longitudinal displacement. The road element determines the current ground elevation by linearly interpolating between the profile points and passes the elevation to the tire model.

CHAPTER 4

FIELD TEST PROGRAM

4.1 Introduction

In most military vehicle missions, long periods of off-road movement are required which expose the vehicle and crew to discrete shock responses and severe vehicle/terrain induced vibrations. The shock level experienced and the energy absorbed by the vehicle system, and particularly by the driver, has a limiting effect on the speed at which a driver will voluntarily operate his vehicle and on the structural life of the vehicle. To determine the effects of non-deformable terrain on a vehicle system and its occupants, standard shock and ride tests have been developed. The standard practice is to conduct shock tests over several different obstacle heights and ride tests on a variety of rough-surface terrains to quantify the effects of suspensions, tire designs and tire inflation pressures. The results of the shock tests are analyzed in a plot of the vehicle's speed which generated 2.5 g's of vertical acceleration on the floorboard under the driver's seat versus the different obstacle hieghts tested on. The ride tests are analyzed in a plot of the vehicle's speed which generated 6 watt vertical absorbed power, AP_{vt}, on the

driver's seat versus the different ride course roughnesses. These 2.5-g level shock and 6 watts AP_{vt} ride curves can then be analyzed to determine the vehicle's performance. From these results, existing vehicle systems can be modified to improve the ride and shock response of the vehicle, which will ultimately extend the structural life of the vehicle system and increase the vehicles' off-road operational speeds.

4.2 Discrete Shock Levels

The ability of a vehicle to negotiate minor discrete obstacles is an important aspect of vehicle ground mobility. Logs, small ditches, boulders, and rice paddy dikes are frequently encountered in off-road travel. These obstacles produce speed-controlling shock loads that depend on the obstacle size, vehicle traction element, and vehicle impact speed. Results of past WES studies (Murphy, 1981) have indicated that obstacle height is a suitable descriptor for characterizing such discrete obstacles. The response criterion currently used as a standard for limiting vehicle speed over obstacles is that speed at which the driver's station vertical acceleration (measured on the floor under the driver's seat) reaches 2.5 g's when the left and right vehicle running gear simultaneously strike an obstacle. The curve of 2.5-g speed versus obstacle height that is developed in this manner was used for predicting driver

tolerance to mechanical shock-limiting speeds over discrete obstacles.

4.3 General Shock Test Procedures

Shock tests are started at speeds slow enough to create low initial g-levels. Test speeds are incrementally increased until g-levels greater than 2.5 g's are measured. The g-levels are measured by an accelerometer on the floorboard under the driver's seat as the vehicle passes over a half round steel obstacle. After the vehicle enters an entrance timing lane (for speed checks), the vehicle speed is maintained as constant as possible until after the vehicle has impacted the obstacle and damped most of the dynamic effects. The peak g-level measured during testing could be generated as the vehicle impacts the obstacle or after the suspension has passed over the obstacle. After the tests are performed, the data are reduced to a g-level speed curve representing the level of g's the driver was experiencing at different vehicle speeds on the tested obstacle height. These test procedures are then repeated for each obstacle height selected. The results are finalized in the form of speed versus obstacle height at 2.5 g's. (For each vehicle configuration tested.)

4.4 Quantifying Terrains

To best quantify the surface roughness of random terrain, a roughness index was adopted by WES in 1968 which effectively represents the surface roughness of a terrain in terms of an rms elevation (inches) after the raw terrain survey profile has been passed through a specific filter (Van Deusen, 1965). The rms elevation has been related to human tolerance to continuous vibration in terms of AP_{vt}.

4.5 Absorbed Power

Ride quality over off-road terrain is presently quantified by AP_{vt} at the driver's seat and is used as a basis for assessing the speeds at which a driver will operate a vehicle. Six watts of AP_{vt} was established as a reasonable standard human tolerance limit when vibration was in the vertical direction only (Pradko, 1966). While results of field tests indicate that a driver will often subject himself to 10-15 watts of AP_{vt} or more for short periods of time (Murphy, 1981), he will not normally subject himself to more than 6 watts of AP_{vt} for prolonged periods. WES tests with numerous wheeled and tracked vehicles indicate that the AP_{vt} at the driver's seat best agrees with the driver's opinion of ride quality and generally appears to be the most critical factor in determining ride quality performance. Six watts of AP_{vt} at the driver's seat is the measurement of ride quality presently used in assigning

speeds at which a driver will operate a vehicle for long periods of time. The relation of vehicle speed at 6 watts AP_{vt} versus rms surface elevation roughness is the standard performance relation used for predicting vehicle speed over continuous terrain.

4.6 Ride Dynamics Test Procedures

Ride dynamics test are started at a slow speed, usually 5 mph, with increasing speeds as the testing continues. Ride dynamics data collection in the form of vertical accelerations is started after the vehicle enters the test course at a constant test speed. The test courses are constructed of several inches of small well-graded gravel to reduce course deformation. The courses are also constructed to present a two-dimension, height and length, terrain profile so both left and right vehicle suspensions experience the same change in surface elevation as they traverse the test course. This is done to isolate the pitch and vertical vehicle displacements and simplify the dynamic analysis. Once the test has started, the driver must maintain as constant a speed as possible throughout the length of the test course. The tests are conducted in both directions over the test lane to eliminate directional effects in the course. On occasion, a directional ride course is encountered which allows the vehicle to traverse in one direction at a measured AP_{vt} and then traverse the

same course in the opposite direction at a different AP_{vt}. After the tests are performed the data are reduced to a ride course speed curve which indicates the amount of AP_{vt} the driver is experiencing at the different vehicle speeds tested on the given rms ride course. Testing continues until a speed is reached which generates approximately 12-watts of AP_{vt} on the driver's seat or the vehicle is able to operate at its maximum safe velocity over the test course without generating 12 watts of AP_{vt}. These test procedures are repeated for each ride course selected, and the results finalized in the form of a speed versus rms elevation at 6 watt AP_{vt}.

4.7 Test Vehicle

The M998 HMMWV Utility Truck, presented in Figure 3.1, was used for dynamics testing by WES. The vehicle was tested in an empty configuration. The M998 HMMWV is currently deployed with standard Goodyear Wrangler R/T II, 36X12.50-16.5LT bias ply tires which were used in WES dynamics testing. During ride dynamics and shock response testing the bias ply tires were operated at the vehicle manufacturer's suggested tire inflation pressures of 20 psi in the front tires and 30 psi in the rear tires.

4.8 Vehicle Instrumentation and Data Collection

The M998 HMMWV was instrumented for dynamics tests with accelerometers at thirteen points-of-interest and one pitch rate transducer (Jones, 1992). These instrumented locations were selected to determine the resultant effects of the terrain on the dynamics of the vehicle. Also, 5 of the 14 locations were selected due to past structural failures of components on the vehicle. Of these 14 locations, 4 were selected for further model validation analysis. These locations are presented in Figure 4.1 and represent points-of-interest on the front left suspension, driver's seat, floorboard under the driver's seat, and center of cargo.

The accelerometers used during testing were selected with a range of operation to capture the induced vertical accelerations at the various locations. The design of the accelerometers was such that a zero decibel (db) offset could be expected for frequencies up to 1000 hertz (Hz). The natural resonant frequency of the accelerometers was 4700 Hz. The calibration range of each accelerometer was selected based upon the expected vertical acceleration level at each location. The pitch rate transducer had an operational range of 100 degrees per sec and was located at the center of cargo.

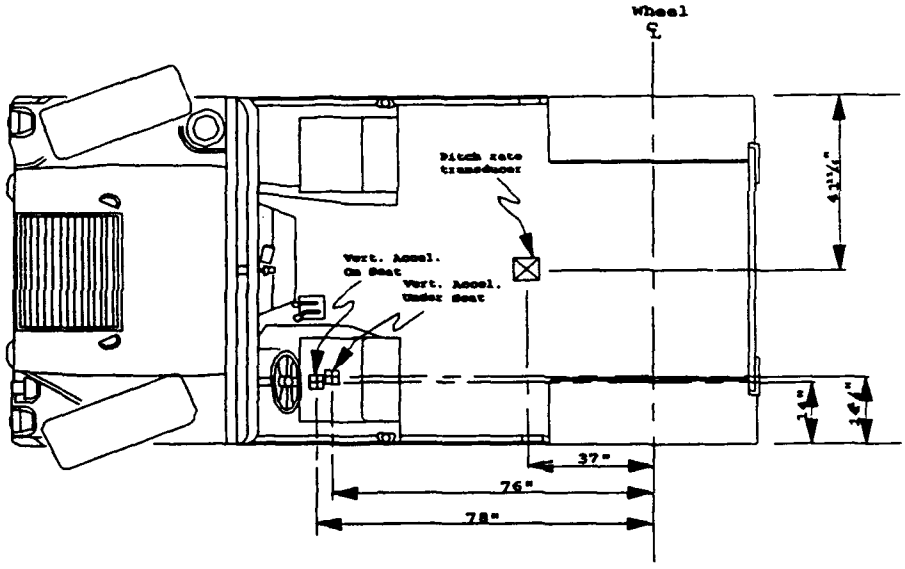

a. Location of instrumentation on vehicle chassis

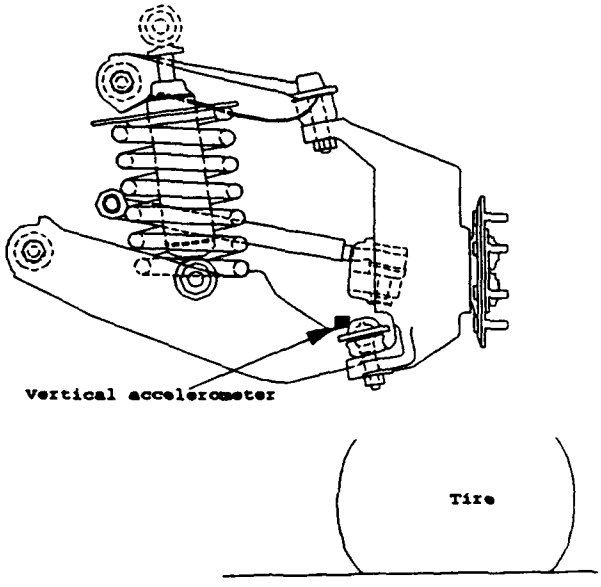

b. Location of instrumentation on front left suspension

Figure 4.1. Location of instrumentation

During dynamics testing the accelerometer and pitch rate data were transferred from the instrumented vehicle to a data collection van via a telemetry system. The telemetry system in the instrumentation van was the front end to a 400 Hz analog discriminator system which separated each data channel and passed the data to a 21 track analog tape recorder. After completion of the dynamics testing the analog data were passed to a 500-samples-per-second-per-channel analog-to-digital sampling board housed in an IBM PC. After digital transformation of the analog data, ASCII data files were created for data storage.

4.9 Field Test Data

To obtain a clear understanding of the dynamic range of the M998 HMMWV during operational scenarios, the field test program involved a total of 1040 dynamics tests. These tests were conducted with the HMMWV in several different vehicle configurations: empty and loaded, without and with a towed trailer, and using bias ply and radial tires and while operating at several different tire inflation pressures. From these tests, 10 shock tests and 16 ride tests were selected to represent the M998 HMMWV's range of dynamic responses when operating empty without a towed trailer and using bias ply tires. This M998 HMMWV configuration was selected because it was the most commonly deployed configuration in the US Army at the time of testing. As

indicated by the test numbers used in Chapter 5 to represent each dynamics test, the 26 field tests chosen to validate the dynamic models were conducted at the middle and latter stages of the M998 test program. The field test data were in the form of digital vertical accelerations and pitch rate time histories. These data were to be used for AP_{vt} calculations and peak g-analysis. The peak g's and pitch rates, either positive or negative, measured by the accelerometers and pitch rate transducer on the vehicle for each shock test were reported after filtering the test data through a low pass 50 Hz digital Butterworth filter. The vertical acceleration time histories for ride tests were also filtered using a low pass digital filter at 50 Hz prior to calculating AP_{vt}.

CHAPTER 5

MODEL VALIDATION

5.1 Methods of Data Analysis

Several different data analysis techniques were employed to ana`vze the field test results and model predictions. These techniques evolved from the basic premise that all results must be analyzed using the same processes. To accomplish this, several FORTRAN computer code routines were written and structured to accommodate the different data bases.

As mentioned in Section 4.6, the direction in which the vehicle traverses over the ride course can be critical to the resultant AP_{vt}. Therefore, the direction the vehicle traversed the ride course determined how the profile was entered into the simulation.

5.1.1 Data Filtering Technique

Typical analog data filtering is accomplished through the electronic implementation of a lowpass four-pole Butterworth filter. The formula for the theoretical frequency response is shown by equation 5.1. The *db* is a

standard unit in electronics for expressing transmission gain or loss and relative levels among power, voltage, and current. Equation 5.1 shows that regardless of the number of poles, $db = 3.01$ when f is equal to f_c, which is characteristic of all Butterworth filters. As K increases, the filter approaches the ideal lowpass response.

$$db = 10 \log \left[1+\left(\frac{f}{f_c}\right)^{2K}\right] \qquad (5.1)$$

where

f = Any arbitrary frequency

f_c = Cutoff frequency

K = Number of poles

db = Decibel

However, practical difficulties make such a filter hard to construct. Theoretically, if a sinusoidal wave form is passed through a filter with a K value of 4 and $db = 3.01$, the resultant output wave form would contain 70 percent of the original amplitude at the cutoff frequency. Therefore, the cutoff frequency chosen for filtering vehicle shock and ride accelerations was 50 Hz. Based on experience (Murphy 1981), this frequency is believed to be a sufficient cutoff for passing the relevant signals and filtering out irrelevant noise.

In order to perform the same functions with a digital computer on the digitized field data and model predictions,

a lowpass four-pole Butterworth filter was programmed using the FORTRAN assembly language. The program followed the same computational methods as presented by Stearns (1975).

5.1.2 Absorbed Power Calculations

Vertical absorbed power, with units of watts, is used to determine human tolerance to vibration of a vehicle as it negotiates rough terrain and is the measure of the rate at which vibrational energy is absorbed by a human. Average absorbed power is calculated from the product of the force and velocity vectors experienced by the driver during a given time interval as shown in equation 5.2.

$$P = \lim_{T \to \infty} \frac{1}{T} \int_0^T F(t)\, V(t)\ dt \qquad (5.2)$$

where

P = Average absorbed power

$F(t)$ = Force on subject

$V(t)$ = Velocity of subject

T = Time interval

Pradko, Lee and Kaluza, (1966) established the relationships between human fatigue and vertical absorbed power and developed a distinct relation between absorbed power and acceleration which does not depend explicitly on the force-velocity product. The absorbed power-acceleration relation is concerned with the acceleration-frequency

relation and the fact that, at a given frequency, absorbed power varies directly as the square of the input rms acceleration. Equation 5.3 is the result of the absorbed power-acceleration relationship, where K relates a gain factor to the magnitude and phase of the individual's effective mass.

$$P = \sum_{i=0}^{N} K_{iv} A_i^2 \qquad (5.3)$$

where

P = Average absorbed power

K_{iv} = Gain factor in vertical direction

A = Rms acceleration

N = Total number of samples

It has been shown from these human response studies that the most sensitive range for whole-body vibrations is at the low frequencies from approximately 0.5 to about 10 Hz. Values of K have been determined for those frequencies at which humans are most susceptible (Lins, 1972).

To compute the acceleration rms of the continuous analog signal, an exponentially weighted rms acceleration circuit is used, as represented by equation 5.4.

$$[f_\lambda(t)]^2 = \sqrt{\lambda \int_{-\infty}^{t} [f(\beta)]^2 \, e^{-\lambda(t-\beta)} d\beta} \qquad (5.4)$$

where

$[f_\lambda(t)]^2$ = rms of the acceleration time history

λ = 1/RC, the reciprocal of the time constant

RC = Product of the resultant resistance and capacitance elements in the circuit

$[f(\beta)]^2$ = Acceleration time history squared

β = Variable of integration

To calculate digitally the AP_{vt}, frequencies of the accelerations experienced by the driver had to be determined, then equation 5.3 could be used to calculate the resultant average absorbed power. A FORTRAN program was written which used a Cooley-Tukey Fast Fourier Transformation, FFT, (Stearns, 1975) to calculate the frequency response and associated amplitudes of the vehicle's vertical accelerations from the field tests and model predictions. Since the FFT transforms a complex waveform into discrete sine and cosine frequencies and amplitudes, the rms acceleration of the FFT is equal to the product of a sine or cosine rms with an amplitude of 1.0 and the amplitudes of the FFT. Equation 5.5 illustrates a sine wave rms with an amplitude of 1.0. Using this method, the rms of the amplitudes of each FFT frequency can be

calculated. By employing equation 5.3, the resultant average absorbed power can be determined.

$$Y = d \sin 2\pi t$$

$$let\ d = 1.0$$

$$let\ t = 0.1, 0.2, 0.3, \ldots, 1$$

$$rms\ Y = \sqrt{\sum \frac{Y^2}{N}}$$

$$Y^2 = 5.0$$

$$N = 10.0$$

$$\therefore\ rms\ Y = 0.7071 \qquad (5.5)$$

5.1.3 Peak Acceleration

A method was adopted to determine peak acceleration for the digital data by searching the time history arrays for the largest acceleration value. For model validation it was important to know in which direction, positive or negative, the event occurred. Therefore, the associated signs of the peak accelerations were reported.

5.2 Discrete Obstacle Simulations

The first step taken in determining the accuracy of each model prediction was to obtain a general feel for the systems response to simplistic inputs. This was accomplished through the comparison of the measured vertical

accelerometer and pitch rate time histories and the model predictions. The controlling frequencies during obstacle testing were determined from FFT's of the measured tests and model simulations. The rms of each associated pitch rate time history was calculated and plotted. Finally, to determine if the model predictions could be used for predicting peak vertical accelerations, the model simulations and measured tests were compared in a 2.5-g level response curve. The magnitude of the differences between the predicted and measured data were determined by plotting the predicted versus measured peak g-values. This plot clearly indicated the general direction and magnitude of differences.

5.2.1 Time History Analysis

The following time history analysis was performed using the three points on the vehicle previously discussed.

5.2.1.1 DADS Results

As shown in Figure 5.1, the DADS predicted vertical acceleration time history of the point on the floorboard under the driver's seat closely matched that from a similar measured test. The bump event can been seen by the sudden positive acceleration that occurred at approximately 0.5 sec and again at 1.25 sec. These two positive peaks occurred as the front and rear suspensions passed over the bump. The

negative peaks were caused by the rebound of the chassis after each suspension passed over the obstacle.

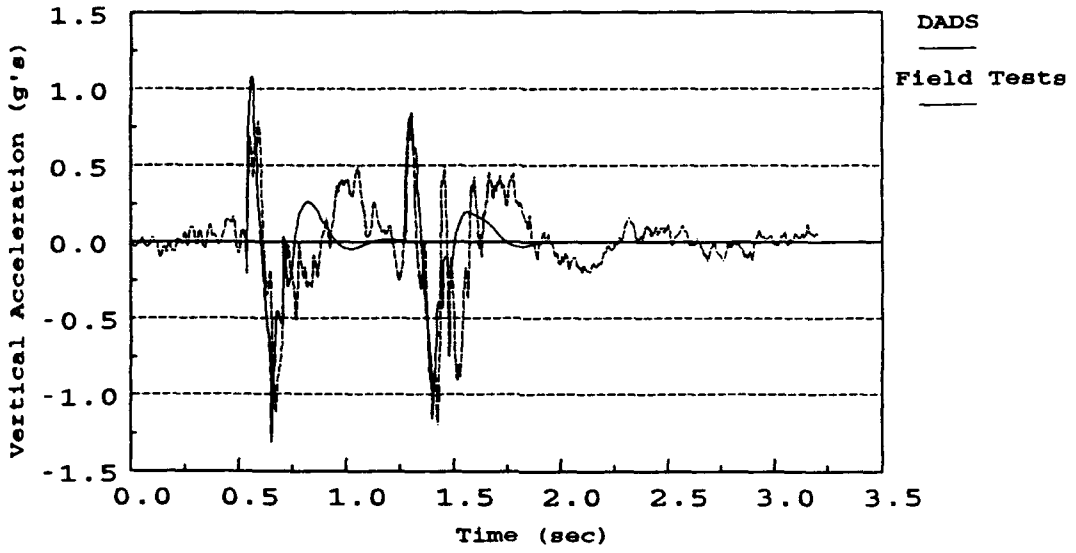

Figure 5.1. Vertical acceleration time history of point under driver's seat as vehicle passed over a 4-in. high half-round obstacle at 10 mph

Figures 5.2 and 5.3 are similar time history plots of the vehicle passing over different obstacle heights.

As shown in Figure 5.2, the DADS simulated vertical acceleration trace was a very close match to the measured test. The difference between the DADS simulation and measured result was the absence of higher frequency responses in the simulation. However, as shown in Figure 5.3, the rigid model was able to reproduce the oscillations of the suspension as it moved through the jounce and rebound positions at 1.3 and 1.8 sec.

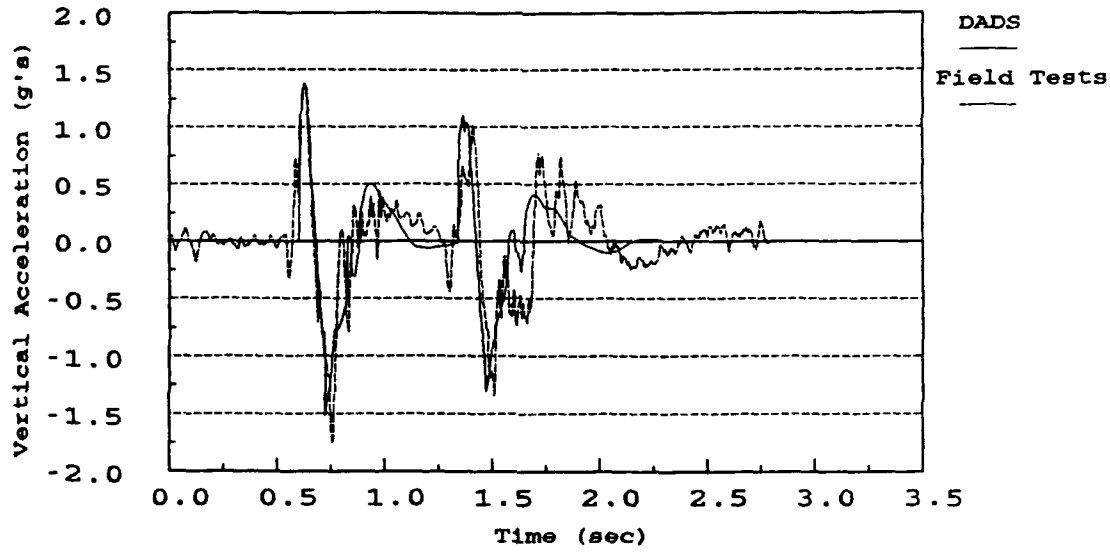

Figure 5.2. Vertical acceleration time history of point under driver's seat as vehicle passed over a 6-in. high half-round obstacle at 10 mph

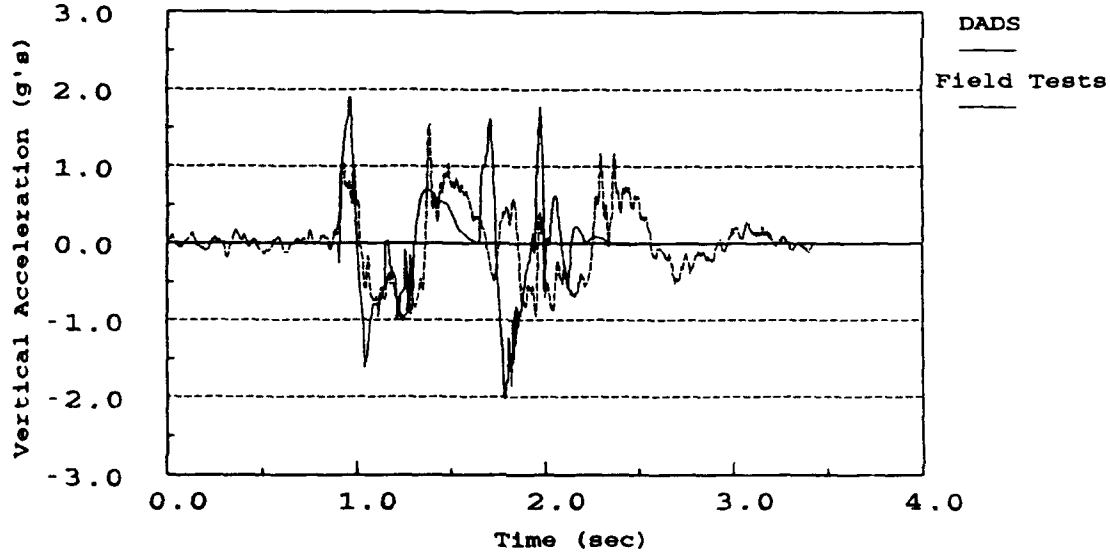

Figure 5.3. Vertical acceleration time history of point under driver's seat as vehicle passed over a 8-in. high half-round obstacle at 10 mph

These higher frequency responses were reproduced by the imposed bump stops in the suspension's force/displacement curves. Although the DADS simulated time history in Figure 5.3 was slightly higher at the peaks, it followed the same pattern as that of the measured test. The simulation in Figure 5.3 shows the front suspension impacting the obstacle at the same time as the measured. However, the predicted rear suspension impacts the obstacle before the measured. This can be seen by the time difference between the third positive acceleration peaks in the simulated and measured results. The simulated rear suspension impact event occurred at 1.6 sec and the measured event occurred at 1.7 sec. This was caused by the velocity controller in the DADS model. Although it was able to closely approximate the velocity traces of the measured tests on the smaller obstacles, there were slight speed variations between the measured and predicted during higher obstacle simulations. These speed differences contribute to the discrepancies between the predicted and measured results.

Figure 5.4 shows the vertical acceleration traces of the front left suspension for the DADS simulation and associated measured test. Although the peaks of the positive and negative accelerations were much greater for the simulation, both traces follow a very similar pattern. The DADS simulations in Figures 5.5 and 5.6 did not reproduce the higher frequency responses. But the simulations did follow the general trends of the measured tests.

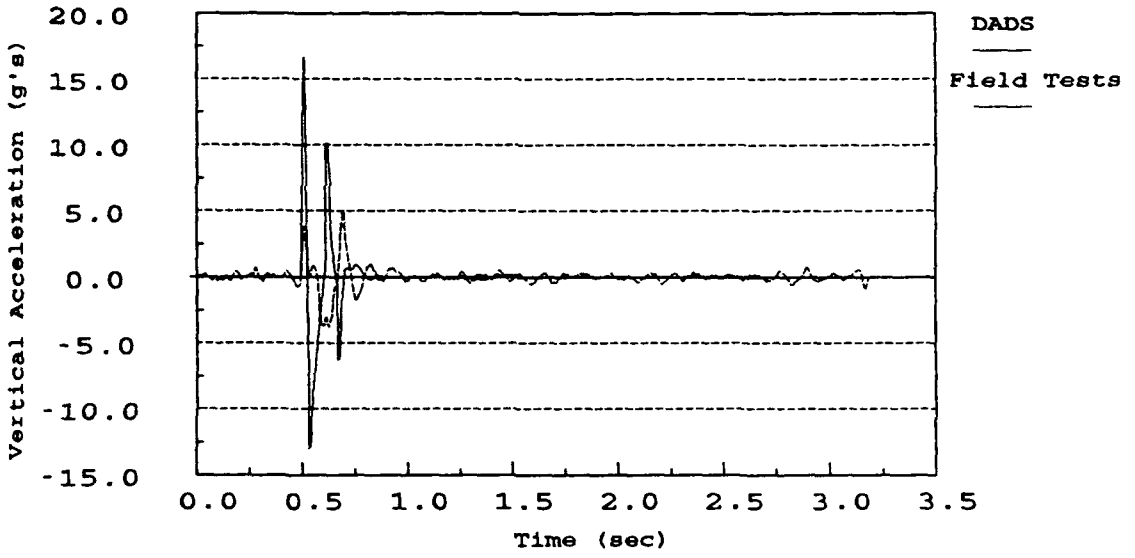

Figure 5.4. Vertical acceleration time history of point on the front left suspension as vehicle passed over a 4-in. high half-round obstacle at 10 mph

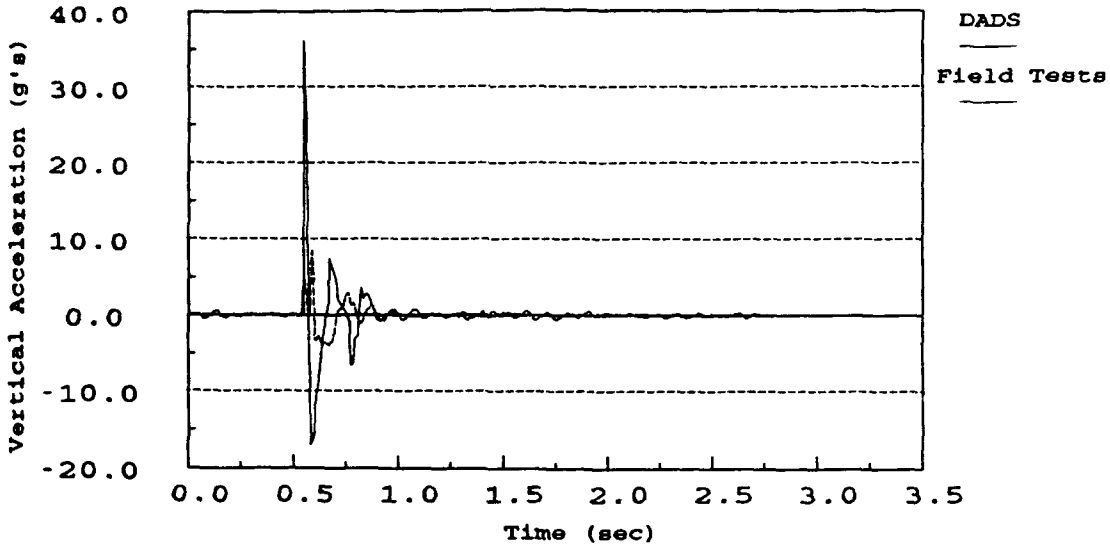

Figure 5.5. Vertical acceleration time history of point on the front left suspension as vehicle passed over a 6-in. high half-round obstacle at 10 mph

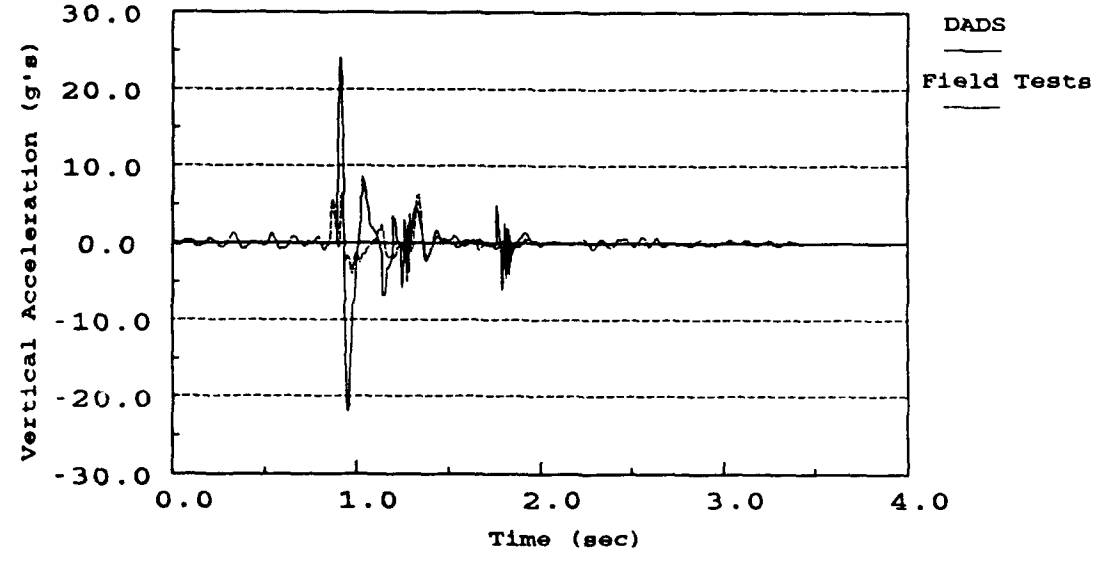

Figure 5.6. Vertical acceleration time history of point on the front left suspension as vehicle passed over a 8-in. high half-round obstacle at 10 mph

Figures 5.7 through 5.9 show the time histories of the vehicle's pitch rate as it passed over the different obstacle heights. As seen in Figure 5.7, the two traces followed the same trends, but the DADS simulation damped the vehicle quicker. However, in Figure 5.8, other than a slightly higher initial pitch rate, and a faster damped effect after the obstacle event, the DADS simulation was very successful in reproducing the measured pitch rate time history.

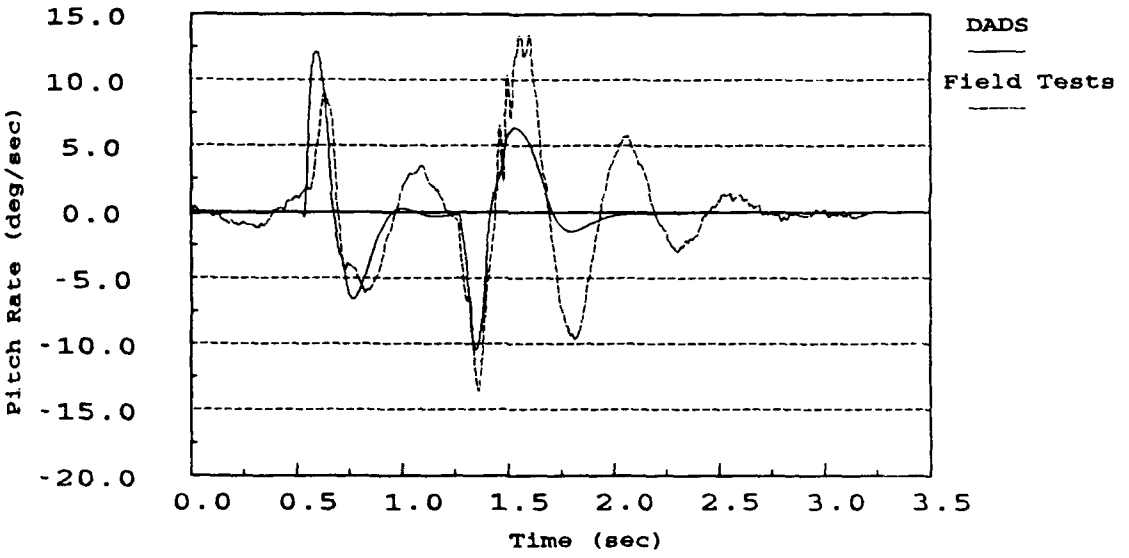

Figure 5.7. Pitch rate time history as vehicle passed over a 4-in. high half-round obstacle at 10 mph

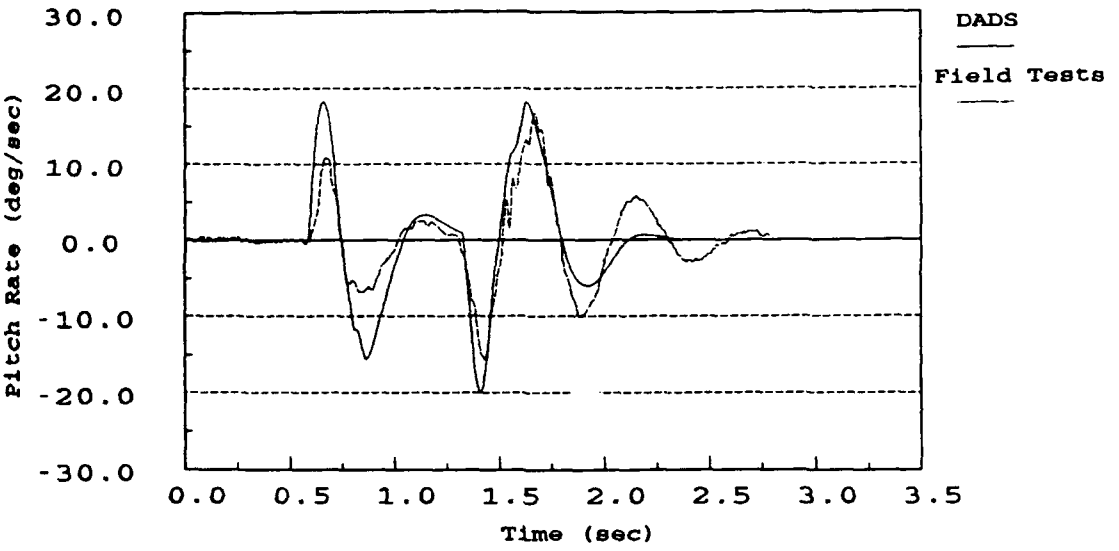

Figure 5.8. Pitch rate time history as vehicle passed over a 6-in. high half-round obstacle at 10 mph

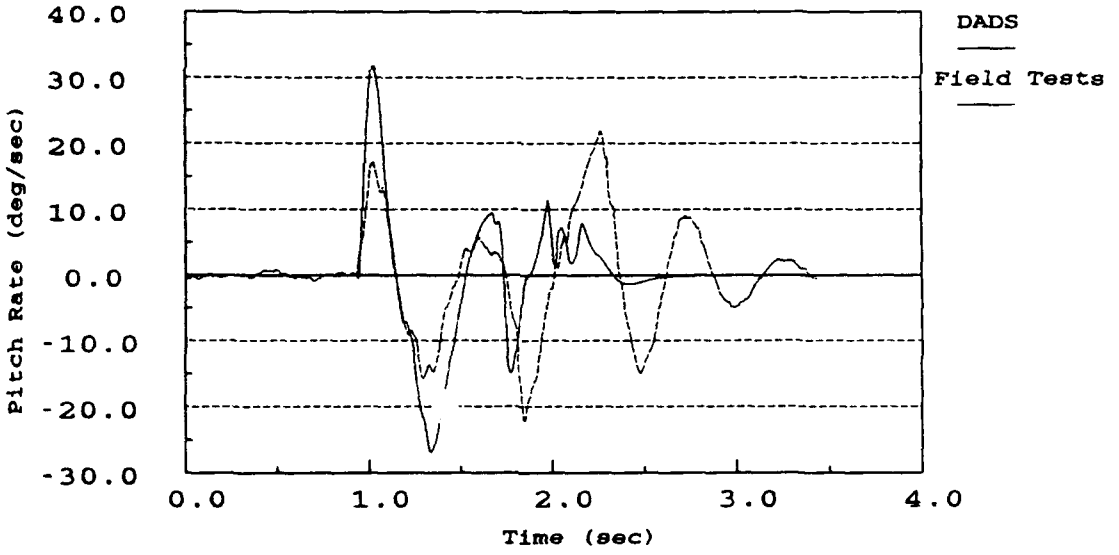

Figure 5.9. Pitch rate time history as vehicle passed over a 8-in. high half-round obstacle at 10 mph

In Figure 5.9 the DADS simulated time trace followed the measured results until the rear suspension impacted the obstacle, close to the 1.7 sec mark. The rear suspension's impact can also be seen in Figure 5.3. In the simulation, the rear suspension's impact effected the pitch rate and caused the vehicle's pitch to oscillate slightly and dampen much sooner than what occurred in the measured test.

5.2.1.2 VEHDYN Results

Figures 5.10 through 5.12 are time histories of the vertical acceleration of the point under the driver's seat from the VEHDYN predictions and corresponding measured tests. Figures 5.10 and 5.11 show the VEHDYN predictions closely matched the measured tests. The predicted positive and negative peaks occurred at the proper time and the traces followed the same trends as seen in the measured tests.

Figure 5.12 shows that the VEHDYN prediction had the general shape of the associated field test, but as with the DADS prediction, it showed a time shift for the rear suspension's impact, and did not accurately reproduce the positive peaks. As shown, the simulation's rear suspension impacted the bump slightly sooner. The time shift can be attributed to the constant velocity driver used in the VEHDYN model, and was a contributing factor to the variance between the predicted and measured results.

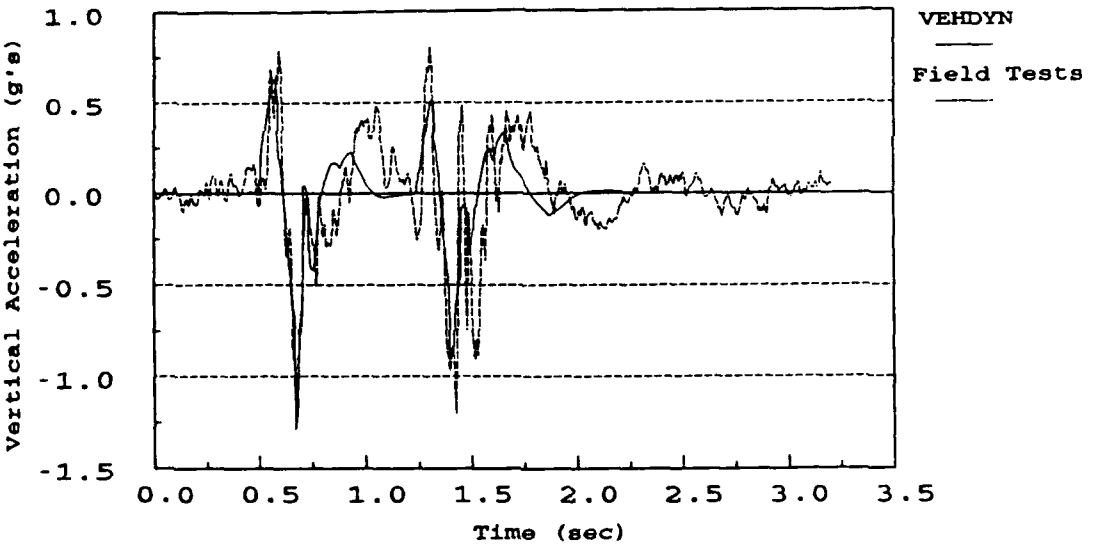

Figure 5.10. Vertical acceleration time history of point under driver's seat as vehicle passed over a 4-in. high half-round obstacle at 10 mph

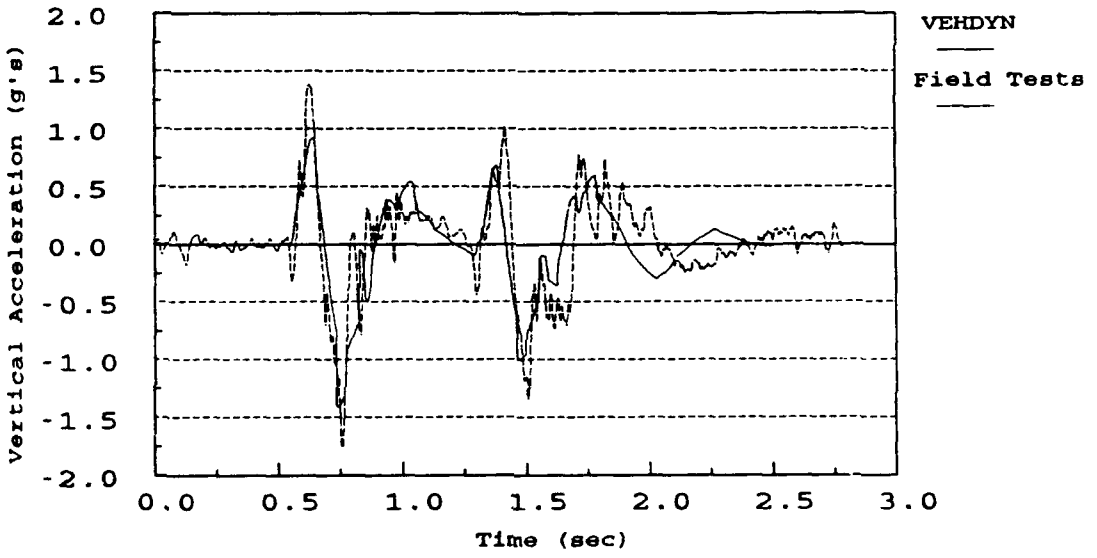

Figure 5.11. Vertical acceleration time history of point under driver's seat as vehicle passed over a 6-in. high half-round obstacle at 10 mph

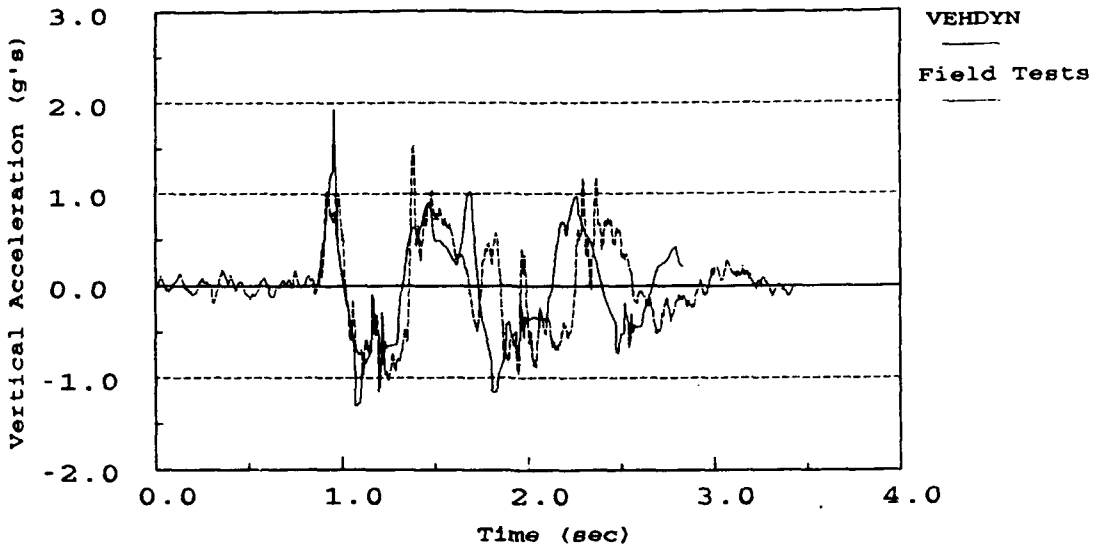

Figure 5.12. Vertical acceleration time history of point under driver's seat as vehicle passed over a 8-in. high half-round obstacle at 10 mph

Figures 5.13 through 5.15 present the vertical acceleration time histories of the point on the front left suspension from the measured tests and the front suspension from the VEHDYN predictions. In Figures 5.13 through 5.15, the simulations produced higher amplitudes but closely matched the trends. In Figure 5.14, the simulation was able to recreate the same frequency responses as the measured results.

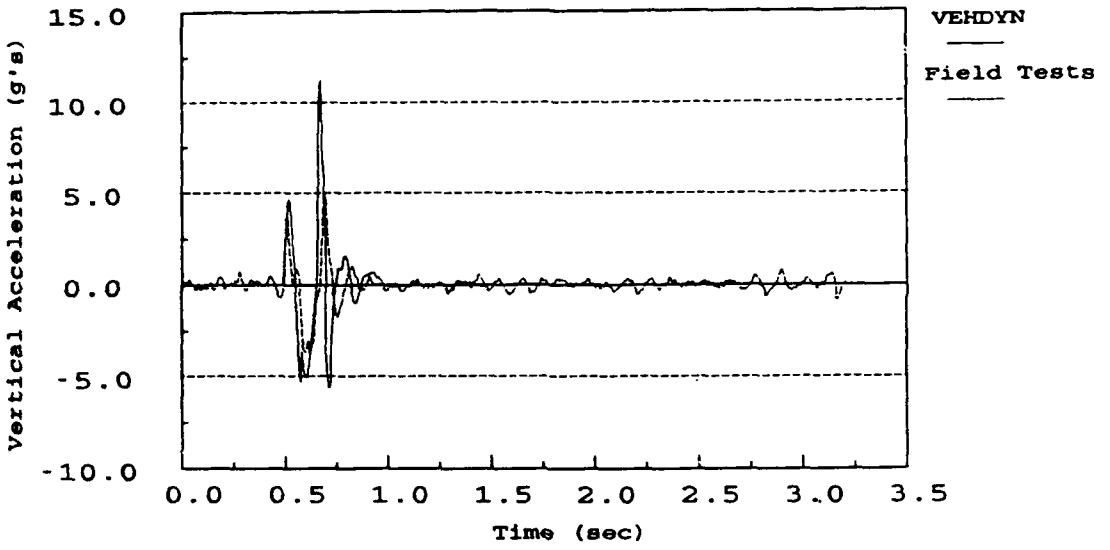

Figure 5.13. Vertical acceleration time history of point on the front left suspension as vehicle passed over a 4-in. high half-round obstacle at 10 mph

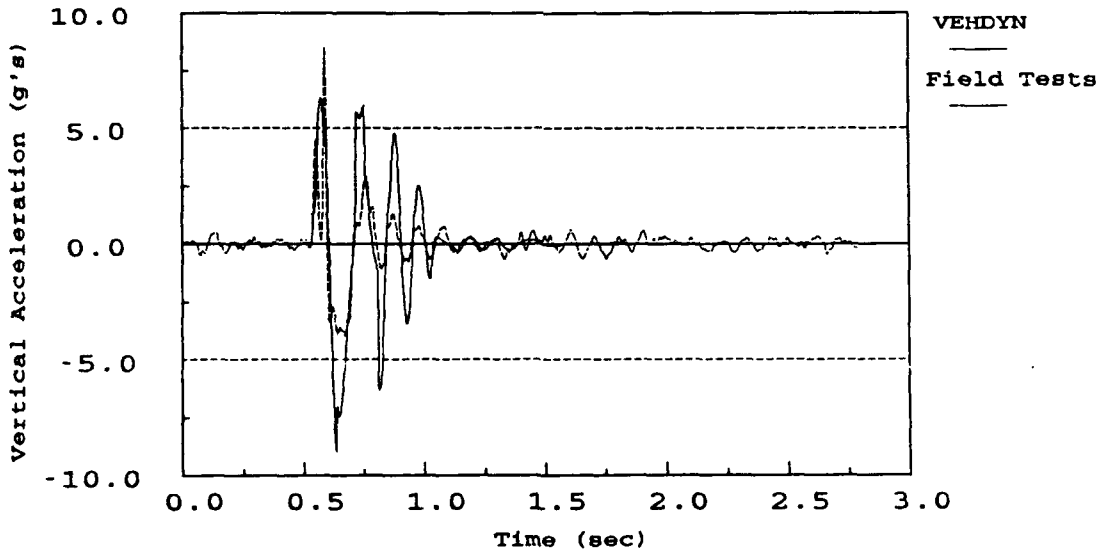

Figure 5.14. Vertical acceleration time history of point on the front left suspension as vehicle passed over a 6-in. high half-round obstacle at 10 mph

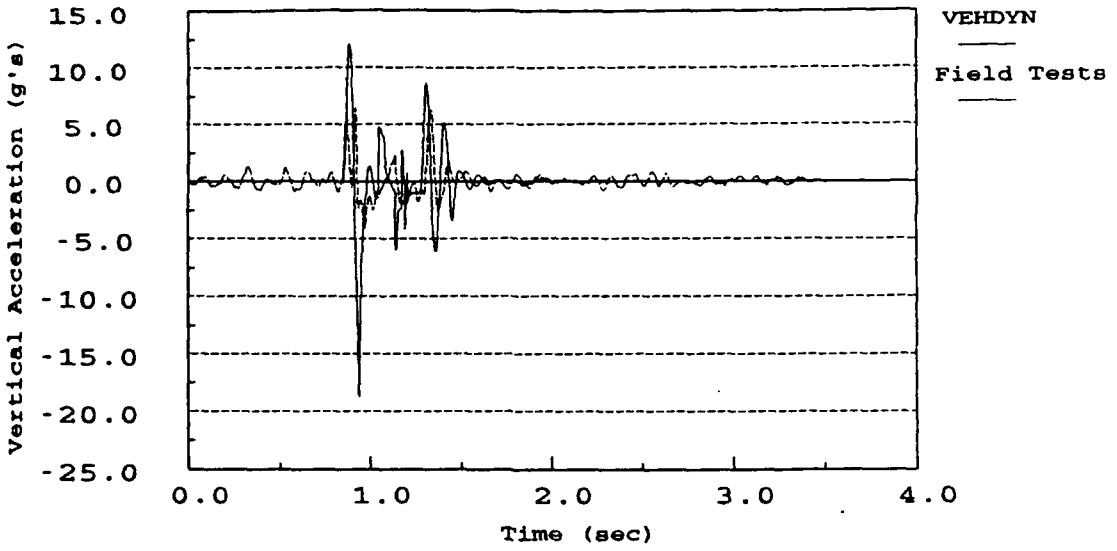

Figure 5.15. Vertical acceleration time history of point on the front left suspension as vehicle passed over a 8-in. high half-round obstacle at 10 mph

Figures 5.16 through 5.18 present the time histories of the vehicle's pitch rate as it passed over the different obstacle heights. The results in Figure 5.16 produced a close correlation between the predicted and measured, but the simulated time trace appeared to follow the same trend seen in the DADS prediction. The predicted pitch rate was damped quicker than the measured test at the 1.0 and 2.0 sec marks. In Figure 5.17 and 5.18, the VEHDYN predictions closely followed the measured trends, but consistently predicted higher amplitudes.

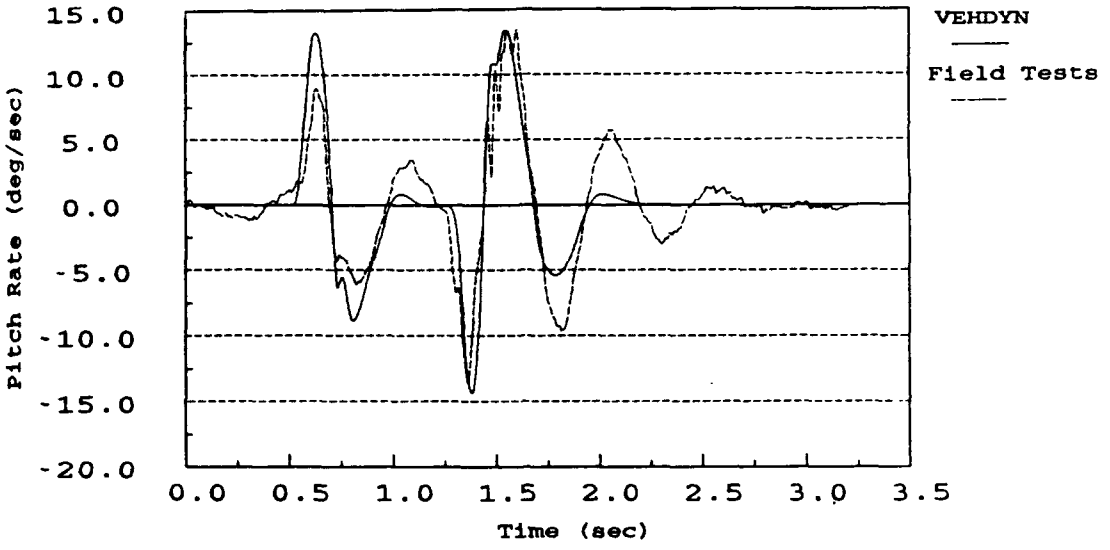

Figure 5.16. Pitch rate time history as vehicle passed over a 4-in. high half-round obstacle at 10 mph

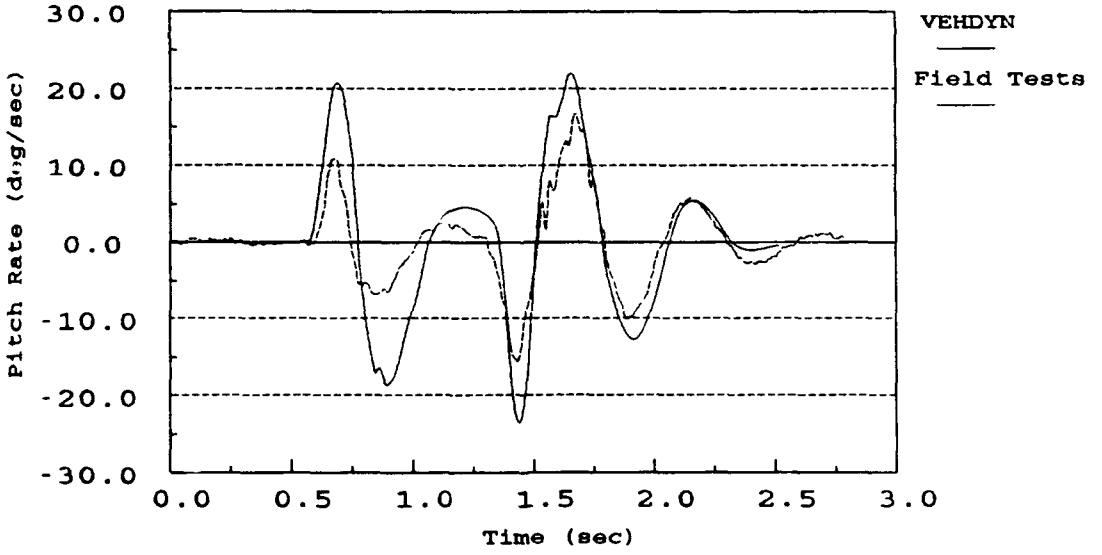

Figure 5.17. Pitch rate time history as vehicle passed over a 6-in. high half-round obstacle at 10 mph

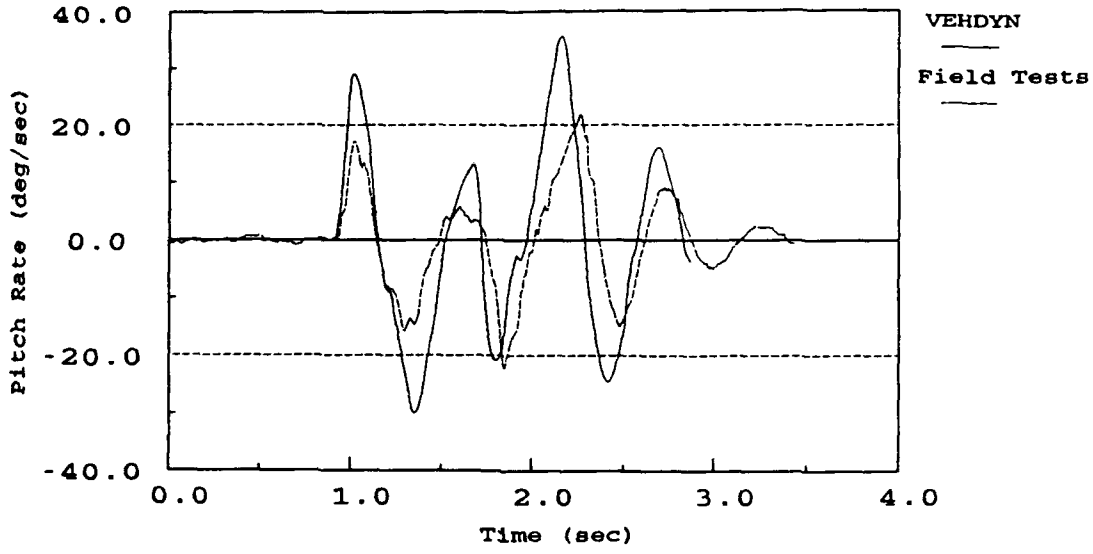

Figure 5.18. Pitch rate time history as vehicle passed over a 8-in. high half-round obstacle at 10 mph

5.2.2 FFT Analysis

5.2.2.1 DADS Results

As seen in Figure 5.1 and 5.2, the DADS predictions of the vertical acceleration time history from the point on the floorboard under the driver's seat produced good correlations to the measured tests. The correlation is also evident in the FFT of the data, as shown in Figures 5.19 and 5.20. Although the FFT's of the measured tests generally had slightly higher amplitudes, it was evident that the predictions reasonably followed the measured frequency trends.

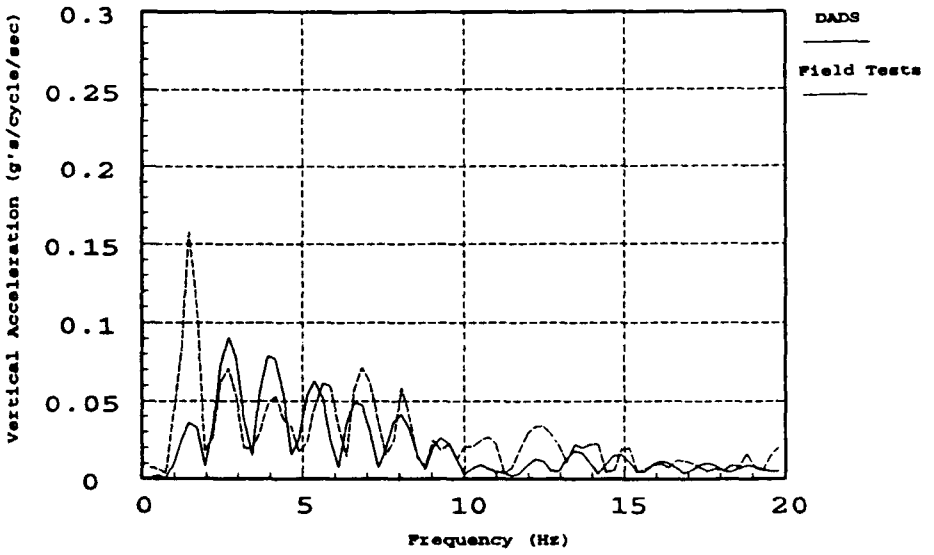

Figure 5.19. FFT of vertical acceleration of point on floorboard under the driver's seat as vehicle passed over a 4-in. half-round obstacle at 10 mph

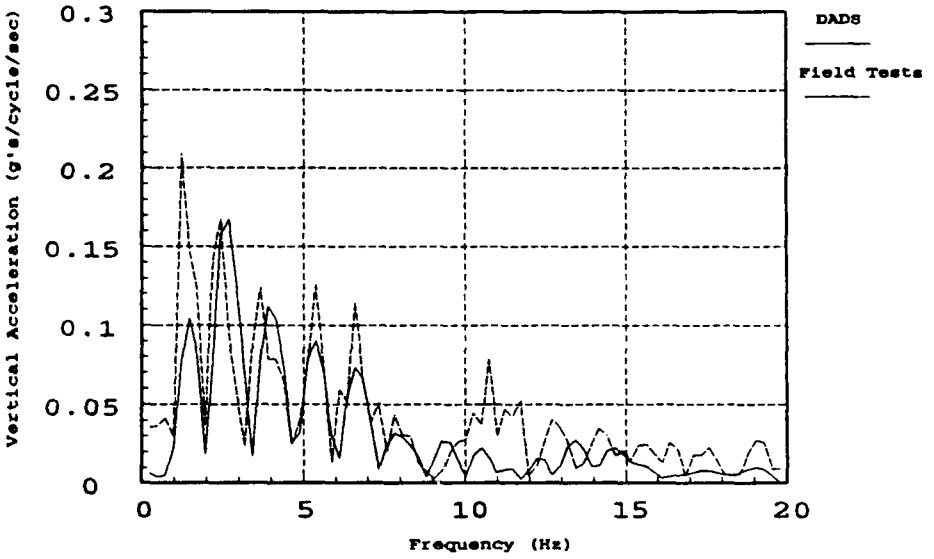

Figure 5.20. FFT of vertical acceleration of point on floorboard under the driver's seat as vehicle passed over a 6-in. half-round obstacle at 10 mph

The same correlation seen in Figure 5.3 was also evident in Figure 5.21. Where the field results produced a higher amplitude for the lowest frequency in Figure 5.21, the DADS prediction produced higher amplitudes for the remaining frequency distribution.

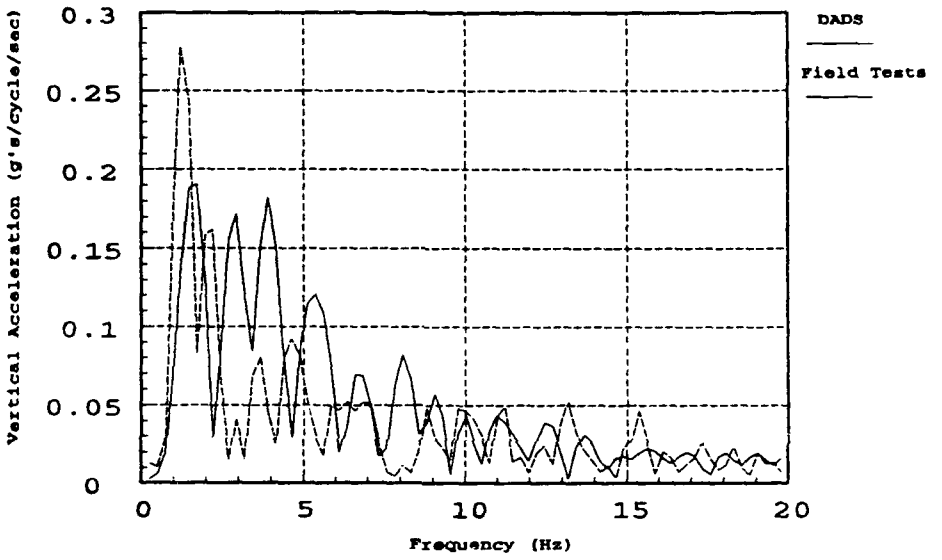

Figure 5.21. FFT of vertical acceleration of point on floorboard under the driver's seat as vehicle passed over a 8-in. half-round obstacle at 10 mph

Figures 5.22 through 5.24 present the FFT's of the suspension's vertical acceleration time history data. Similar trends, as seen in Figures 5.4 through 5.6, were seen in their FFT's. Figures 5.22 through 5.24 revealed parallel frequency trends between the measured and predicted data, but the amplitudes of the DADS predictions were higher than the measured tests.

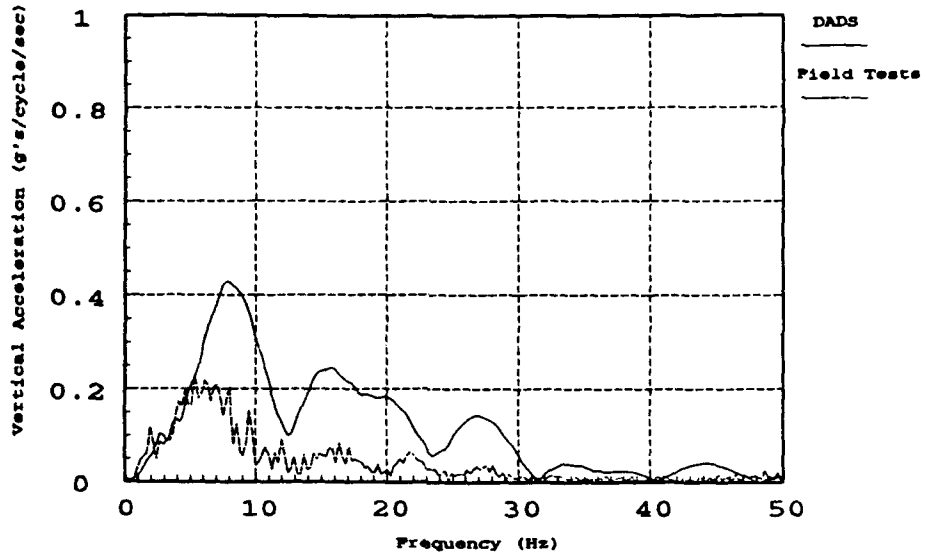

Figure 5.22. FFT of vertical acceleration of point on front left suspension as vehicle passed over a 4-in. half-round obstacle at 10 mph

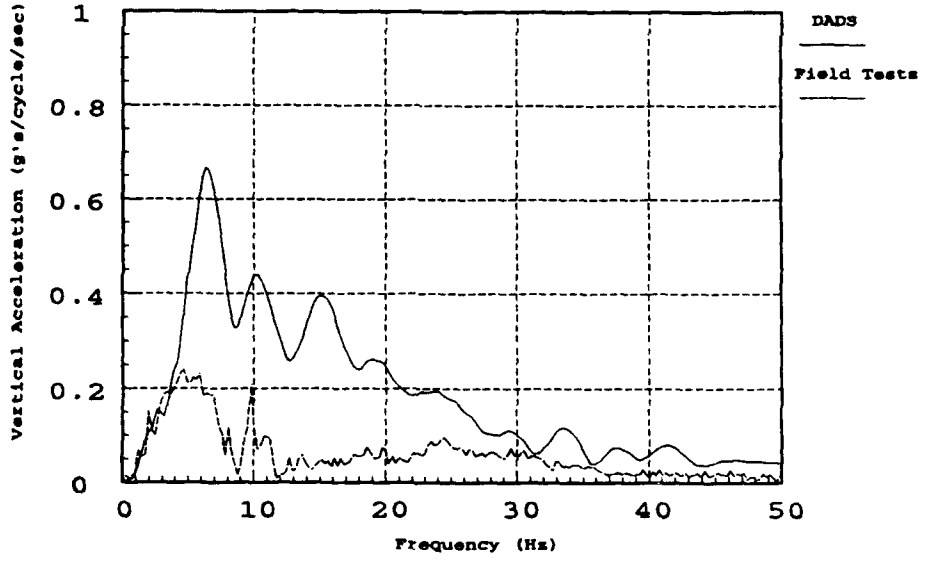

Figure 5.23. FFT of vertical acceleration of point on front left suspension as vehicle passed over a 6-in. half-round obstacle at 10 mph

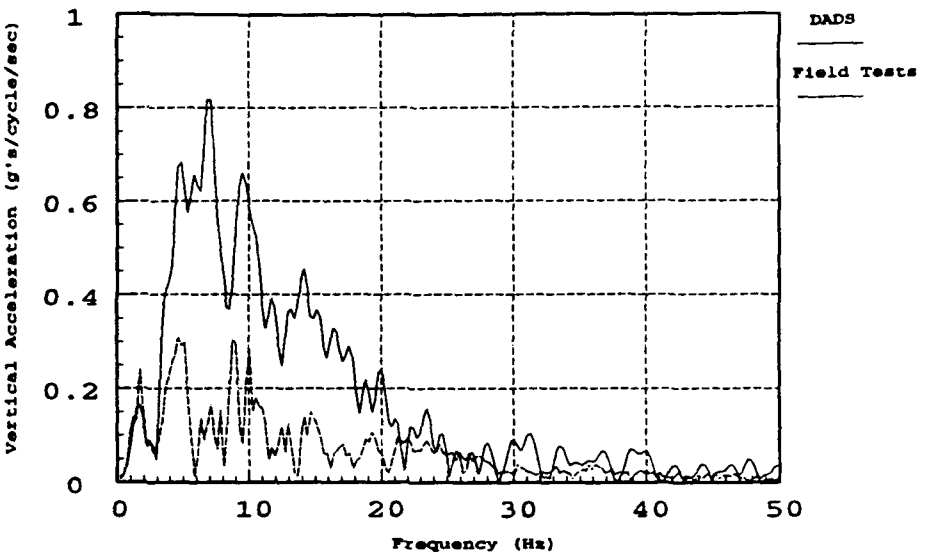

Figure 5.24. FFT of vertical acceleration of point on front left suspension as vehicle passed over a 8-in. half-round obstacle at 10 mph

5.2.2.2 VEHDYN Results

VEHDYN was able to reproduce the trend of the frequency distributions, but like DADS was unable to match the amplitudes of the measured responses. The predicted amplitudes were generally higher. As seen in Figures 5.10 through 5.12, the VEHDYN predictions of the vertical acceleration time histories from the point on the floorboard under the driver's seat produced good correlations with the measured tests. The correlations were evident in the frequency distributions shown in Figure 5.25 through 5.27.

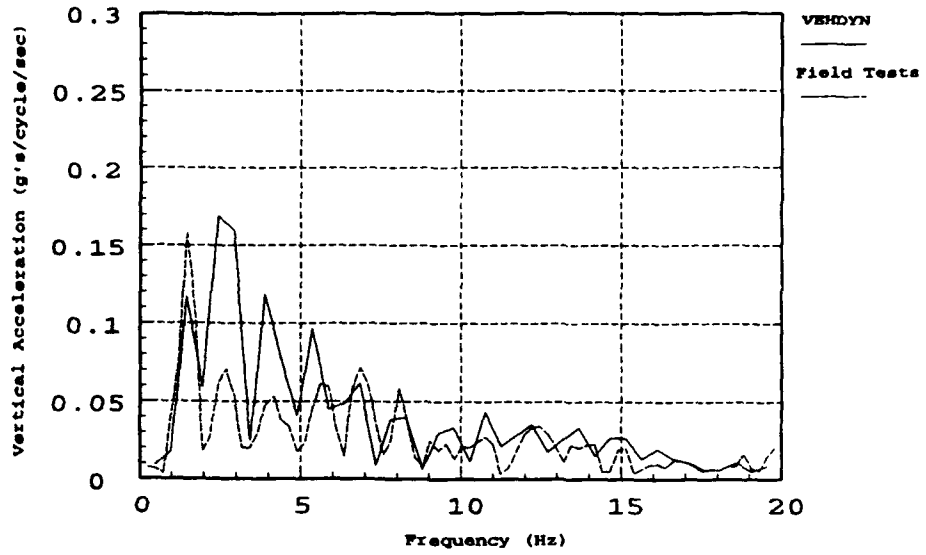

Figure 5.25. FFT of vertical acceleration of point on floorboard under the driver's seat as vehicle passed over a 4-in. half-round obstacle at 10 mph

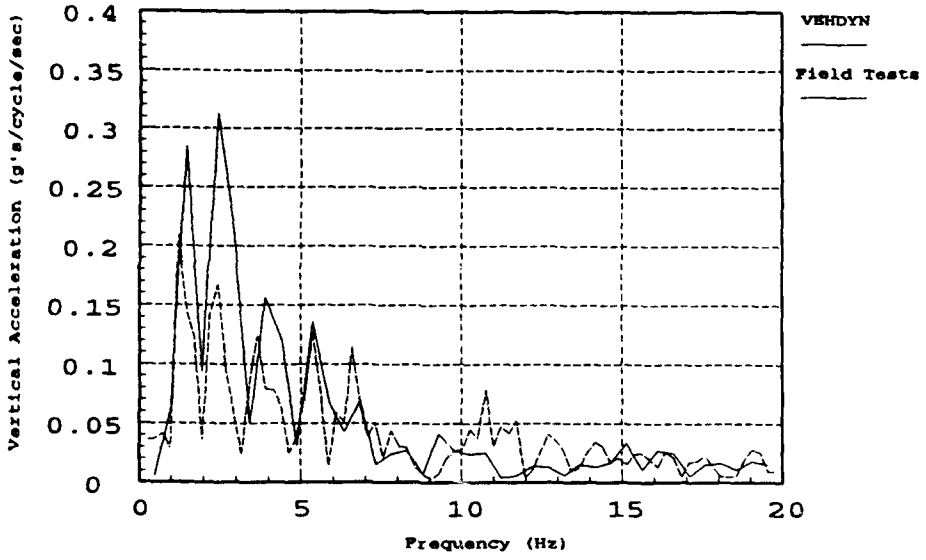

Figure 5.26. FFT of vertical acceleration of point on floorboard under the driver's seat as vehicle passed over a 6-in. half-round obstacle at 10 mph

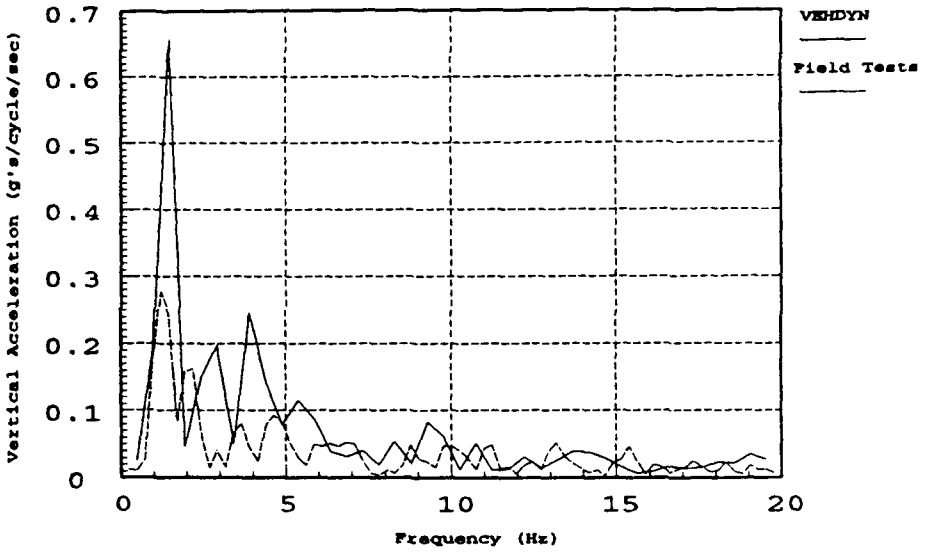

Figure 5.27. FFT of vertical acceleration of point on floorboard under the driver's seat as vehicle passed over a 8-in. half-round obstacle at 10 mph

Figures 5.28 through 5.30 present the FFT's of the suspension's vertical acceleration time history data. The predicted amplitudes were higher than the measured, but the frequency distributions were similar.

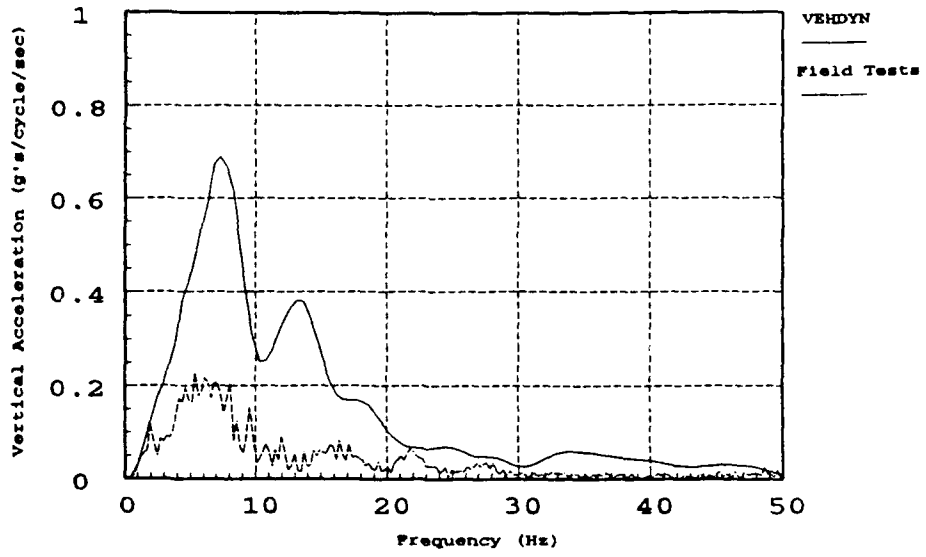

Figure 5.28. FFT of vertical acceleration of point on front left suspension as vehicle passed over a 4-in. half-round obstacle at 10 mph

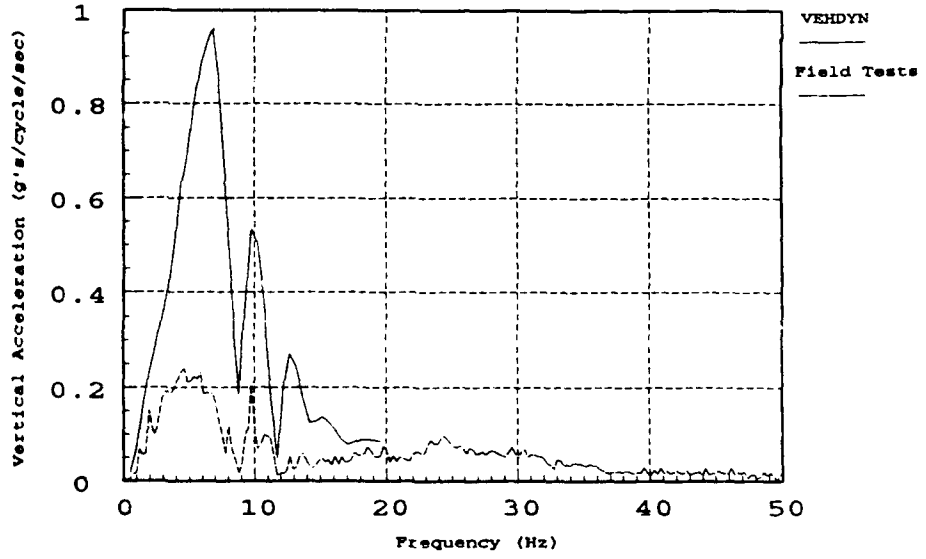

Figure 5.29. FFT of vertical acceleration of point on front left suspension as vehicle passed over a 6-in. half-round obstacle at 10 mph

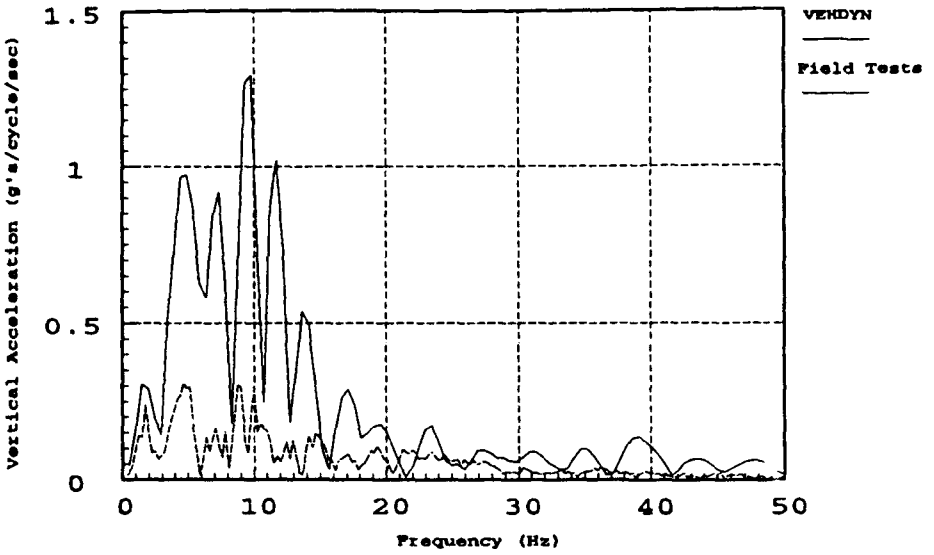

Figure 5.30. FFT of vertical acceleration of point on front left suspension as vehicle passed over a 8-in. half-round obstacle at 10 mph

The time histories and FFT results of the simulations exhibited the deviation between predicted and measured results. But, they also demonstrated the model's accuracy in simulating responses at the appropriate time increments and frequencies.

5.2.3 Peak Vertical Acceleration Analysis

To determine the accuracy of the vehicle models in their intended use, predictions of peak vertical accelerations and rms pitch rates were compared with results of corresponding measured tests.

5.2.3.1 DADS Results

Figure 5.31 shows predicted versus measured peak vertical accelerations on the floorboard under the driver's seat, for 5 speeds as the vehicle passed over a 4-in. high half-round obstacle. The data are also presented in Table 5.1. The predicted peak vertical acceleration in Figure 5.31 decreased slightly as the speed increased. However, the measured results produced a steady increase in peak accelerations as speeds increased, up to 30 mph. The predicted and measured accelerations at 10 mph overlay each other. That is the speed at which several model iterations were performed in order to develop force/velocity damper relationships while traversing over a 6-in. obstacle.

The relationship between the predicted and measured peak vertical accelerations on the floorboard under the driver's seat traversing a 6-in. half-round obstacle in Figure 5.32 were close for the 5 and 10 mph speeds, but diverged significantly at 15 mph.

The predictions for the 8-in. obstacle produced better correlations between the predicted and measured, but as shown in Figure 5.33 the predicted result at 15 mph was lower than the measured result.

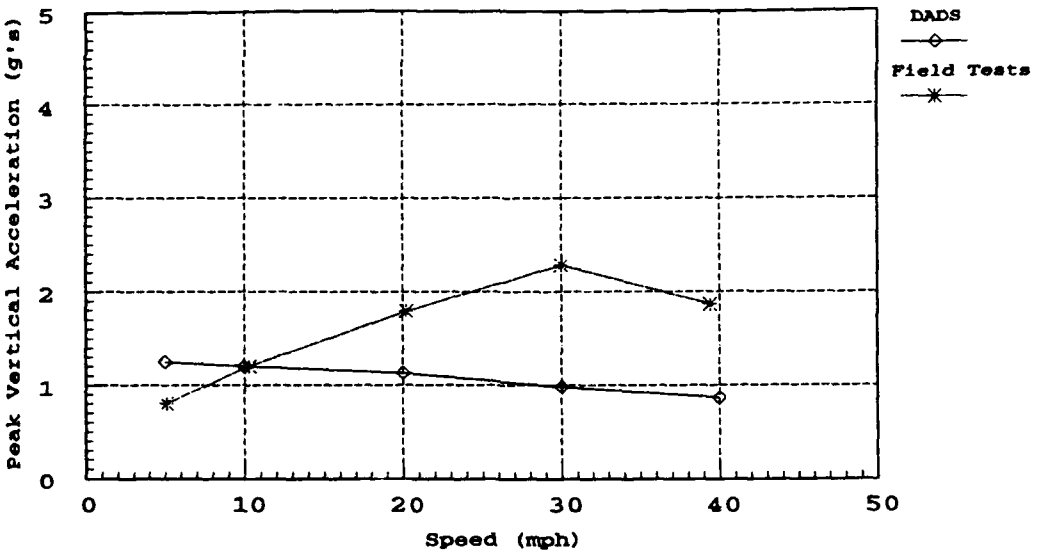

Figure 5.31. Peak vertical acceleration on the floorboard under the driver's seat as vehicle passed over a 4-in. half-round obstacle at different speeds

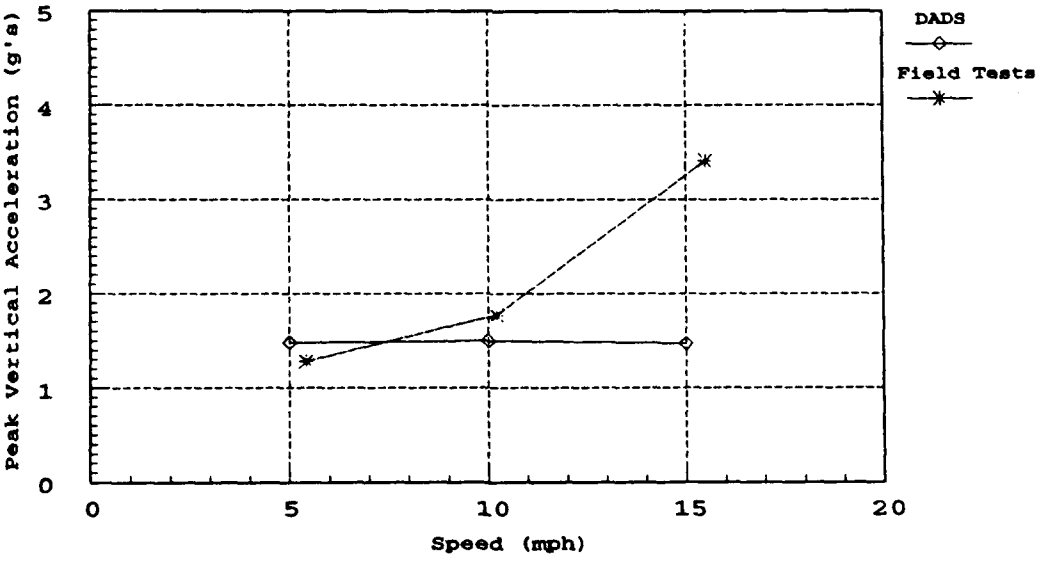

Figure 5.32. Peak vertical acceleration on the floorboard under the driver's seat as vehicle passed over a 6-in. half-round obstacle at different speeds

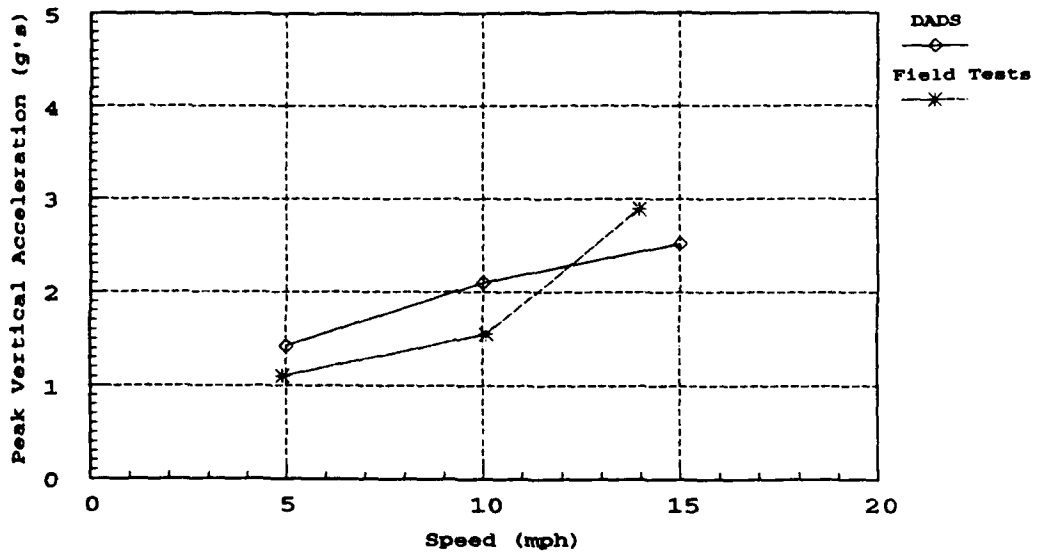

Figure 5.33. Peak vertical acceleration on the floorboard under the driver's seat as vehicle passed over a 8-in. half-round obstacle at different speeds

Figure 5.34 presents the resultant 2.5-g peak vertical acceleration speed versus obstacle height curves for the DADS predictions and the measured field tests. The data presented in Figure 5.34 represents speeds that produced 2.5 g's of vertical acceleration on the floorboard under the driver's seat and were derived by interpolating between the results presented in Figures 5.31 through 5.33. The arrows represent conditions that did not produce 2.5 g's of accelerations. The speeds which would have produced 2.5 g's were higher than the indicated point.

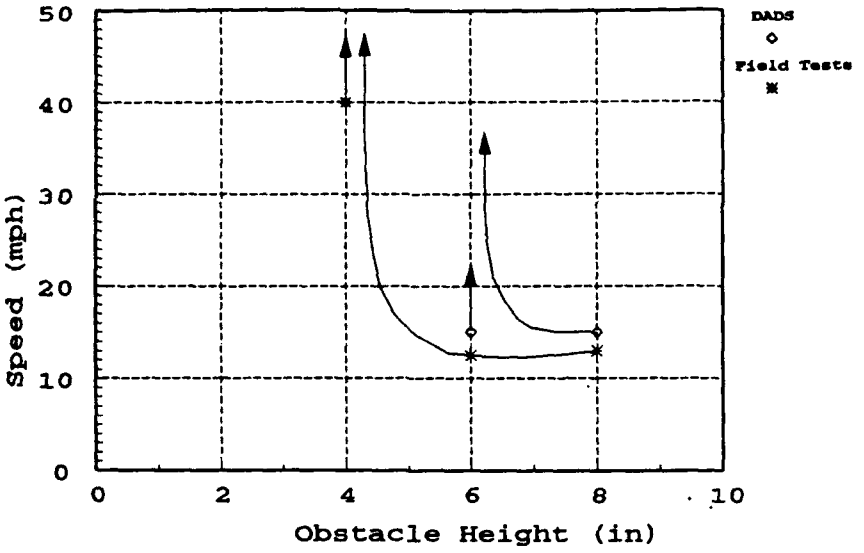

Figure 5.34. Speeds which generate 2.5 g's of vertical acceleration measured on the floorboard under the driver's seat as vehicle passed over different obstacle heights

The curves shown in Figure 5.34 indicate the measured tests were able to produce speeds greater than 40 mph as the vehicle passed over a 4-in. half-round obstacle without experiencing 2.5 g's. As the obstacle height increased to 6-in., the 2.5 g's speed decreased to 13 mph. The same speed was achieved on the 8-in. obstacle. DADS predicted that the vehicle was able to traverse both 4- and 6-in. half-round obstacles without reaching the 2.5 g's speed limit and was limited to about 15 mph over an 8-in. obstacle. These results indicate that the DADS model was better able to predict for higher obstacle heights at slow vehicle speeds.

The data presented in Figure 5.35 compare measured versus predicted rms pitch rates as the vehicle passed over the different obstacle heights at various speeds. The scatter about the one-to-one line indicates that the DADS model slightly under predicted for low pitch rates up to about 5 deg/sec, and slightly over predicted beyond that value. Predictions of the rms values tend to agree more closely with the measured results than the predictions of a discrete event such as peak acceleration as seen in Figure 5.36.

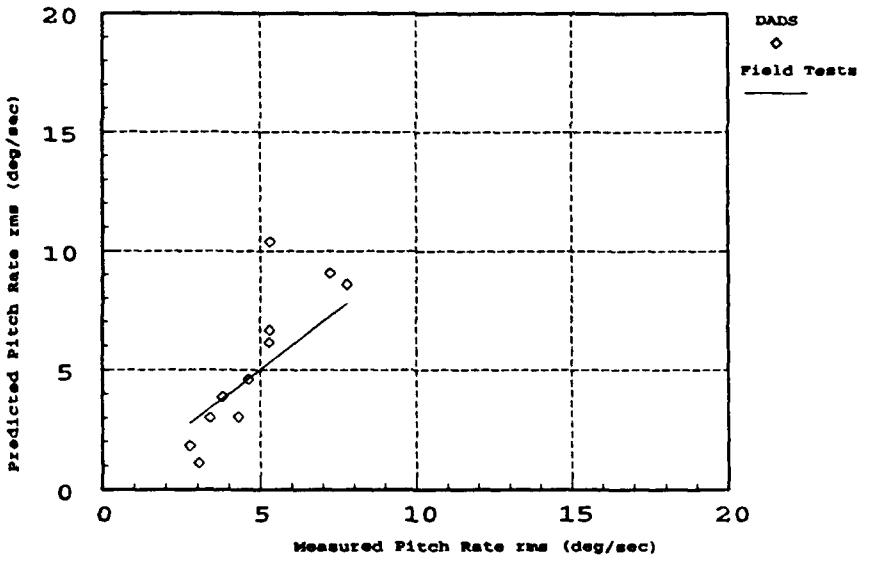

Figure 5.35. DADS predicted rms pitch rates versus measured rms pitch rate on the floorboard under the driver's seat as vehicle passed over different obstacle heights at various speeds

Data presented in Figure 5.36 show the relationship between the measured and DADS predicted peak vertical acceleration on the floorboard under the driver's seat as the vehicle passed over the different obstacle heights at various speeds.

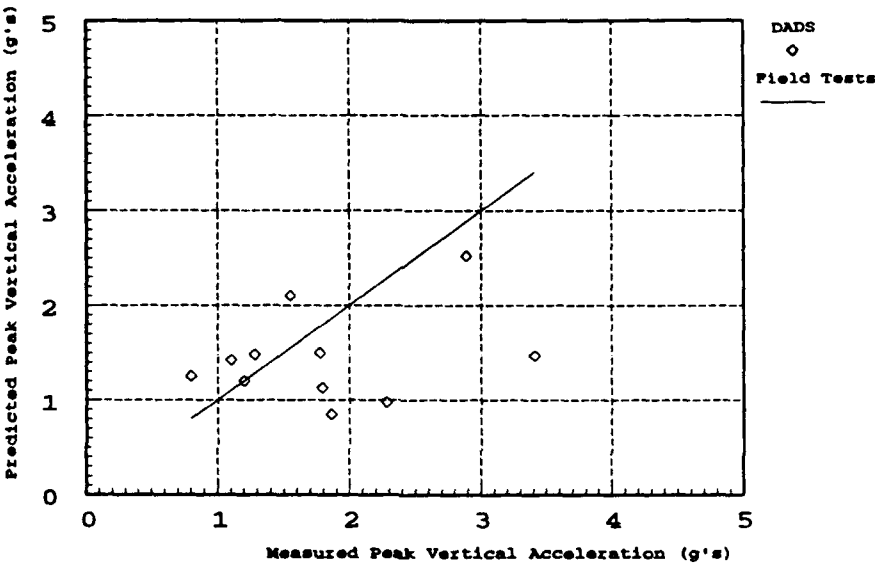

Figure 5.36. DADS predicted peak vertical g's versus measured peak vertical g's on the floorboard under the driver's seat as vehicle passed over different obstacle heights at various speeds

The DADS results were plotted versus the associated measured test which best matched the DADS speed and associated obstacle height. The resultant relationship indicates that the DADS model was able to better predict for low level vertical accelerations, and predicted low for higher levels of vertical acceleration.

Table 5.1. DADS Predicted Peak Vertical g's as Measured on Floorboard Under the Driver's Seat

Test Number	Obstacle Height in.	Test Speed mph	Model Speed mph	Field Test Peak g's	DADS Test Peak g's
690	4	5.1	5.0	-0.80	-1.25
691	4	10.3	10.0	-1.20	-1.20
693	4	20.2	20.0	1.79	1.13
695	4	30.0	30.0	2.28	0.98
697	4	39.4	40.0	1.86	0.85
700	6	5.4	5.0	-1.28	-1.48
701	6	10.2	10.0	-1.77	-1.50
702	6	15.5	15.0	3.41	-1.47
704	8	4.9	5.0	-1.10	1.42
706	8	10.1	10.0	1.55	-2.10
708	8	14.0	15.0	2.89	2.52

5.2.3.2 VEHDYN Results

The VEHDYN results presented in Figures 5.37 through 5.39 show trends similar to those seen in the DADS predictions. AS shown in Figure 5.37, the predicted peak vertical acceleration decreased as the vehicle speed increased. The simulated results for a 6-in. obstacle shown in Figure 5.38, indicate better correlations for speeds below 10 mph, but diverged as the speeds increased. Figure 5.39 presents the predictions for a 8-in. obstacle which produced peak g-values that were close to the measured values for 5 and 10 mph speeds. The predictions also followed the measured trends for the faster speeds.

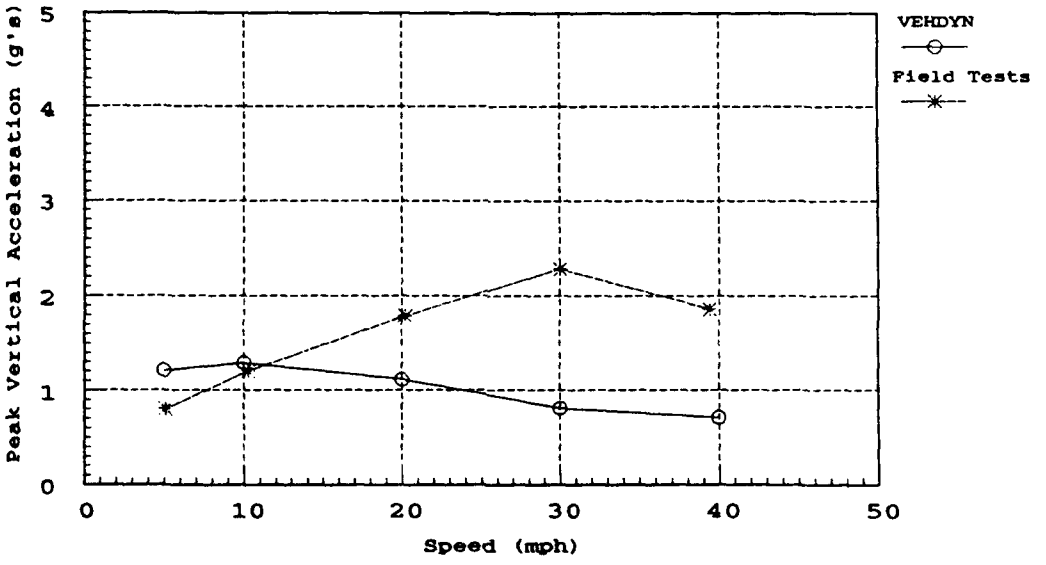

Figure 5.37. Peak vertical acceleration on the floorboard under the driver's seat as vehicle passed over a 4-in. half-round obstacle at different speeds

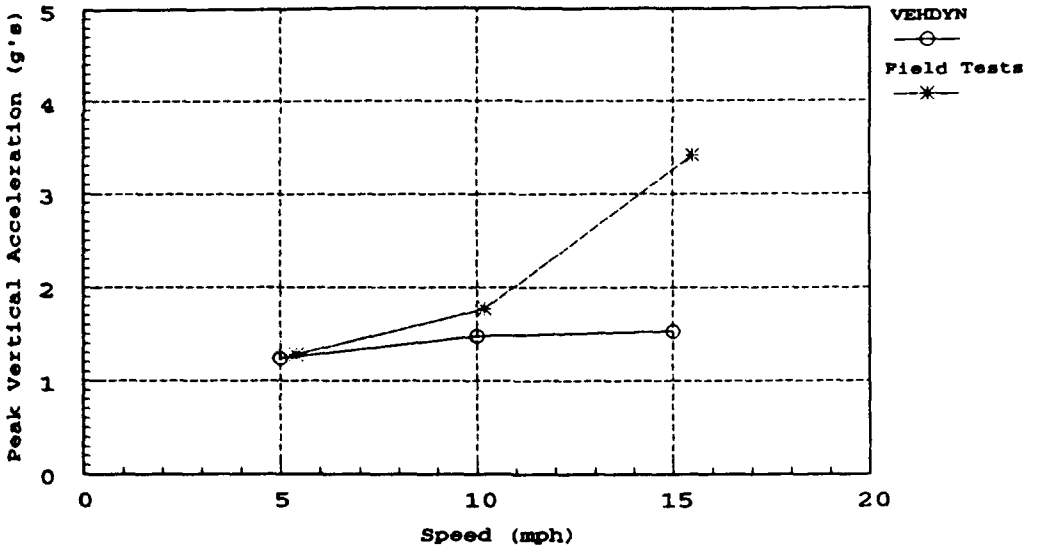

Figure 5.38. Peak vertical acceleration on the floorboard under the driver's seat as vehicle passed over a 6-in. half-round obstacle at different speeds

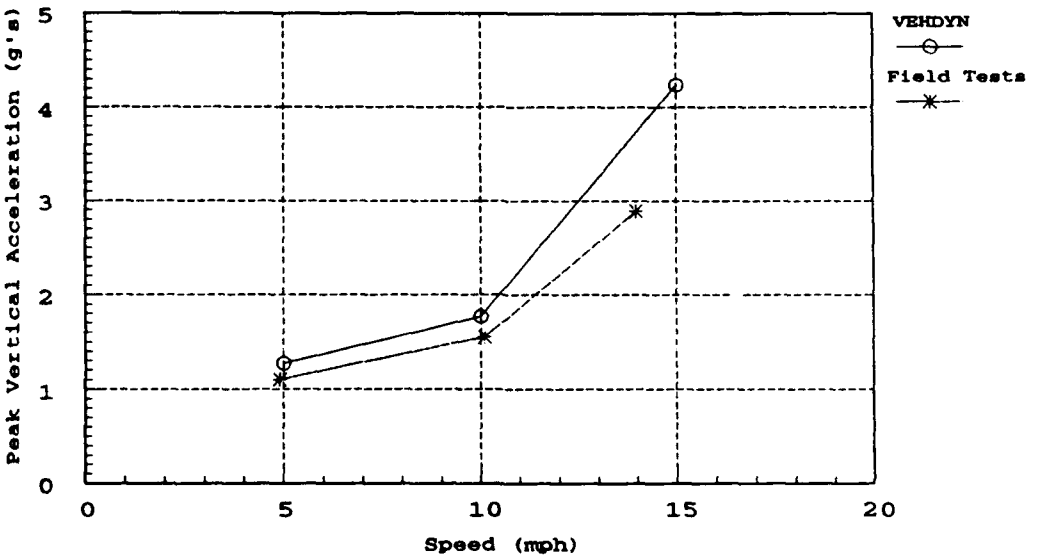

Figure 5.39. Peak vertical acceleration on the floorboard under the driver's seat as vehicle passed over a 8-in. half-round obstacle at different speeds

The resultant 2.5-g speed curves, in Figure 5.40, show that the simulated testing did not predict a 2.5-g level for the 6-in. obstacle. As previously shown, the vertical g-level trend of the simulated data passing over a 6-in. obstacle decreased as the speeds increased. Therefore, a 2.5-g level speed was not predicted. As the simulated obstacle height increased, the 2.5-g level predicted speed decreased to slightly under the field measured level. The results, similar to those of D/DS, indicate the VEHDYN model was better able to predict for higher obstacle heights at slow vehicle speeds. The resultant peak g's for all field test and VEHDYN simulations are presented in Table 5.2.

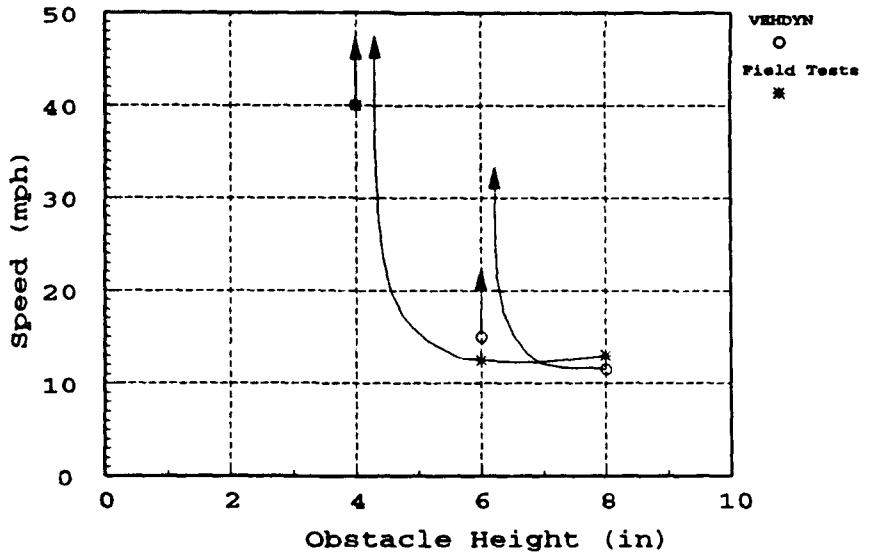

Figure 5.40. Speeds which generate 2.5 g's of vertical acceleration measured on the floorboard under the driver's seat as vehicle passed over different obstacle heights

The data presented in Figure 5.41 compare measured versus predicted rms pitch rates. The pitch rate rms predictions were of the simulated vehicle passing over the three different obstacle heights at the various speeds.

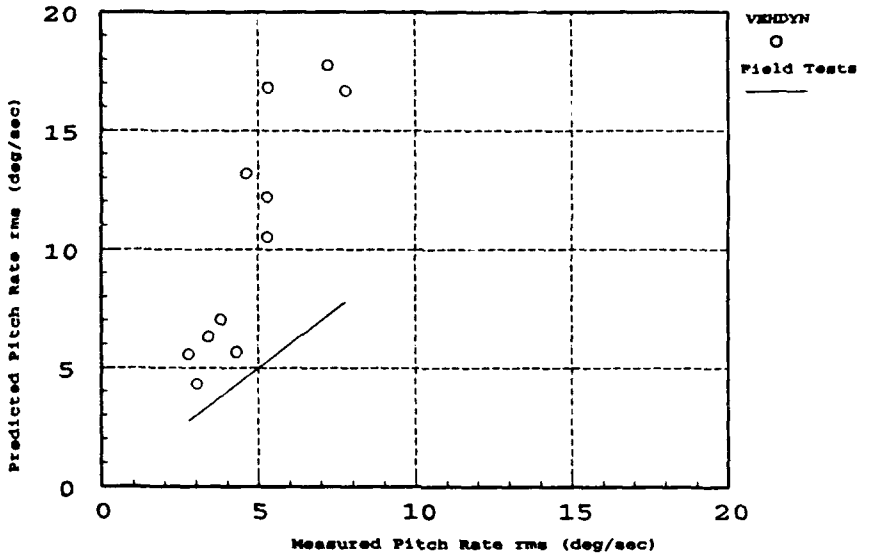

Figure 5.41. VEHDYN predicted rms pitch rates versus measured rms pitch rates on the floorboard under the driver's seat as vehicle passed over different obstacle heights at various speeds

The scatter about the one-to-one line indicates that the VEHDYN model was better able to correlate with the measured data at lower pitch rate levels.

The data presentation in Figure 5.42 is similar in plotting style to Figure 5.41. The data in Figure 5.42 are the resultant peak vertical acceleration from the point on the floorboard under the driver's seat. The VEHDYN model produced better correlations with the measured tests at

lower level accelerations. As the measured peak vertical acceleration increased, the accuracy of the VEHDYN predictions decreased. This was the same trend seen in the DADS model.

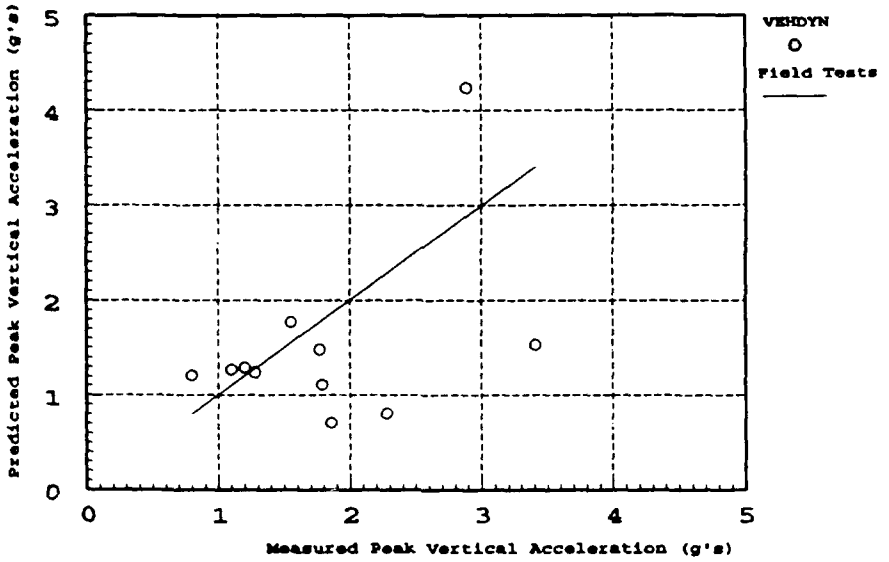

Figure 5.42. VEHDYN predicted peak vertical g's versus measured peak vertical g's on the floorboard under the driver's seat as vehicle passed over different obstacle heights at various speeds

Table 5.2. VEHDYN Predicted Peak Vertical g's as Measured on Floorboard Under the Driver's Seat

Test Number	Obstacle Height in.	Test Speed mph	Model Speed mph	Field Test Peak g's	VEHDYN Test Peak g's
690	4	5.1	5.0	-0.80	-1.21
691	4	10.3	10.0	-1.20	-1.29
693	4	20.2	20.0	1.79	-1.11
695	4	30.0	30.0	2.28	-0.81
697	4	39.4	40.0	1.86	-0.71
700	6	5.4	5.0	-1.28	-1.24
701	6	10.2	10.0	-1.77	-1.48
702	6	15.5	15.0	3.41	-1.53
704	8	4.9	5.0	-1.10	1.27
706	8	10.1	10.0	1.55	-1.77
708	8	14.0	15.0	2.89	4.24

5.2.4 Shock Test Conclusions

It was shown that both models produced vertical acceleration and pitch rate time histories which were closely matched to the measured test for 10 mph speeds. Also, the resultant FFT's simulated the frequency distributions seen in the measured tests. But, when the 2.5-g level speed curves were developed, for both models, the model predictions were unable to match the g-level response of the measured tests at the faster speeds. These deficiencies could be caused by several factors, the two most probable factors are the method employed to develop the damper force/velocity data used in both models, and the horizontal velocity differences between the predicted and measured results. Another factor that could contribute to the variations in the predicted versus measured was the style of modeling used to simulate the measured testing. Since both models were generated using rigid body dynamics, the models were unable to reproduce the effects caused by the flexing of the vehicle's frame and displacements occurring in the bushing components in the suspensions.

To determine the accuracy of the shock test predictions, percent variations were determined using the absolute peak vertical acceleration values under the driver's seat for the individual obstacle tests. The DADS model yielded, on average, a 91 percent accuracy, with a maximum low of 43 percent and a maximum high of 135 percent.

The VEHDYN model also yielded, on average, a 91 percent accuracy with a maximum low of 45 percent and a maximum high of 147 percent.

5.3 Ride Test Analysis

To determine the dominant frequencies in the vehicle during ride course simulations and field testing, the FFT was calculated from the resultant vertical acceleration time histories while traversing a smooth (0.69 in rms), medium (1.34 in rms), and rough (2.41 in rms) ride course. The associated pitch rates during the same tests were analyzed by calculating and plotting the rms of the pitch rate time histories. The average vertical absorbed power for the model simulations and field tests were calcualted and compared by means of a 6 watt speed curve. To analyze the magnitude of the differences between predicted and measured results, a predicted AP_{vt} versus measured AP_{vt} plot was generated. The plot included all measured testing and simulations and indicated the general direction and magnitude of the differences.

5.3.1 FFT Analysis

5.3.1.1 DADS Results

Figures 5.43 through 5.48 represent the vertical acceleration amplitudes and frequencies experienced by the driver during ride tests over three different rms elevation ride courses. Figures 5.43 and 5.44 show that the dominant frequency range for the sprung mass was between 1.5 and 2.5 Hz. The DADS simulations predicted higher amplitudes for the three ride courses shown, but was able to simulate the measured frequency distributions. The design parameters for springs, shocks, and tires used in vehicles, generally cause the sprung mass to have a maximum amplitude of vertical acceleration occurring above 1 Hz and below 4 Hz. The natural frequency of the sprung mass at about 2 Hz can been seen in Figures 5.43 through 5.48. In the results shown in Figures 5.43 and 5.44, the DADS simulations were able to predict the natural frequency of the sprung mass, and followed the measured trends of the associated amplitudes. The same amplitudes and frequency distribution trends were also present in the results shown in Figures 5.46 through 5.48.

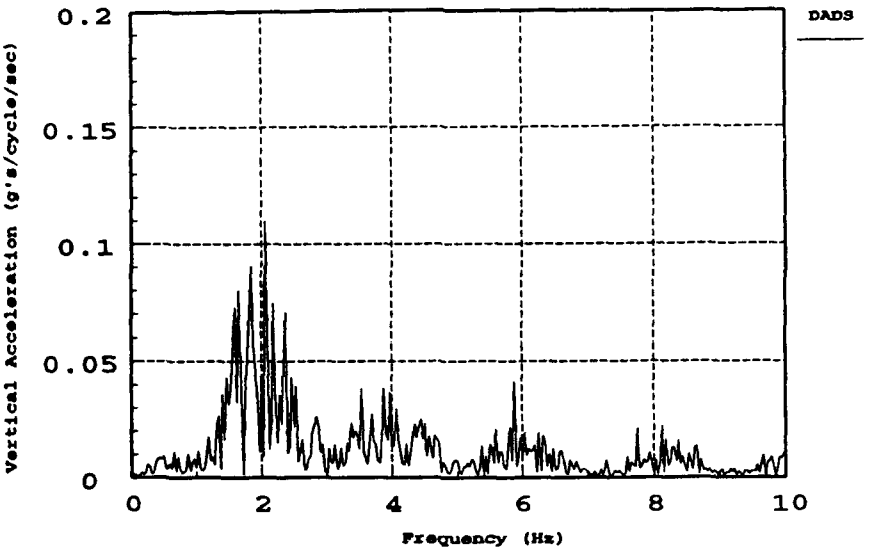

Figure 5.43. FFT of DADS predicted vertical acceleration of point on driver's seat as vehicle passed over a 0.69-in. rms ride course at 15.0 mph

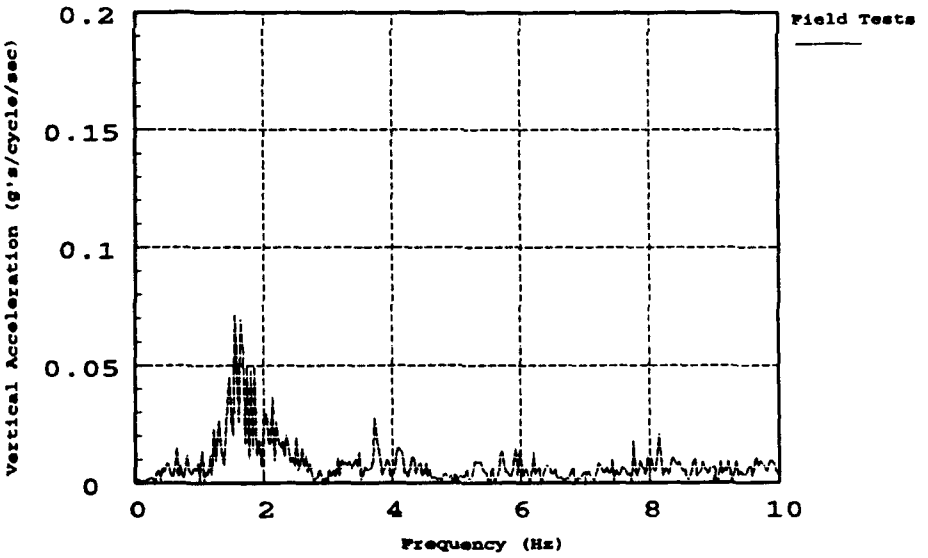

Figure 5.44. FFT of measured vertical acceleration of point on driver's seat as vehicle passed over a 0.69-in. rms ride course at 14.5 mph

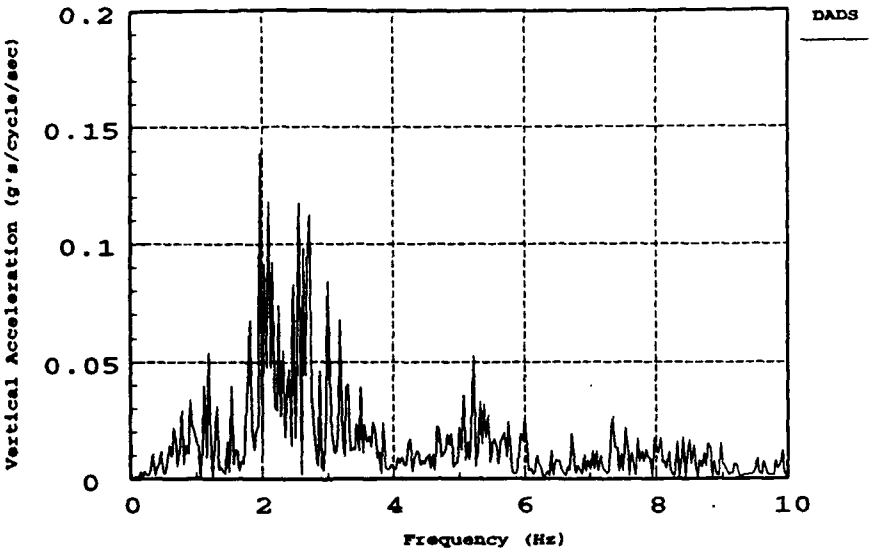

Figure 5.45. FFT of DADS predicted vertical acceleration of point on driver's seat as vehicle passed over a 1.34-in. rms ride course at 20.0 mph

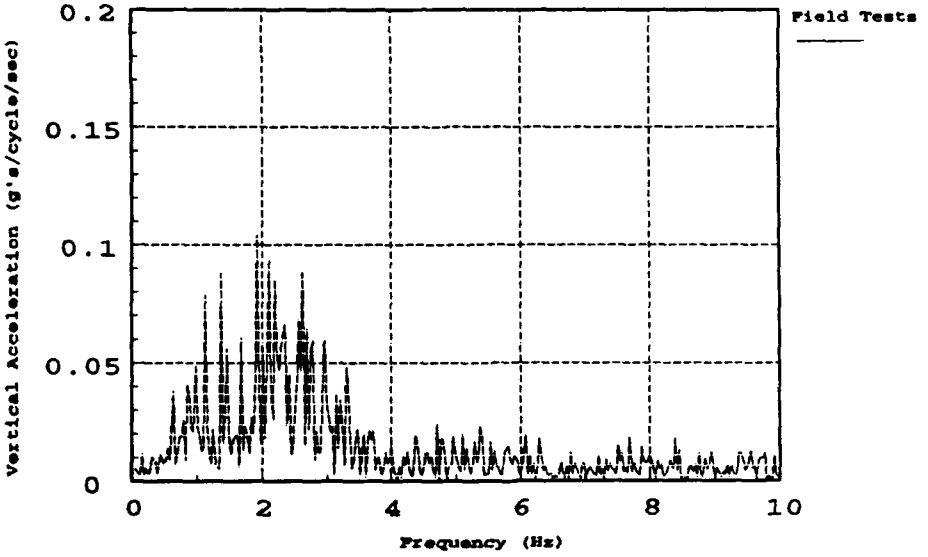

Figure 5.46. FFT of measured vertical acceleration of point on driver's seat as vehicle passed over a 1.34-in. rms ride course at 19.5 mph

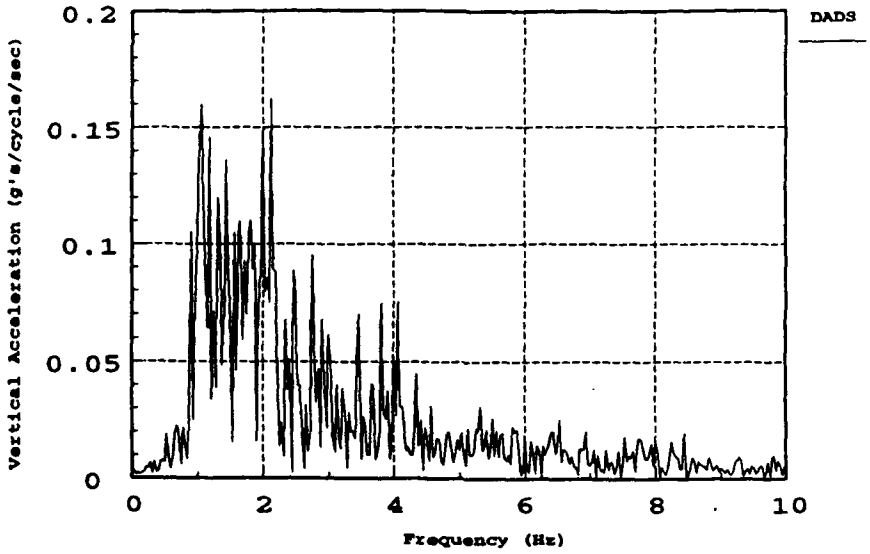

Figure 5.47. FFT of DADS predicted vertical acceleration of point on driver's seat as vehicle passed over a 2.41-in. rms ride course at 15.0 mph

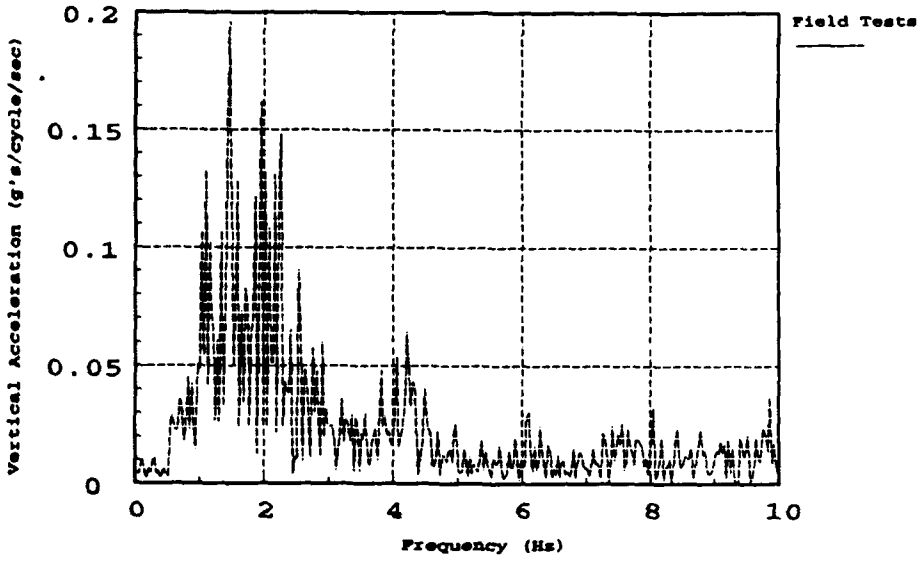

Figure 5.48. FFT of measured vertical acceleration of point on driver's seat as vehicle passed over a 2.41-in. rms ride course at 15.0 mph

Figures 5.49 through 5.54 present the vertical acceleration amplitudes and frequencies generated in the front left suspension for the same three test results shown in Figures 5.43 through 5.48. The DADS simulations predicted higher amplitudes for a wider range of frequencies, but the simulations generally followed the trends found in the measured frequency distribution. A vehicle's unsprung mass generally has a natural frequency between 5 and 15 Hz. As shown by peak amplitudes between 7 Hz and 11 Hz, the natural frequency for the unsprung mass was apparent in Figure 5.50. The predicted results in Figure 5.49 produced a natural frequency around 5 Hz. Generally, the larger the input to a suspension becomes, the harder it is to recognize the natural frequency of the suspension from a frequency distribution plot. This was evident in both the simulated and measured results presented in Figure 5.51 through 5.54.

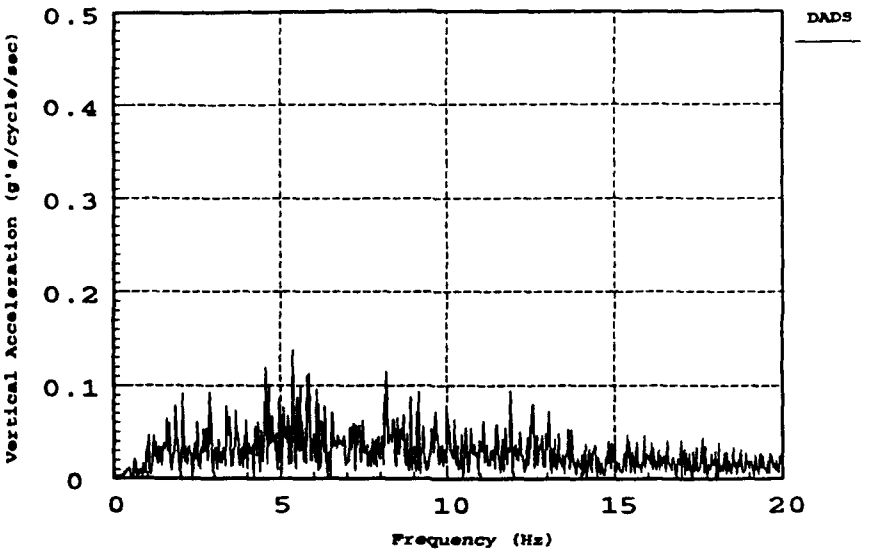

Figure 5.49. FFT of DADS predicted vertical acceleration of point on front left suspension as vehicle passed over a 0.69-in. rms ride course at 15.0 mph

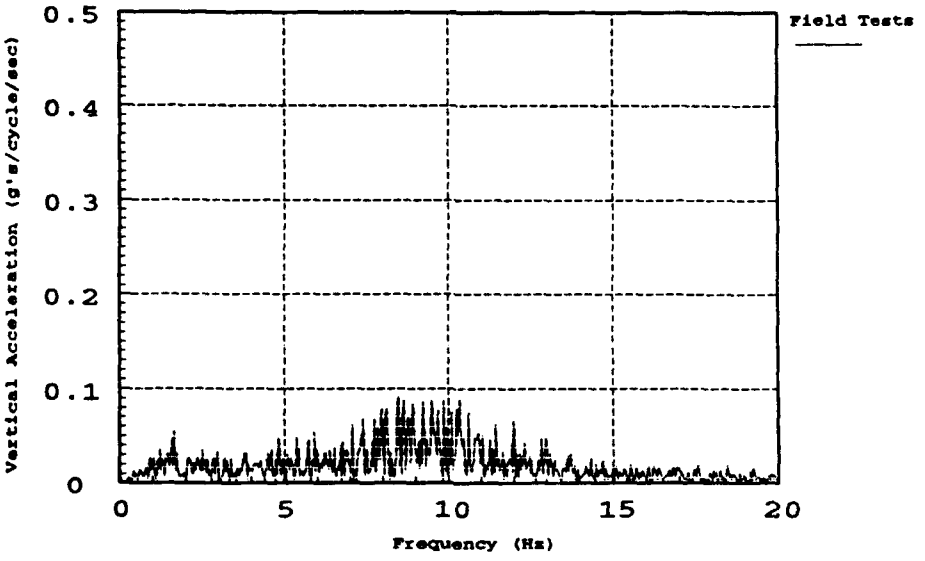

Figure 5.50. FFT of measured vertical acceleration of point on front left suspension as vehicle passed over a 0.69-in. rms ride course at 15.5 mph

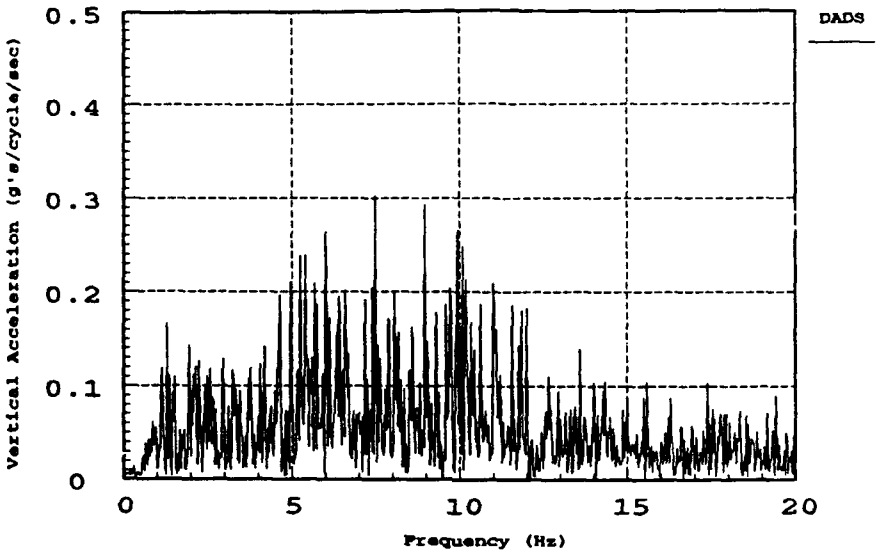

Figure 5.51. FFT of DADS predicted vertical acceleration of point on front left suspension as vehicle passed over a 1.34-in. rms ride course at 20.0 mph

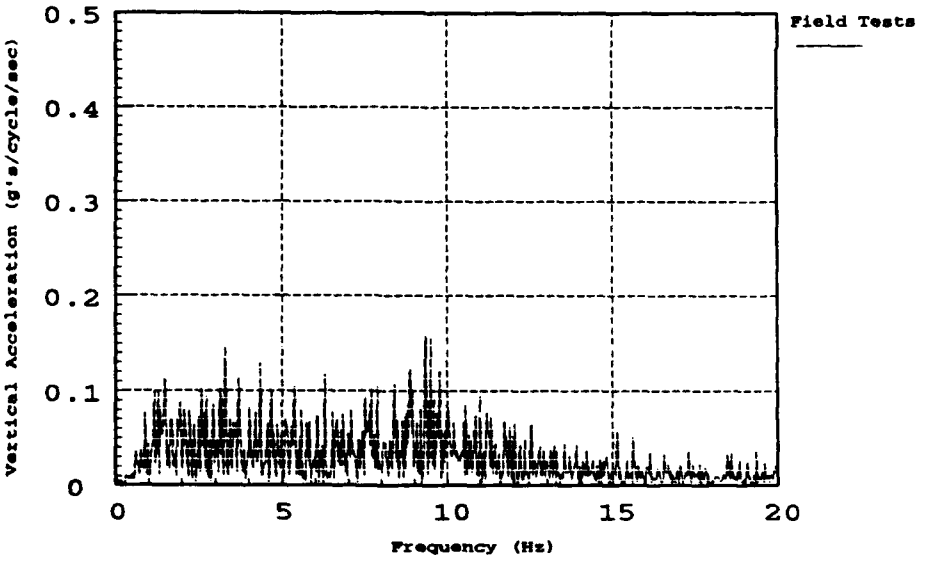

Figure 5.52. FFT of measured vertical acceleration of point on front left suspension as vehicle passed over a 1.34-in. rms ride course at 19.5 mph

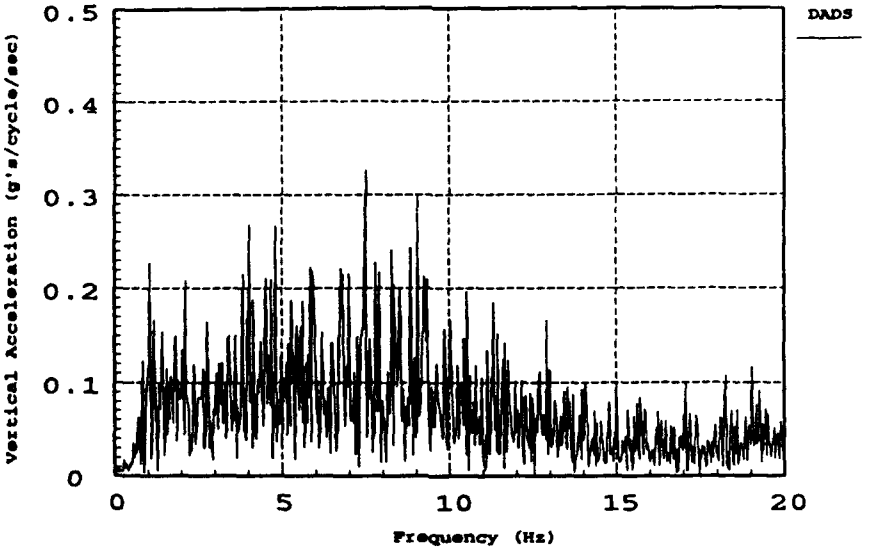

Figure 5.53. FFT of DADS predicted vertical acceleration of point on front left suspension as vehicle passed over a 2.41-in. rms ride course at 15.0 mph

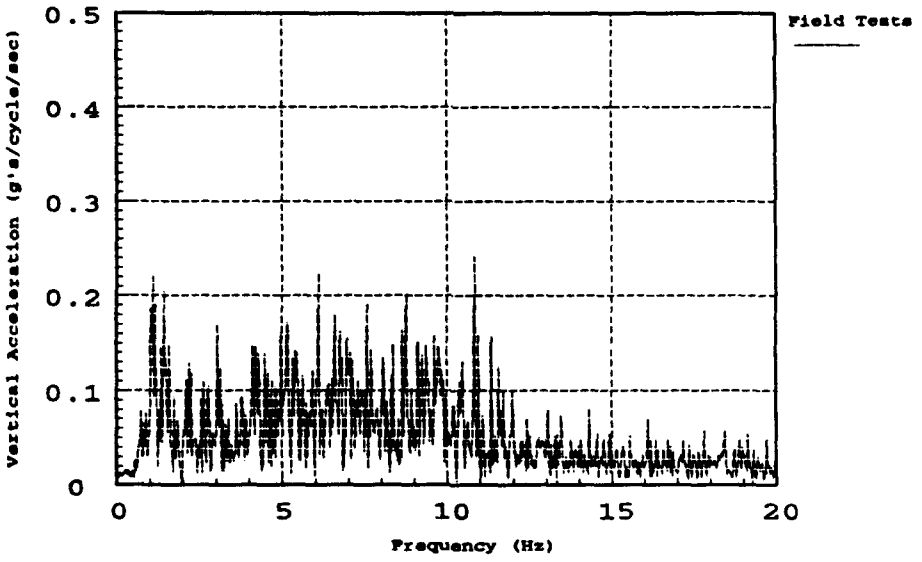

Figure 5.54. FFT of measured vertical acceleration of point on front left suspension as vehicle passed over a 2.41-in. rms ride course at 15.0 mph

5.3.1.2 VEHDYN Results

Figures 5.55 through 5.57 represent the predicted vertical acceleration amplitudes and frequencies experienced by the driver during ride tests over three different rms elevation ride courses. Figure 5.55 shows that the dominant predicted frequency range for the sprung mass was between 1.5 and 2.5 Hz. The VEHDYN predictions followed the same amplitude and frequency trends seen in the DADS predictions. That is, higher predicted vertical acceleration amplitudes, but reasonable frequency distributions.

Figures 5.58 through 5.60 present the vertical acceleration amplitudes and frequencies generated in the front left suspension for the same three test results shown in Figures 5.55 through 5.57. The VEHDYN predictions differed from the DADS in that VEHDYN predicted much higher amplitudes, but produced better natural frequency predictions for the suspension.

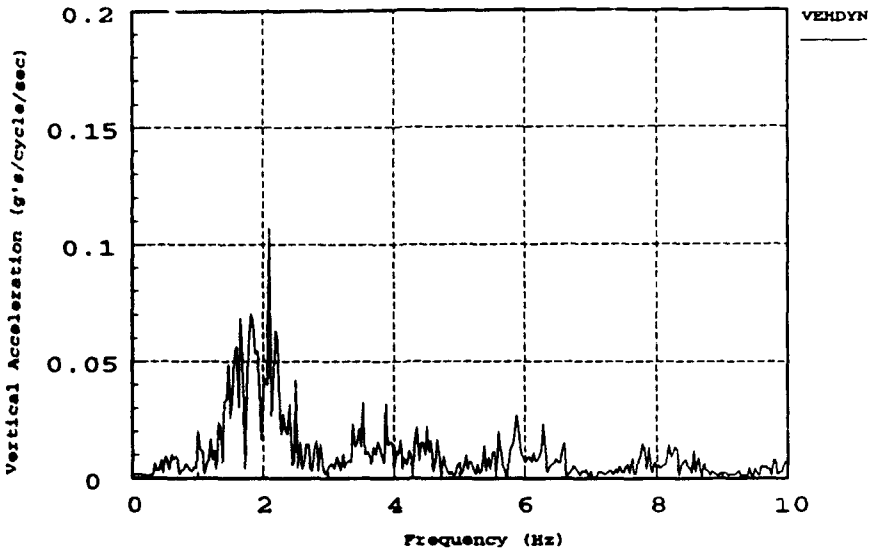

Figure 5.55. FFT of VEHDYN predicted vertical acceleration of point on driver's seat as vehicle passed over a 0.69-in. rms ride course at 15.0 mph

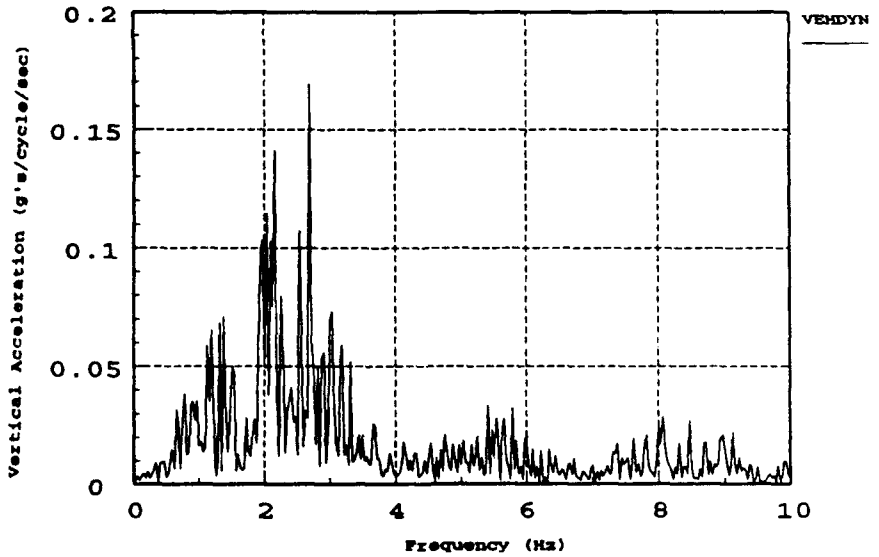

Figure 5.56. FFT of VEHDYN predicted vertical acceleration of point on driver's seat as vehicle passed over a 1.34-in. rms ride course at 20.0 mph

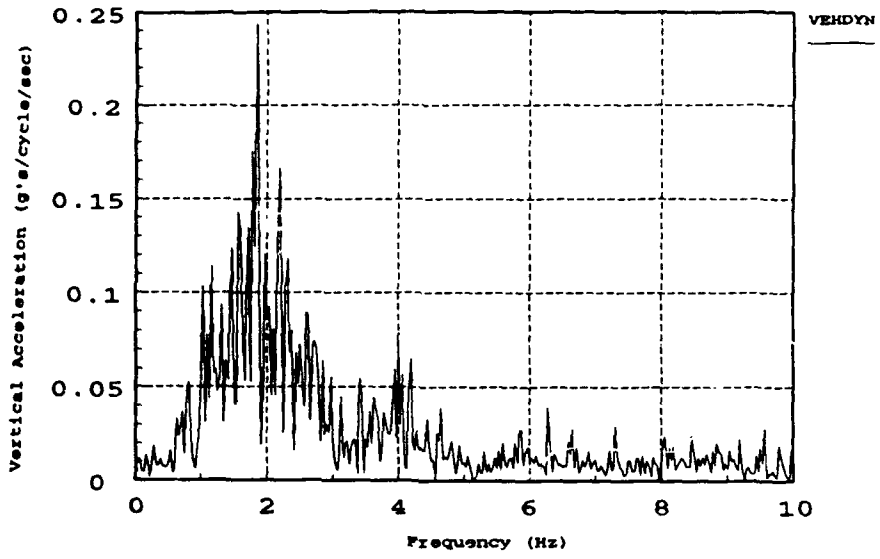

Figure 5.57. FFT of VEHDYN predicted vertical acceleration of point on driver's seat as vehicle passed over a 2.41-in. rms ride course at 15.0 mph

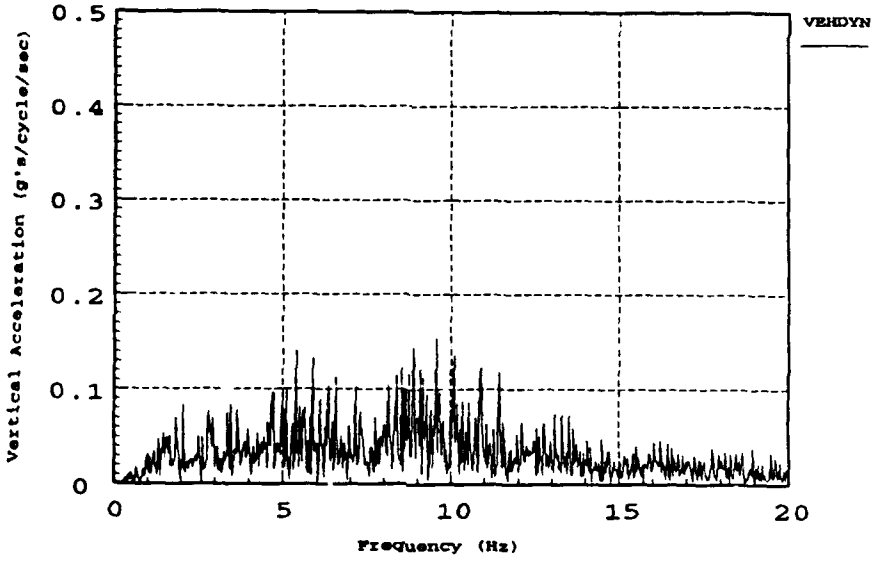

Figure 5.58. FFT of VEHDYN predicted vertical acceleration of point on front suspension as vehicle passed over a 0.69-in. rms ride course at 15.0 mph

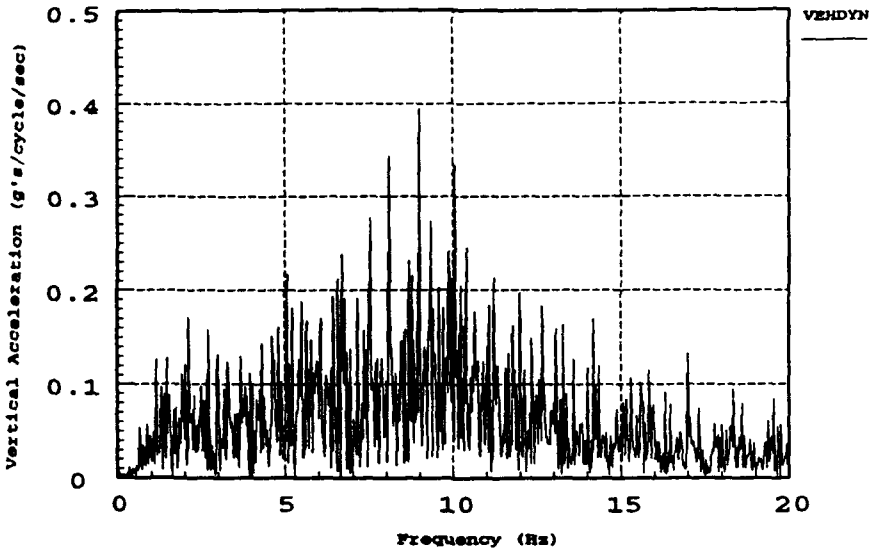

Figure 5.59. FFT of VEHDYN predicted vertical acceleration of point on front suspension as vehicle passed over a 1.34-in. rms ride course at 20.0 mph

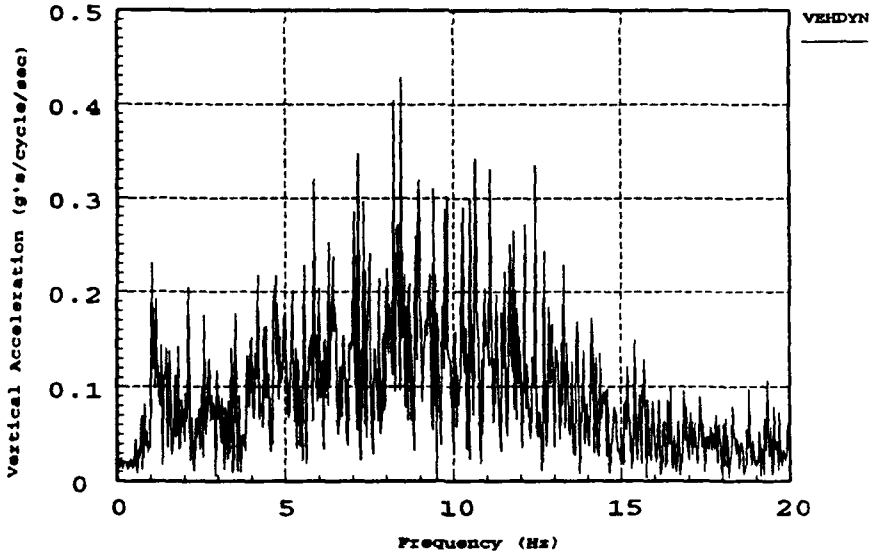

Figure 5.60. FFT of VEHDYN predicted vertical acceleration of point on front suspension as vehicle passed over a 2.41-in. rms ride course at 15.0 mph

The FFT results of the simulated ride tests show similar trends to the results of the simulated shock tests, which demostrate that the models were capable of simulating the measured frequencies. The simulated results also reveal that high vertical accelerations in the suspension did not cause excessively high vertical acceleration predictions for the chassis.

5.3.2 Pitch Rate Analysis

To analyze the pitch rate of the vehicle during the ride course field testing and simulations, the rms of the pitch rate time histories for all measured and simulated ride testing were plotted.

The test data presented in Figures 5.61 and 5.62 compare the relationship between the measured and predicted rms pitch rates as the vehicle passed over the different ride courses at various speeds. As shown in Figure 5.61, the DADS predictions plot close to the measured results one-to-one line, and produced a good correlation for all ride test simulations. The VEHDYN results, presented in Figure 5.62, show a little more scatter, but followed the trend of the measured data.

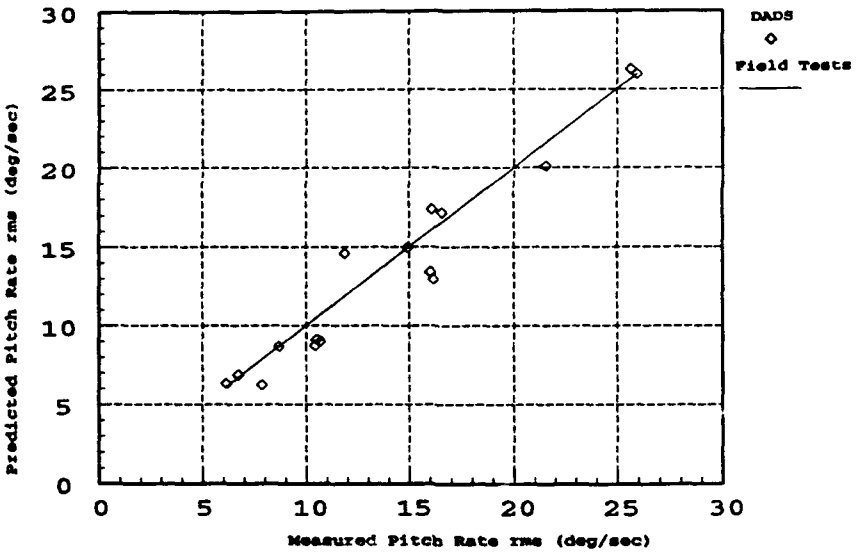

Figure 5.61. DADS predicted pitch rate rms versus measured pitch rate rms on the driver's seat as vehicle passed over different ride courses at various speeds

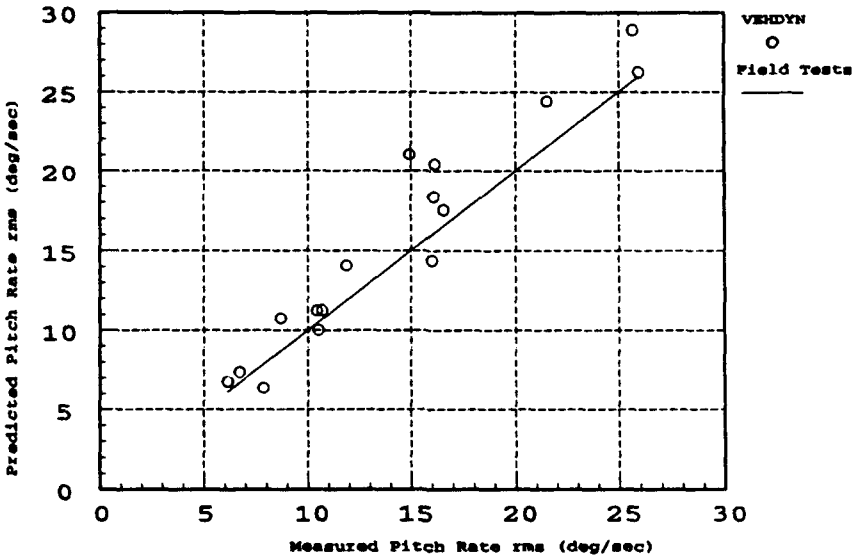

Figure 5.62. *VEHDYN* predicted pitch rates rms versus measured pitch rate rms on the driver's seat as vehicle passed over different ride courses at various speeds

5.3.3 Absorbed Power Analysis

The measured and predicted average AP_{vt} on the drivers seat was plotted for three ride courses, to show the general speed versus AP_{vt} trends. The AP_{vt} results for all field tests and model simulations are presented in Tables 5.3 and 5.4.

5.3.3.1 DADS Results

The results presented in Figures 5.63 through 5.65 show that as the vehicle speed increased, for both measured testing and DADS predictions, so did the AP_{vt}. The level of AP_{vt} for each DADS prediction was higher than the measured AP_{vt}, but the same trend as seen in the measured results was present in the DADS predictions.

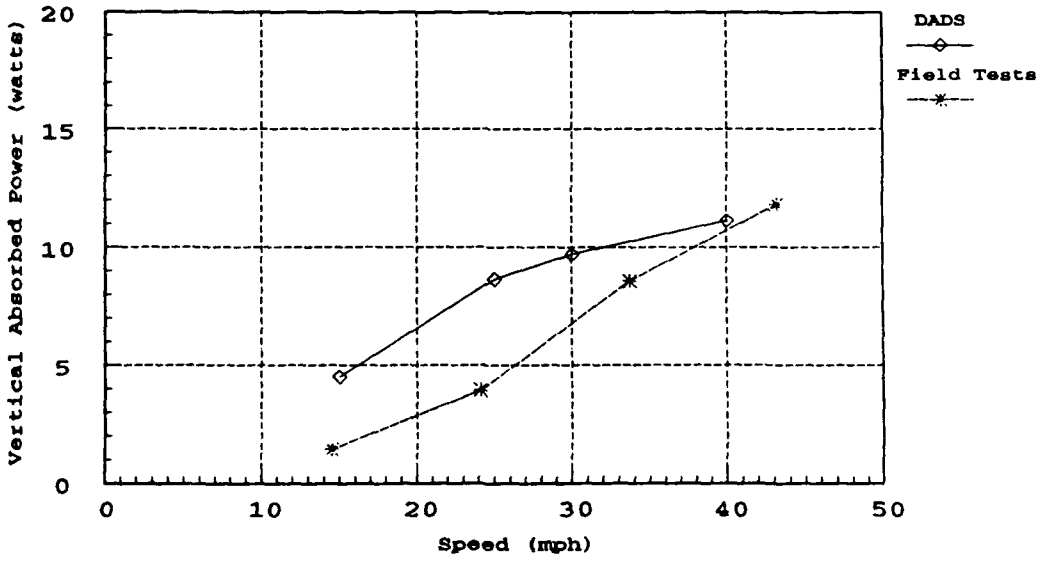

Figure 5.63. Average vertical absorbed power of point on the driver's seat as vehicle passed over a 0.69-in. rms ride course at different speeds

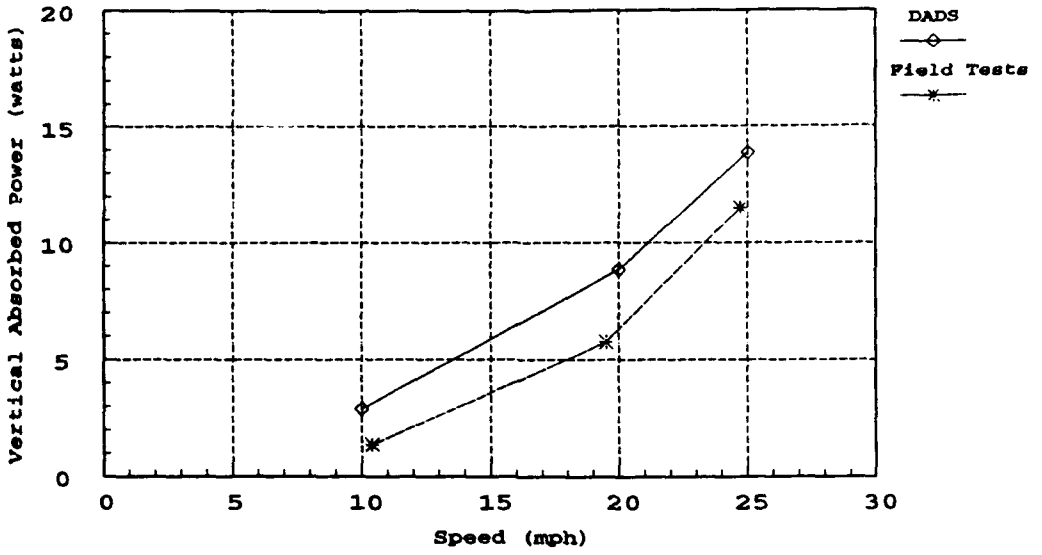

Figure 5.64. Average vertical absorbed power of point on the driver's seat as vehicle passed over a 1.34-in. rms ride course at different speeds

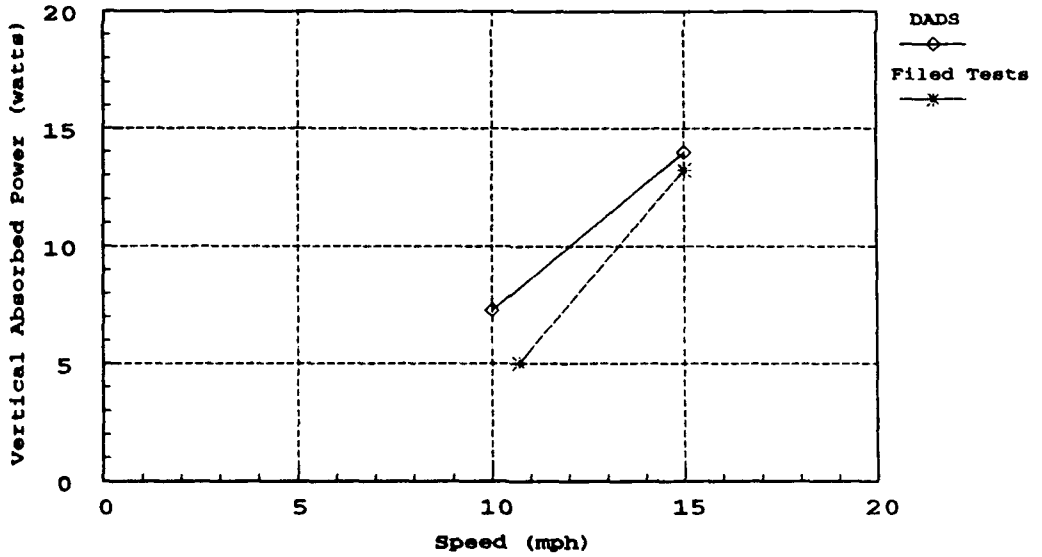

Figure 5.65. Average vertical absorbed power of point on the driver's seat as vehicle passed over a 2.41-in. rms ride course at different speeds

The resultant speed versus rms roughness at 6 watts of AP_{vt} is shown in Figure 5.66. The plot indicates that at a low rms value the vehicle was not speed limited. The curves used to represent this portion of the plot were extrapolated from the general shape and distribution of the data points. As the rms roughness increased the vehicle was forced to reduce its speed. As shown in Figure 5.66, the amount of speed reduction necessary to maintain a 6 watt level over the increasing rms values was significant. The speeds ranged from 29 to 11 mph for the measured tests and from 19 to 5 mph for the DADS predictions. In comparing the measured and DADS predicted speeds, it can be seen that the difference over the range of rms values was smaller for the higher rms values. This trend was the same as seen in the shock tests and the FFT's of the ride test results. As the amount of input energy to the vehicle increased, through higher obstacles and rougher ride courses, so did the correlation between the measured and predicted results.

The test data presented in Figure 5.67 shows the relationship between the measured and predicted AP_{vt} on the driver's seat as the vehicle passed over the different ride courses at various speeds. The solid line represents a one-to-one plot of the measured results. As shown in Figure 5.67, the DADS predictions were higher for the lower levels of AP_{vt}, and closer to the measured results for the higher levels of

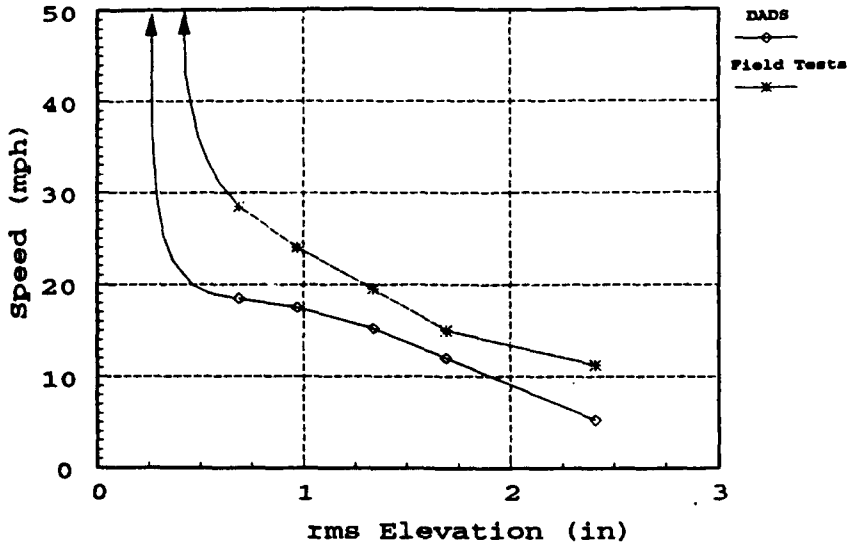

Figure 5.66. Speeds which generate 6 watts of average vertical absorbed power on the driver's seat as the vehicle passed over different ride courses

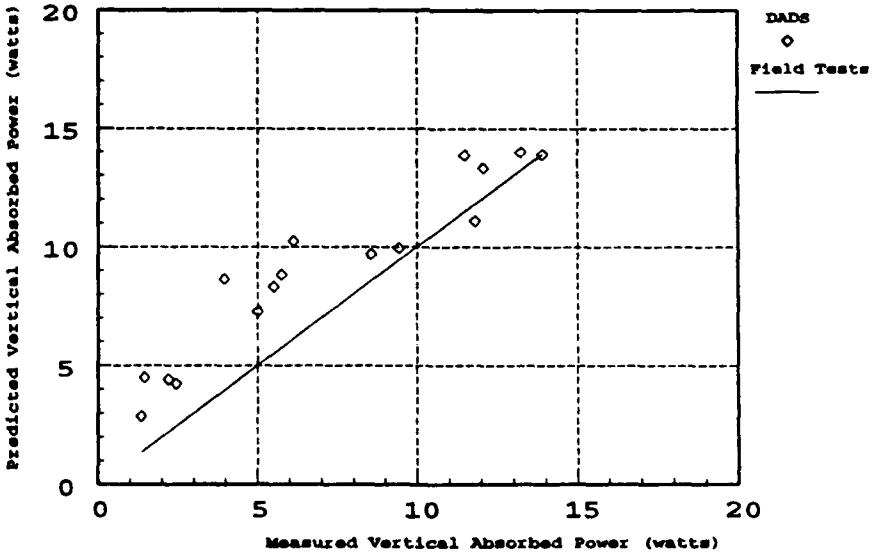

Figure 5.67. DADS predicted average vertical absorbed power versus measured average vertical absorbed power on the driver's seat as vehicle passed over different ride courses

AP_{vt}. This, again, follows the trend seen in the previous simulations. As the input energy increases so did the correlation.

Table 5.3. DADS Predicted Vertical Absorbed Power

Test Number	rms Value in.	Test Speed mph	Model Speed mph	Field Test AP_{vt}	DADS Test AP_{vt}
553	0.69	14.5	15.0	1.45	4.50
557	0.69	24.1	25.0	3.95	8.64
561	0.69	33.7	30.0	8.55	9.69
565	0.69	43.2	40.0	11.81	0.98
541	0.97	14.5	15.0	2.20	4.41
543	0.97	24.5	25.0	6.12	10.24
544	0.97	28.7	30.0	9.43	9.94
546	0.97	39.1	40.0	13.91	13.91
578	1.34	10.4	10.0	1.35	2.81
580	1.34	19.5	20.0	5.75	8.82
582	1.34	24.7	25.0	11.49	13.87
570	1.69	10.2	10.0	2.44	4.24
571	1.69	14.4	15.0	5.50	8.32
573	1.69	20.9	20.0	12.07	13.34
588	2.41	10.7	10.0	5.01	7.27
589	2.41	15.0	15.0	13.23	14.00

5.3.3.2 VEHDYN Results

The results presented in Figures 5.68 through 5.70 show that as the vehicle speed increased, for both measured testing and VEHDYN predictions, so did the AP_{vt}. The level of AP_{vt} for each VEHDYN prediction was higher than the measured AP_{vt}, but the same trend as seen in the measured results and DADS predictions was also present in the VEHDYN predictions.

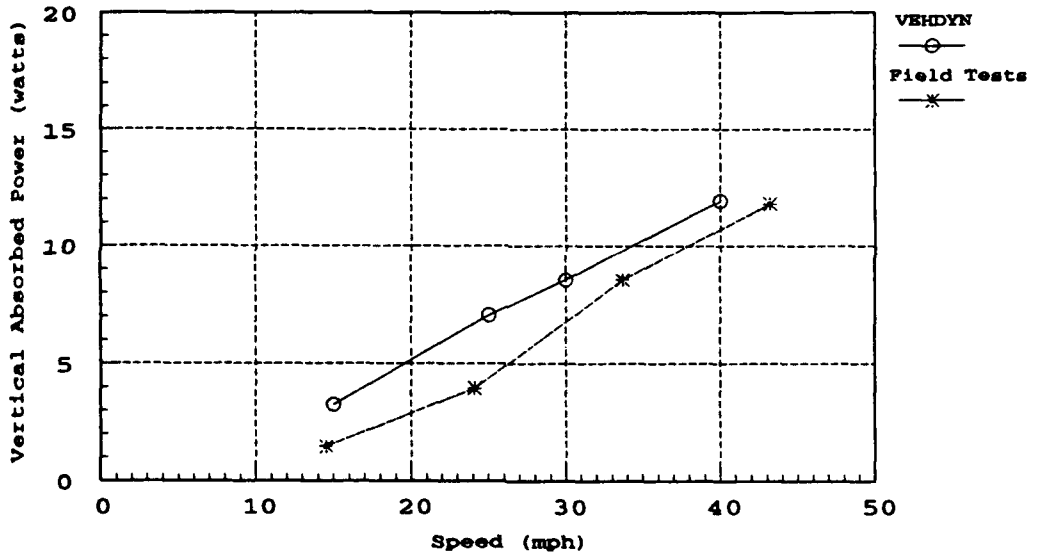

Figure 5.68. Average vertical absorbed power of point on the driver's seat as vehicle passed over a 0.69-in. rms ride course at different speeds

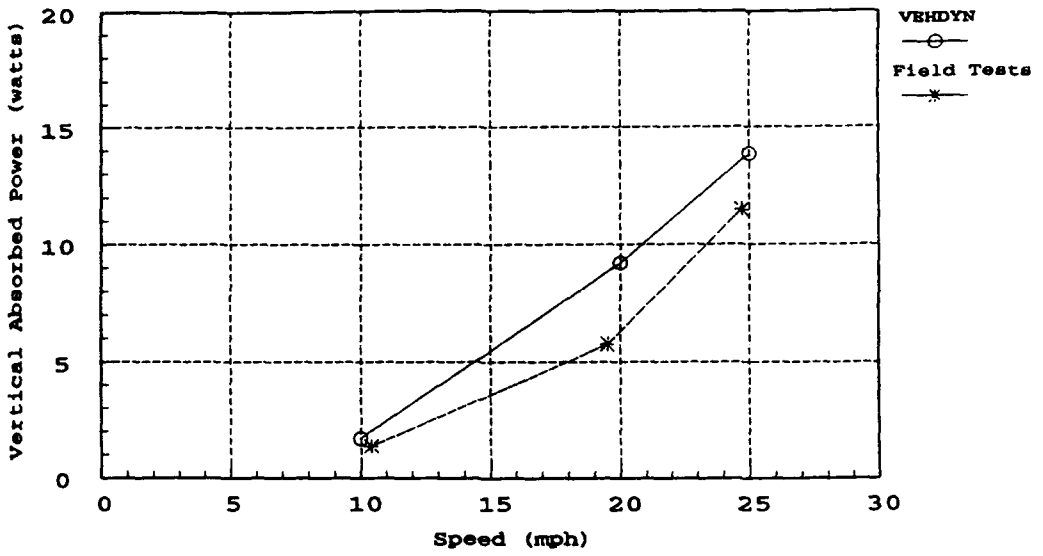

Figure 5.69. Average vertical absorbed power of point on the driver's seat as vehicle passed over a 1.34-in. rms ride course at different speeds

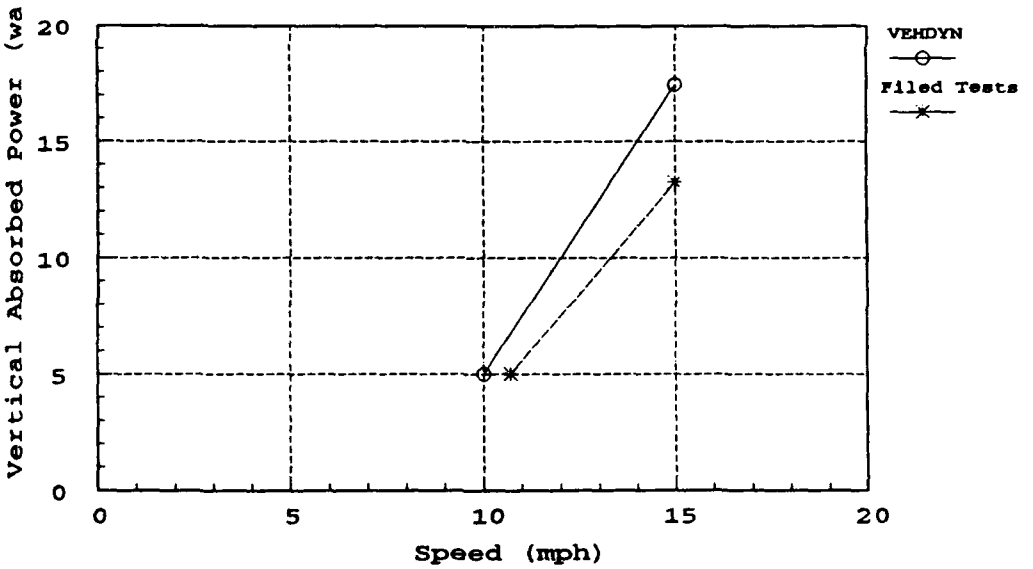

Figure 5.70. Average vertical absorbed power of point on the driver's seat as vehicle passed over a 2.41-in. rms ride course at different speeds

The resultant speed versus rms roughness at 6 watts of AP_{vt} is shown in Figure 5.71. The plot shows the same trends seen in the DADS comparison. As the rms roughness increased the vehicle was forced to reduce its speed. As shown in Figure 5.71, the amount of predicted speed reduction necessary to maintain a 6 watt level over the increasing rms values ranged from 22 to 10 mph. In comparing the measured and predicted speeds, the difference over the range of rms values was smaller for the higher rms values. This followed the same trends seen in the shock tests and the FFT's of the ride test results. As the amount of input energy to the vehicle increased, through higher obstacles and rougher ride courses, so did the correlation between the measured and predicted results.

The test data presented in Figure 5.72 shows the relationship between the measured and predicted AP_{vt} on the driver's seat as the vehicle passed over the different ride courses at various speeds. As shown in Figure 5.72, the predictions parallel the measured on the high side with several falling on the measured slope. This was a better correlation than seen in the shock tests.

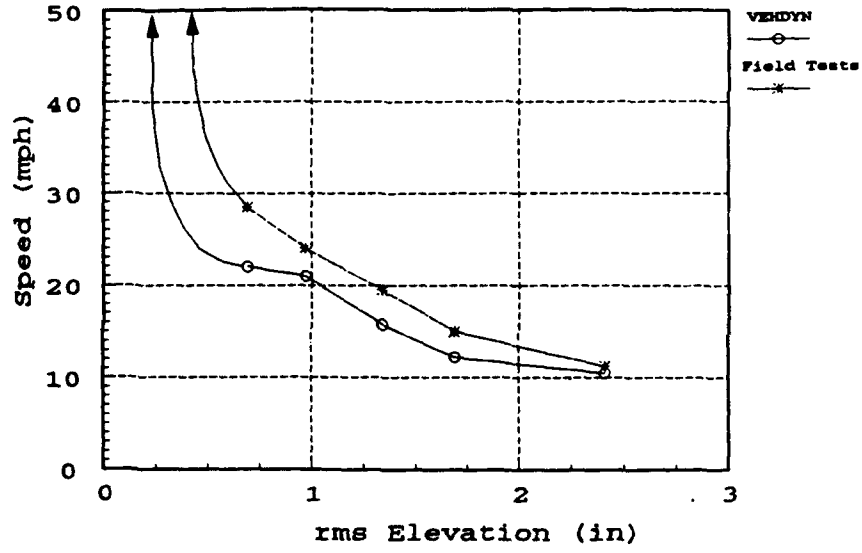

Figure 5.71. Speeds which generate 6 watts of average vertical absorbed power on the driver's seat as the vehicle passed over different ride courses

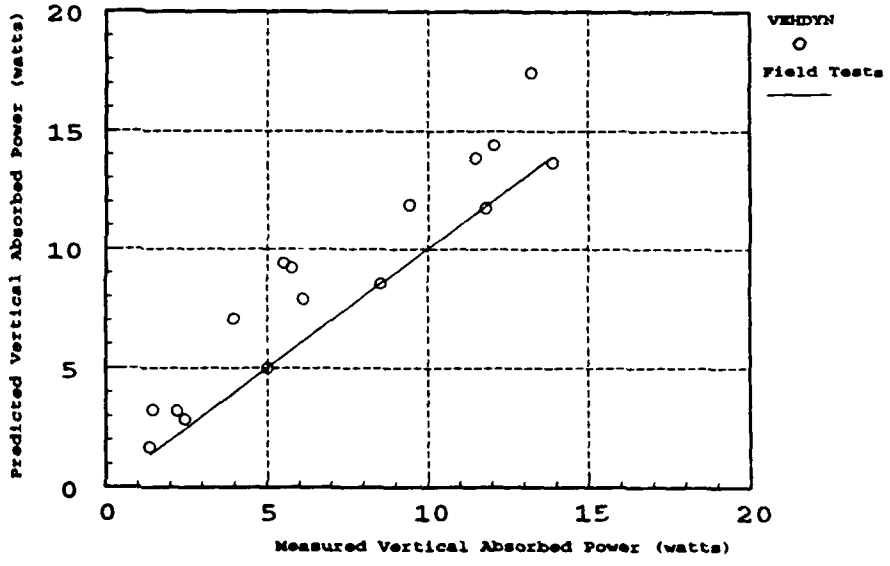

Figure 5.72. VEHDYN predicted average vertical absorbed power versus measured average vertical absorbed power on the driver's seat as vehicle passed over different ride courses

Table 5.4. VEHDYN Predicted Vertical Absorbed Power

Test Number	rms Value in.	Test Speed mph	Model Speed mph	Field Test AP_{vt}	VEHDYN Test AP_{vt}
553	0.69	14.5	15.0	1.45	3.25
557	0.69	24.1	25.0	3.95	7.06
561	0.69	33.7	30.0	8.55	8.55
565	0.69	43.2	40.0	11.81	11.74
541	0.97	14.5	15.0	2.20	3.22
543	0.97	24.5	25.0	6.12	7.89
544	0.97	28.7	30.0	9.43	11.88
546	0.97	39.1	40.0	13.91	13.66
578	1.34	10.4	10.0	1.35	1.69
580	1.34	19.5	20.0	5.75	9.21
582	1.34	24.7	25.0	11.49	13.86
570	1.69	10.2	10.0	2.44	2.86
571	1.69	14.4	15.0	5.50	9.40
573	1.69	20.9	20.0	12.07	14.40
588	2.41	10.7	10.0	5.01	5.00
589	2.41	15.0	15.0	13.23	17.45

5.3.4 Ride Test Conclusions

The ride test analysis revealed very similar trends to those developed in the shock test analysis. As the amount of energy into the system increased, in the from of rougher ride courses, the correlation between the measured and predicted improved. This would follow the assumption that in the actual system a certain level of energy was absorbed by the vehicle's flexing and bushing displacements. As the energy level into the system increased, the flexing of the chassis would reach its maximum along with the displacements of the bushings in the suspension components. The energy in the system above the saturation level would be seen in the resultant AP_{vt} levels. This also facilitates the possibility of inaccurate damper data. If the damper force data was too low, the predictions for lower level rms ride courses at faster speeds would also be on the low end, since the modeled suspension would absorb more of the energy, through larger suspension displacements, instead of transferring the energy to the chassis.

To determine the accuracy of the simulated ride tests, the 6 watt AP_{vt} curves were used to calculate the percent variation of the predicted and measured. The DADS model predicted, on average, a 69 percent accuracy, with a maximum low of 65 percent and maximum high of 80 percent. The VEHDYN model predicted, on average, a 84 percent accuracy,

with a maximum low of 77 percent and a maximum high of 93 percent.

5.4 Validation Conclusions and Recommendations

On the basis of the results of this study, the following conclusions are made:

a. Both dynamic codes provided sufficient design flexibility for creating and simulating vehicle dynamics.

b. Both models successfully simulated sprung mass vertical accelerations and pitch rates.

c. Both models successfully simulated sprung and unsprung mass frequency distributions, but tended to predict higher amplitudes than measured.

e. Both models successfully simulated shock and ride test trends.

f. Both models were similar in either over or under predicting dynamic responses.

g. Both models were sensitive to user supplied force element data.

h. The method used to characterize suspension damping was not appropriate for all simulations.

i. Field test speed fluctuations are not reproducible in the current vehicle models.

i. The differences between measured and predicted speeds influenced the relationship between the measured and predicted responses.

It is recommended that:

a. The DADS and VEHDYN codes be used for predicting vehicle dynamic responses.

b. The HMMWV models be used for shock and ride test analysis.

c. Research be conducted to develop better methods of characterizing suspension damping forces for model use.

d. Research be conducted to develop methods to accurately simulate vehicle speed.

e. A sensitivity analysis of both HMMWV models be conducted.

CHAPTER 6

OBSERVATIONS

6.1 Future Model Validations

Field tests are normally performed with enough repetition to determine the variation in the measured data. The measured variation indicates a certain amount of inherent nonreproducibility within each test. To gain an understanding of model predictability relative to measured variations, future vehicle models should be validated stochastically.

6.2 Model Geometry

The amount of time required to construct the dynamic models varied greatly. The DADS vehicle model required approximately 6 weeks to create. Half of this time was used to calculate the suspension geometry from the chassis layout drawings. The remainder was needed to input the data and debug the model. The VEHDYN model required approximately one week to map the geometry, construct, and debug the model. The time saver in the VEHDYN model was the predesigned suspension components.

6.3 Computer CPU Time

Both the DADS and VEHDYN models were operated on comparable UNIX systems. For the shock test simulations the DADS model required 20 to 40 cpu minutes and the VEHDYN model required approximately 2 min. For ride test simulations, the DADS model required approximately 4 to 5 hrs and the VEHDYN required approximately 5 min. The cpu time difference can be attributed to the complexity of the DADS model. Where the VEHDYN model was accounting for a 3 body, 4 DOF system, the DADS model was determining the dynamics of a 13 body, 10 DOF system.

6.4 Model Uses

Since it has been shown from the results of this study that both models were capable of simulating vehicle dynamics, the appropriate use of each model is an important consideration.

The VEHDYN model was developed specifically for simulating planar vehicle motion. The basic programming concept was to provide a quick and reliable method for determining the planar dynamics of a vehicle system. Since the model operates in a two dimensional environment, the potentials of the model are limited to a planar analysis. This places the VEHDYN in a limited use category.

The amount of effort required to generate the DADS model will pay off in the types of analyses the spatial

model offers. Once a model has been created and validated in the spatial environment, a larger variety of simulations can be performed such as, steering and roll stability. Also, each modeled component is available for dynamic analysis.

One area of joint effort between the two models would be the use of the VEHDYN model to perform initial validations on basic vehicle components such as: tire spring rates, suspension spring rates and damper forces, body inertias, etc. and then transform the data to the spatial model geometry. This would reduce the time required in making DADS validation iterations.

REFERENCES

Beck, R. R., Schmuhl, J. C., March-April 1992. "Role of Simulation at the Army Tank-Automotive Command," pg. 33-35, Army Research, Development and Acquisition Bulletin, Headquarters Department of the Army, Washington D.C.

Bechert, A. B., May 1991. "Hugging the Track with Dynamic Analysis", pg. 32-33, Computer-Aided Engineering, San Diego, CA.

CADSi, 1991. DADS User's Manual, Computer Aided Design Software, Inc., Oakdale, IA.

Creighton, D. C., 1986. "Revised Vehicle Dynamics Module: User's Guide for Computer Program VEHDYN II," Technical Report SL-86-9, US Army Engineer Waterways Experiment Station, MS.

Grohnke, D., Kalell-Fox, S., August 1991. "Navistar mobilizes design improvements by simulating steering system dynamics", pg. 26-28, Automotive Engineering.

Haug, E. J., 1989. Computer Aided Kinematics and Dynamics of Mechanical Systems, Allyn and Beacon, Needham Heights, MA.

Jones, R. A., 1992. "Mobility Performance Tests of the High Mobility Multipurpose Wheeled Vehicle with a Central Tire Inflation System and Towed Trailer," Technical Report GL-92-12, US Army Engineer Waterways Experiment Station, Vicksburg, MS.

Lessem, A. S., 1968. "Dynamics of Wheeled Vehicles, Report 1, A Mathematical Model for the Traversal of Rigid Obstacles by a Pneumatic Tire," Technical Report M-68-1, US Army Engineer Waterways Experiment Station, Vicksburg, MS.

Lins, W. F., 1972. "Human Vibration Response Measurements," Technical Report 11551, US Army Tank-Automotive Command, Warren, MI.

McGill University, 1982. "NATO Reference Mobility Model, Edition 1, Vehicle Dynamics Module," Serial #25SU78-00254, McGill University, Geotechnical Research Centre, Montreal, PQ, Canada.

Murphy, N. R., Ahlvin, R. B., 1976. "AMC-74 Vehicle Dynamics Module," Technical Report M-76-1, US Army Waterways Experiment Station, Vicksburg, Ms.

Murphy, N. R., 1981, "Armored Combat Vehicle Technology (ACVT) Program," Technical Report GL-81-13, US Army Waterways Experiment Station, Vicksburg, MS.

Murphy, N. R., Lessem, A. S., 1987. "Stress in M1 Tank Tracks, Report 1, Initial Field and Simulation Studies," Technical Report GL-87-7, US Army Waterways Experiment Station, Vicksburg, MS.

Pradko, F., Lee, R., Kaliza, V., 1966. "Theory of Human Vibration Response," Presentation at the Winter Annual Meeting and Energy Systems Exposition, American Society of Mechanical Engineers, New York, NY.

Stearns, S. D., 1975. Digital Signal Analysis, Hayden Book Company, Inc., Rochelle Park, NJ.

Van Deusen, B. D., 1965 (Mar). "A Study of the Vehicle Ride Dynamics Aspect of Ground Mobility MERS Project," Vol 1, prepared by Chrysler Corporation for US Army Engineer Waterways Experiment Station, Vicksburg, MS.

APPENDIX

A.1 DADS Vehicle Input File

```
ANALYSIS
CREATE SYSTEM.DATA
   UNITS                        := 'INCHES'
   ANALYSIS.TYPE                := 'DYNAMIC'
   STARTING.TIME                := '0.0'
   ENDING.TIME                  := '5.0'
   PRINT.INTERVAL               := '0.002'
   GRAVITY.SEA.LEVEL            := '386.088'
   X.GRAVITY                    := '0.0'
   Y.GRAVITY                    := '0.0'
   Z.GRAVITY                    := '-1.0'
   SCALE.GRAVITY.COEF           := '1.0'
   MATRIX.OPERATIONS            := 'SPARSE'
   REDUNDANCY.CHECK             := 'TRUE'
   LU.TOL                       := '1.0D-12'
   ASSEMBLY.TOL                 := '1.0D-3'
   BYPASS.ASSEMBLY              := 'FALSE'
   OUTPUT.FILE                  := 'BINARY_ONLY'
   REFERENCE.FRAME              := 'GLOBAL'
   DEBUG.FLAG                   := 'FALSE'
UP
CREATE DYNAMIC.DATA
   REACTION.FORCES              := 'FALSE'
   FORCE.COORDINATES            := 'GLOBAL'
   PRINT.METHOD                 := 'INTERPOLATED'
   MAX.INT.STEP                 := '0.001'
   SOLUTION.TOL                 := '0.001'
   INTEGRATION.TOL              := '0.0001'
   METHOD.INTEGRATION           := 'PECE'
   PRINT.FREQ                   := '0'
UP
UP
CONSTRAINTS
CREATE DISTANCE.CONSTRAINT
   NAME                         := 'RAD-ROD.RL'
   BODY.1.NAME                  := 'CHASSIS'
   BODY.2.NAME                  := 'WHEEL.RL'
   P.ON.BODY.1                  := ( -16.380, -161.980, 33.080 )
   P.ON.BODY.2                  := ( -32.327, -164.066, 30.405 )
   Q.ON.BODY.1                  := ( -16.380, -161.980, 34.080 )
   Q.ON.BODY.2                  := ( -32.327, -164.066, 31.405 )
```

```
   R.ON.BODY.1                := ( -15.380, -161.980, 33.080 )
   R.ON.BODY.2                := ( -31.327, -164.066, 30.405 )
   DISTANCE                   := '16.303798023773'
   NODE.1                     := '0'
   NODE.2                     := '0'
UP
CREATE DISTANCE.CONSTRAINT
   NAME                       := 'RAD-ROD.RR'
   BODY.1.NAME                := 'CHASSIS'
   BODY.2.NAME                := 'WHEEL.RR'
   P.ON.BODY.1                := ( 16.380, -161.980, 33.080 )
   P.ON.BODY.2                := ( 32.327, -164.066, 30.405 )
   Q.ON.BODY.1                := ( 16.380, -161.980, 34.080 )
   Q.ON.BODY.2                := ( 32.327, -164.066, 31.405 )
   R.ON.BODY.1                := ( 17.380, -161.980, 33.080 )
   R.ON.BODY.2                := ( 33.327, -164.066, 30.405 )
   DISTANCE                   := '16.303798023773'
   NODE.1                     := '0'
   NODE.2                     := '0'
UP
CREATE DISTANCE.CONSTRAINT
   NAME                       := 'Tierod.FL'
   BODY.1.NAME                := 'CHASSIS'
   BODY.2.NAME                := 'WHEEL.FL'
   P.ON.BODY.1                := ( -17.655, -47.635, 32.905 )
   P.ON.BODY.2                := ( -32.327, -44.702, 30.127 )
   Q.ON.BODY.1                := ( -17.655, -47.635, 33.905 )
   Q.ON.BODY.2                := ( -32.327, -44.702, 31.127 )
   R.ON.BODY.1                := ( -16.655, -47.635, 32.905 )
   R.ON.BODY.2                := ( -31.327, -44.702, 30.127 )
   DISTANCE                   := '15.217994513076'
   NODE.1                     := '0'
   NODE.2                     := '0'
UP
CREATE DISTANCE.CONSTRAINT
   NAME                       := 'Tierod.FR'
   BODY.1.NAME                := 'CHASSIS'
   BODY.2.NAME                := 'WHEEL.FR'
   P.ON.BODY.1                := ( 17.655, -47.635, 32.905 )
   P.ON.BODY.2                := ( 32.327, -44.702, 30.127 )
   Q.ON.BODY.1                := ( 17.655, -47.635, 33.905 )
   Q.ON.BODY.2                := ( 32.327, -44.702, 31.127 )
   R.ON.BODY.1                := ( 18.655, -47.635, 32.905 )
   R.ON.BODY.2                := ( 33.327, -44.702, 30.127 )
   DISTANCE                   := '15.21799453076'
   NODE.1                     := '0'
   NODE.2                     := '0'
UP
UP
FORCE
CREATE TIRE
```

```
   NAME                    := 'TIRE.FL'
   TIRE.BODY               := 'WHEEL.FL'
   CHASSIS.BODY            := 'CHASSIS'
   TYPE                    := 'INTERMEDIATE'
   P.ON.TIRE               := ( -35.815, -39.370, 29.735 )
   RADIUS                  := '18.150'
   ROLLING.RESISTANCE      := '0.0'
   DAMPING.CONSTANT        := '10.00'
   VERTICAL.STIFF          := '1800.00'
   LATERAL.STIFF           := '233.33'
   STEER.ANGLE             := '0.0'
   FRICTION.COEFF          := '0.8'
   CURVE.UTILITY           := 'NONE'
   CURVE.VERTICAL          := 'NONE'
   CURVE.TORQUE            := 'NONE'
   CURVE.STEER             := 'NONE'
   ANGULAR.UNITS           := 'DEGREES'
   ALIGN.COEFF             := '0.0'
UP
CREATE TIRE
   NAME                    := 'TIRE.FR'
   TIRE.BODY               := 'WHEEL.FR'
   CHASSIS.BODY            := 'CHASSIS'
   TYPE                    := 'INTERMEDIATE'
   P.ON.TIRE               := ( 35.815, -39.370, 29.735 )
   RADIUS                  := '18.150'
   ROLLING.RESISTANCE      := '0.0'
   DAMPING.CONSTANT        := '10.00'
   VERTICAL.STIFF          := '1800.00'
   LATERAL.STIFF           := '233.33'
   STEER.ANGLE             := '0.0'
   FRICTION.COEFF          := '0.8'
   CURVE.UTILITY           := 'NONE'
   CURVE.VERTICAL          := 'NONE'
   CURVE.TORQUE            := 'NONE'
   CURVE.STEER             := 'NONE'
   ANGULAR.UNITS           := 'DEGREES'
   ALIGN.COEFF             := '0.0'
UP
CREATE TIRE
   NAME                    := 'TIRE.RL'
   TIRE.BODY               := 'WHEEL.RL'
   CHASSIS.BODY            := 'CHASSIS'
   TYPE                    := 'INTERMEDIATE'
   P.ON.TIRE               := ( -35.815, -169.370, 29.735 )
   RADIUS                  := '18.150'
   ROLLING.RESISTANCE      := '0.0'
   DAMPING.CONSTANT        := '10.00'
   VERTICAL.STIFF          := '2000.00'
   LATERAL.STIFF           := '233.33'
   STEER.ANGLE             := '0.0'
```

```
   FRICTION.COEFF              := '0.8'
   CURVE.UTILITY               := 'NONE'
   CURVE.VERTICAL              := 'NONE'
   CURVE.TORQUE                := 'NONE'
   CURVE.STEER                 := 'NONE'
   ANGULAR.UNITS               := 'DEGREES'
   ALIGN.COEFF                 := '0.0'
UP
CREATE TIRE
   NAME                        := 'TIRE.RR'
   TIRE.BODY                   := 'WHEEL.RR'
   CHASSIS.BODY                := 'CHASSIS'
   TYPE                        := 'INTERMEDIATE'
   P.ON.TIRE                   := ( 35.815, -169.370, 29.735 )
   RADIUS                      := '18.150'
   ROLLING.RESISTANCE          := '0.0'
   DAMPING.CONSTANT            := '10.00'
   VERTICAL.STIFF              := '2000.00'
   LATERAL.STIFF               := '233.33'
   STEER.ANGLE                 := '0.0'
   FRICTION.COEFF              := '0.8'
   CURVE.UTILITY               := 'NONE'
   CURVE.VERTICAL              := 'NONE'
   CURVE.TORQUE                := 'NONE'
   CURVE.STEER                 := 'NONE'
   ANGULAR.UNITS               := 'DEGREES'
   ALIGN.COEFF                 := '0.0'
UP
CREATE TSDA
   NAME                        := 'SPRING.FL'
   BODY.1.NAME                 := 'CHASSIS'
   BODY.2.NAME                 := 'ARM.LFL'
   SPRING.CONSTANT             := '0.0'
   FREE.LENGTH.SPRING          := '13.36'
   DAMPING.COEFFICIENT         := '0.0'
   ACTUATOR.FORCE              := '0.0'
   P.ON.BODY.1                 := ( -20.070, -33.685, 38.545 )
   P.ON.BODY.2                 := ( -21.385, -33.953, 28.935 )
   Q.ON.BODY.1                 := ( -20.070, -33.685, 39.545 )
   Q.ON.BODY.2                 := ( -21.385, -33.953, 29.935 )
   R.ON.BODY.1                 := ( -19.070, -33.685, 38.545 )
   R.ON.BODY.2                 := ( -20.385, -33.953, 28.935 )
   CURVE.SPRING                := 'F_SPRING.CU'
   CURVE.DAMPER                := 'NONE'
   CURVE.ACTUATOR              := 'NONE'
   NODE.1                      := '0'
   NODE.2                      := '0'
   TYPE                        := 'BIDIRECTIONAL'
UP
CREATE TSDA
   NAME                        := 'SPRING.FR'
```

```
    BODY.1.NAME                 := 'CHASSIS'
    BODY.2.NAME                 := 'ARM.LFR'
    SPRING.CONSTANT             := '0.0'
    FREE.LENGTH.SPRING          := '13.36'
    DAMPING.COEFFICIENT         := '0.0'
    ACTUATOR.FORCE              := '0.0'
    P.ON.BODY.1                 := ( 20.070, -33.685, 38.545 )
    P.ON.BODY.2                 := ( 21.385, -33.953, 28.935 )
    Q.ON.BODY.1                 := ( 20.070, -33.685, 39.545 )
    Q.ON.BODY.2                 := ( 21.385, -33.953, 29.935 )
    R.ON.BODY.1                 := ( 21.070, -33.685, 38.545 )
    R.ON.BODY.2                 := ( 22.385, -33.953, 28.935 )
    CURVE.SPRING                := 'F_SPRING.CU'
    CURVE.DAMPER                := 'NONE'
    CURVE.ACTUATOR              := 'NONE'
    NODE.1                      := '0'
    NODE.2                      := '0'
    TYPE                        := 'BIDIRECTIONAL'
UP
CREATE TSDA
    NAME                        := 'SPRING.RL'
    BODY.1.NAME                 := 'CHASSIS'
    BODY.2.NAME                 := 'ARM.LRL'
    SPRING.CONSTANT             := '0.0'
    FREE.LENGTH.SPRING          := '12.43'
    DAMPING.COEFFICIENT         := '0.0'
    ACTUATOR.FORCE              := '0.0'
    P.ON.BODY.1                 := ( -20.070, -174.865, 38.545 )
    P.ON.BODY.2                 := ( -21.385, -174.597, 28.935 )
    Q.ON.BODY.1                 := ( -20.070, -174.865, 39.545 )
    Q.ON.BODY.2                 := ( -21.385, -174.597, 29.935 )
    R.ON.BODY.1                 := ( -19.070, -174.865, 38.545 )
    R.ON.BODY.2                 := ( -20.385, -174.597, 28.935 )
    CURVE.SPRING                := 'R_SPRING.CU'
    CURVE.DAMPER                := 'NONE'
    CURVE.ACTUATOR              := 'NONE'
    NODE.1                      := '0'
    NODE.2                      := '0'
    TYPE                        := 'BIDIRECTIONAL'
UP
CREATE TSDA
    NAME                        := 'SPRING.RR'
    BODY.1.NAME                 := 'CHASSIS'
    BODY.2.NAME                 := 'ARM.LRR'
    SPRING.CONSTANT             := '0.0'
    FREE.LENGTH.SPRING          := '12.43'
    DAMPING.COEFFICIENT         := '0.0'
    ACTUATOR.FORCE              := '0.0'
    P.ON.BODY.1                 := ( 20.070, -174.865, 38.545 )
    P.ON.BODY.2                 := ( 21.385, -174.597, 28.935 )
    Q.ON.BODY.1                 := ( 20.070, -174.865, 39.545 )
```

```
    Q.ON.BODY.2                 := ( 21.385, -174.597, 29.935 )
    R.ON.BODY.1                 := ( 21.070, -174.865, 38.545 )
    R.ON.BODY.2                 := ( 22.385, -174.597, 28.935 )
    CURVE.SPRING                := 'R_SPRING.CU'
    CURVE.DAMPER                := 'NONE'
    CURVE.ACTUATOR              := 'NONE'
    NODE.1                      := '0'
    NODE.2                      := '0'
    TYPE                        := 'BIDIRECTIONAL'
UP
CREATE TSDA
    NAME                        := 'SHOCK.FL'
    BODY.1.NAME                 := 'CHASSIS'
    BODY.2.NAME                 := 'ARM.LFL'
    SPRING.CONSTANT             := '0.0'
    FREE.LENGTH.SPRING          := '0.0'
    DAMPING.COEFFICIENT         := '0.0'
    ACTUATOR.FORCE              := '0.0'
    P.ON.BODY.1                 := ( -19.598, -33.685, 43.492 )
    P.ON.BODY.2                 := ( -21.415, -33.953, 29.259 )
    Q.ON.BODY.1                 := ( -19.598, -33.685, 44.492 )
    Q.ON.BODY.2                 := ( -21.415, -33.953, 30.259 )
    R.ON.BODY.1                 := ( -18.598, -33.685, 43.492 )
    R.ON.BODY.2                 := ( -20.415, -33.953, 29.259 )
    CURVE.SPRING                := 'NONE'
    CURVE.DAMPER                := 'F_DAMP.CU'
    CURVE.ACTUATOR              := 'NONE'
    NODE.1                      := '0'
    NODE.2                      := '0'
    TYPE                        := 'BIDIRECTIONAL'
UP
CREATE TSDA
    NAME                        := 'SHOCK.FR'
    BODY.1.NAME                 := 'CHASSIS'
    BODY.2.NAME                 := 'ARM.LFR'
    SPRING.CONSTANT             := '0.0'
    FREE.LENGTH.SPRING          := '0.0'
    DAMPING.COEFFICIENT         := '0.0'
    ACTUATOR.FORCE              := '0.0'
    P.ON.BODY.1                 := ( 19.598, -33.685, 43.492 )
    P.ON.BODY.2                 := ( 21.415, -33.953, 29.259 )
    Q.ON.BODY.1                 := ( 19.598, -33.685, 44.492 )
    Q.ON.BODY.2                 := ( 21.415, -33.953, 30.259 )
    R.ON.BODY.1                 := ( 20.598, -33.685, 43.492 )
    R.ON.BODY.2                 := ( 22.415, -33.953, 29.259 )
    CURVE.SPRING                := 'NONE'
    CURVE.DAMPER                := 'F_DAMP.CU'
    CURVE.ACTUATOR              := 'NONE'
    NODE.1                      := '0'
    NODE.2                      := '0'
    TYPE                        := 'BIDIRECTIONAL'
```

```
UP
CREATE TSDA
   NAME                    := 'SHOCK.RL'
   BODY.1.NAME             := 'CHASSIS'
   BODY.2.NAME             := 'ARM.LRL'
   SPRING.CONSTANT         := '0.0'
   FREE.LENGTH.SPRING      := '0.0'
   DAMPING.COEFFICIENT     := '0.0'
   ACTUATOR.FORCE          := '0.0'
   P.ON.BODY.1             := ( -19.598, -174.865, 43.492 )
   P.ON.BODY.2             := ( -21.415, -174.597, 29.259 )
   Q.ON.BODY.1             := ( -19.598, -174.865, 44.492 )
   Q.ON.BODY.2             := ( -21.415, -174.597, 30.259 )
   R.ON.BODY.1             := ( -18.598, -174.865, 43.492 )
   R.ON.BODY.2             := ( -20.415, -174.597, 29.259 )
   CURVE.SPRING            := 'NONE'
   CURVE.DAMPER            := 'R_DAMP.CU'
   CURVE.ACTUATOR          := 'NONE'
   NODE.1                  := '0'
   NODE.2                  := '0'
   TYPE                    := 'BIDIRECTIONAL'
UP
CREATE TSDA
   NAME                    := 'SHOCK.RR'
   BODY.1.NAME             := 'CHASSIS'
   BODY.2.NAME             := 'ARM.LRR'
   SPRING.CONSTANT         := '0.0'
   FREE.LENGTH.SPRING      := '0.0'
   DAMPING.COEFFICIENT     := '0.0'
   ACTUATOR.FORCE          := '0.0'
   P.ON.BODY.1             := ( 19.598, -174.865, 43.492 )
   P.ON.BODY.2             := ( 21.415, -174.597, 29.259 )
   Q.ON.BODY.1             := ( 19.598, -174.865, 44.492 )
   Q.ON.BODY.2             := ( 21.415, -174.597, 30.259 )
   R.ON.BODY.1             := ( 20.598, -174.865, 43.492 )
   R.ON.BODY.2             := ( 22.415, -174.597, 29.259 )
   CURVE.SPRING            := 'NONE'
   CURVE.DAMPER            := 'R_DAMP.CU'
   CURVE.ACTUATOR          := 'NONE'
   NODE.1                  := '0'
   NODE.2                  := '0'
   TYPE                    := 'BIDIRECTIONAL'
UP
UP
JOINTS
CREATE REVOLUTE.JOINT
   NAME                    := 'REV.LFL'
   BODY.1.NAME             := 'CHASSIS'
   BODY.2.NAME             := 'ARM.LFL'
   P.ON.BODY.1             := ( -12.09, -37.78, 30.770 )
   P.ON.BODY.2             := ( -12.09, -37.78, 30.770 )
```

```
   Q.ON.BODY.1                := ( -12.09, -36.78, 30.770 )
   Q.ON.BODY.2                := ( -12.09, -36.78, 30.770 )
   R.ON.BODY.1                := ( -11.09, -37.78, 30.770 )
   R.ON.BODY.2                := ( -11.09, -37.78, 30.770 )
   NODE.1                     := '0'
   NODE.2                     := '0'
UP
CREATE REVOLUTE.JOINT
   NAME                       := 'REV.LFR'
   BODY.1.NAME                := 'CHASSIS'
   BODY.2.NAME                := 'ARM.LFR'
   P.ON.BODY.1                := ( 12.09, -37.78, 30.770 )
   P.ON.BODY.2                := ( 12.09, -37.78, 30.770 )
   Q.ON.BODY.1                := ( 12.09, -36.78, 30.770 )
   Q.ON.BODY.2                := ( 12.09, -36.78, 30.770 )
   R.ON.BODY.1                := ( 13.09, -37.78, 30.770 )
   R.ON.BODY.2                := ( 13.09, -37.78, 30.770 )
   NODE.1                     := '0'
   NODE.2                     := '0'
UP
CREATE REVOLUTE.JOINT
   NAME                       := 'REV.LRL'
   BODY.1.NAME                := 'CHASSIS'
   BODY.2.NAME                := 'ARM.LRL'
   P.ON.BODY.1                := ( -12.09, -170.77, 30.770 )
   P.ON.BODY.2                := ( -12.09, -170.77, 30.770 )
   Q.ON.BODY.1                := ( -12.09, -169.77, 30.770 )
   Q.ON.BODY.2                := ( -12.09, -169.77, 30.770 )
   R.ON.BODY.1                := ( -11.09, -170.77, 30.770 )
   R.ON.BODY.2                := ( -11.09, -170.77, 30.770 )
   NODE.1                     := '0'
   NODE.2                     := '0'
UP
CREATE REVOLUTE.JOINT
   NAME                       := 'REV.LRR'
   BODY.1.NAME                := 'CHASSIS'
   BODY.2.NAME                := 'ARM.LRR'
   P.ON.BODY.1                := ( 12.09, -170.77, 30.770 )
   P.ON.BODY.2                := ( 12.09, -170.77, 30.770 )
   Q.ON.BODY.1                := ( 12.09, -169.77, 30.770 )
   Q.ON.BODY.2                := ( 12.09, -169.77, 30.770 )
   R.ON.BODY.1                := ( 13.09, -170.77, 30.770 )
   R.ON.BODY.2                := ( 13.09, -170.77, 30.770 )
   NODE.1                     := '0'
   NODE.2                     := '0'
UP
CREATE REVOLUTE.JOINT
   NAME                       := 'REV.UFL'
   BODY.1.NAME                := 'CHASSIS'
   BODY.2.NAME                := 'ARM.UFL'
   P.ON.BODY.1                := ( -18.183, -44.003, 39.435 )
```

```
   P.ON.BODY.2                := ( -18.183, -44.003, 39.435 )
   Q.ON.BODY.1                := ( -17.558, -39.670, 40.400 )
   Q.ON.BODY.2                := ( -17.558, -39.670, 40.400 )
   R.ON.BODY.1                := ( -17.193, -44.146, 39.435 )
   R.ON.BODY.2                := ( -17.193, -44.146, 39.435 )
   NODE.1                     := '0'
   NODE.2                     := '0'
UP
CREATE REVOLUTE.JOINT
   NAME                       := 'REV.UFR'
   BODY.1.NAME                := 'CHASSIS'
   BODY.2.NAME                := 'ARM.UFR'
   P.ON.BODY.1                := ( 18.183, -44.003, 39.435 )
   P.ON.BODY.2                := ( 18.183, -44.003, 39.435 )
   Q.ON.BODY.1                := ( 17.558, -39.670, 40.400 )
   Q.ON.BODY.2                := ( 17.558, -39.670, 40.400 )
   R.ON.BODY.1                := ( 19.173, -43.860, 39.435 )
   R.ON.BODY.2                := ( 19.173, -43.860, 39.435 )
   NODE.1                     := '0'
   NODE.2                     := '0'
UP
CREATE REVOLUTE.JOINT
   NAME                       := 'REV.URL'
   BODY.1.NAME                := 'CHASSIS'
   BODY.2.NAME                := 'ARM.URL'
   P.ON.BODY.1                := ( -18.195, -162.380, 39.655 )
   P.ON.BODY.2                := ( -18.195, -162.380, 39.655 )
   Q.ON.BODY.1                := ( -18.195, -161.380, 39.655 )
   Q.ON.BODY.2                := ( -18.195, -161.380, 39.655 )
   R.ON.BODY.1                := ( -17.195, -162.380, 39.655 )
   R.ON.BODY.2                := ( -17.195, -162.380, 39.655 )
   NODE.1                     := '0'
   NODE.2                     := '0'
UP
CREATE REVOLUTE.JOINT
   NAME                       := 'REV.URR'
   BODY.1.NAME                := 'CHASSIS'
   BODY.2.NAME                := 'ARM.URR'
   P.ON.BODY.1                := ( 18.195, -162.380, 39.655 )
   P.ON.BODY.2                := ( 18.195, -162.380, 39.655 )
   Q.ON.BODY.1                := ( 18.195, -161.380, 39.655 )
   Q.ON.BODY.2                := ( 18.195, -161.380, 39.655 )
   R.ON.BODY.1                := ( 19.195, -162.380, 39.655 )
   R.ON.BODY.2                := ( 19.195, -162.380, 39.655 )
   NODE.1                     := '0'
   NODE.2                     := '0'
UP
CREATE SPHERICAL.JOINT
   NAME                       := 'SPH.LFL'
   BODY.1.NAME                := 'ARM.LFL'
   BODY.2.NAME                := 'WHEEL.FL'
```

```
   P.ON.BODY.1              := ( -30.965, -39.180, 26.120 )
   P.ON.BODY.2              := ( -30.965, -39.180, 26.120 )
   Q.ON.BODY.1              := ( -30.757, -39.232, 27.097 )
   Q.ON.BODY.2              := ( -28.170, -39.868, 39.254 )
   R.ON.BODY.1              := ( -31.943, -39.180, 26.328 )
   R.ON.BODY.2              := ( -44.099, -39.180, 28.915 )
   NODE.1                   := '0'
   NODE.2                   := '0'
UP
CREATE SPHERICAL.JOINT
   NAME                     := 'SPH.LFR'
   BODY.1.NAME              := 'ARM.LFR'
   BODY.2.NAME              := 'WHEEL.FR'
   P.ON.BODY.1              := ( 30.965, -39.180, 26.120 )
   P.ON.BODY.2              := ( 30.965, -39.180, 26.120 )
   Q.ON.BODY.1              := ( 30.757, -39.232, 27.097 )
   Q.ON.BODY.2              := ( 28.170, -39.868, 39.254 )
   R.ON.BODY.1              := ( 31.943, -39.180, 26.328 )
   R.ON.BODY.2              := ( 44.099, -39.180, 28.915 )
   NODE.1                   := '0'
   NODE.2                   := '0'
UP
CREATE SPHERICAL.JOINT
   NAME                     := 'SPH.LRL'
   BODY.1.NAME              := 'ARM.LRL'
   BODY.2.NAME              := 'WHEEL.RL'
   P.ON.BODY.1              := ( -30.965, -169.370, 26.120 )
   P.ON.BODY.2              := ( -30.965, -169.370, 26.120 )
   Q.ON.BODY.1              := ( -30.757, -169.422, 27.097 )
   Q.ON.BODY.2              := ( -28.170, -169.370, 39.270 )
   R.ON.BODY.1              := ( -31.943, -169.370, 26.328 )
   R.ON.BODY.2              := ( -44.115, -169.370, 28.915 )
   NODE.1                   := '0'
   NODE.2                   := '0'
UP
CREATE SPHERICAL.JOINT
   NAME                     := 'SPH.LRR'
   BODY.1.NAME              := 'ARM.LRR'
   BODY.2.NAME              := 'WHEEL.RR'
   P.ON.BODY.1              := ( 30.965, -169.370, 26.120 )
   P.ON.BODY.2              := ( 30.965, -169.370, 26.120 )
   Q.ON.BODY.1              := ( 30.757, -169.422, 27.097 )
   Q.ON.BODY.2              := ( 28.170, -169.370, 39.270 )
   R.ON.BODY.1              := ( 31.943, -169.370, 26.328 )
   R.ON.BODY.2              := ( 44.115, -169.370, 28.915 )
   NODE.1                   := '0'
   NODE.2                   := '0'
UP
CREATE SPHERICAL.JOINT
   NAME                     := 'SPH.UFL'
   BODY.1.NAME              := 'ARM.UFL'
```

```
   BODY.2.NAME                 := 'WHEEL.FL'
   P.ON.BODY.1                 := ( -28.170, -39.868, 39.254 )
   P.ON.BODY.2                 := ( -28.170, -39.868, 39.254 )
   Q.ON.BODY.1                 := ( -27.962, -39.920, 40.231 )
   Q.ON.BODY.2                 := ( -25.375, -40.556, 52.388 )
   R.ON.BODY.1                 := ( -29.148, -39.868, 39.462 )
   R.ON.BODY.2                 := ( -41.304, -39.868, 42.049 )
   NODE.1                      := '0'
   NODE.2                      := '0'
UP
CREATE SPHERICAL.JOINT
   NAME                        := 'SPH.UFR'
   BODY.1.NAME                 := 'ARM.UFR'
   BODY.2.NAME                 := 'WHEEL.FR'
   P.ON.BODY.1                 := ( 28.170, -39.868, 39.254 )
   P.ON.BODY.2                 := ( 28.170, -39.868, 39.254 )
   Q.ON.BODY.1                 := ( 27.962, -39.920, 40.231 )
   Q.ON.BODY.2                 := ( 25.375, -40.556, 52.388 )
   R.ON.BODY.1                 := ( 29.148, -39.868, 39.462 )
   R.ON.BODY.2                 := ( 41.304, -39.868, 42.049 )
   NODE.1                      := '0'
   NODE.2                      := '0'
UP
CREATE SPHERICAL.JOINT
   NAME                        := 'SPH.URL'
   BODY.1.NAME                 := 'ARM.URL'
   BODY.2.NAME                 := 'WHEEL.RL'
   P.ON.BODY.1                 := ( -28.170, -169.370, 39.270 )
   P.ON.BODY.2                 := ( -28.170, -169.370, 39.270 )
   Q.ON.BODY.1                 := ( -25.375, -169.370, 52.420 )
   Q.ON.BODY.2                 := ( -25.375, -169.370, 52.420 )
   R.ON.BODY.1                 := ( -41.320, -169.370, 42.065 )
   R.ON.BODY.2                 := ( -41.320, -169.370, 42.065 )
   NODE.1                      := '0'
   NODE.2                      := '0'
UP
CREATE SPHERICAL.JOINT
   NAME                        := 'SPH.URR'
   BODY.1.NAME                 := 'ARM.URR'
   BODY.2.NAME                 := 'WHEEL.RR'
   P.ON.BODY.1                 := ( 28.170, -169.370, 39.270 )
   P.ON.BODY.2                 := ( 28.170, -169.370, 39.270 )
   Q.ON.BODY.1                 := ( 25.375, -169.370, 52.420 )
   Q.ON.BODY.2                 := ( 25.375, -169.370, 52.420 )
   R.ON.BODY.1                 := ( 41.320, -169.370, 42.065 )
   R.ON.BODY.2                 := ( 41.320, -169.370, 42.065 )
   NODE.1                      := '0'
   NODE.2                      := '0'
UP
UP
CONTROLS
```

```
CREATE AMPLIFIER
   NAME                        := 'VEL_TO_FORCE'
   INPUT.NODE                  := 'VEL_DIFF'
   OUTPUT.NODE                 := 'VEL_FORCE'
   TYPE                        := 'CONSTANT'
   GAIN                        := '1000.0'
   CURVE.NAME                  := 'NONE'
UP
CREATE INPUT.FUNCTION
   NAME                        := 'VELOCITY_FEEDBACK'
   NODE.NAME                   := 'CHASSIS_VEL'
   TYPE                        := 'YD'
   BODY.1.NAME                 := 'CHASSIS'
   BODY.2.NAME                 := 'NONE'
   FUNCTION.PARAMETERS         := ( 0.0, 0.0, 0.0, 0.0 )
   P.ON.BODY.1                 := ( 0.0, 0.0, 0.0 )
   P.ON.BODY.2                 := ( 0.0, 0.0, 0.0 )
   Q.ON.BODY.1                 := ( 1.0, 0.0, 0.0 )
   Q.ON.BODY.2                 := ( 1.0, 0.0, 0.0 )
   CURVE.NAME                  := 'NONE'
   JOINT.NAME                  := 'NONE'
   FLEXIBLE.NODE.1             := '0'
   FLEXIBLE.NODE.2             := '0'
   ANGULAR.UNITS               := 'DEGREES'
   EXTNUM                      := '0'
   SAMPLE.RATE                 := '0.0'
   DIGITAL.FLAG                := 'FALSE'
   LINEAR.FLAG                 := 'FALSE'
UP
CREATE INPUT.FUNCTION
   NAME                        := 'REFERENCE_INPUT'
   NODE.NAME                   := 'VEL_REF'
   TYPE                        := 'POLYNOMIAL'
   BODY.1.NAME                 := 'NONE'
   BODY.2.NAME                 := 'NONE'
   FUNCTION.PARAMETERS         := ( 176.00, 0.0, 0.0, 0.0 )
   P.ON.BODY.1                 := ( 0.0, 0.0, 0.0 )
   P.ON.BODY.2                 := ( 0.0, 0.0, 0.0 )
   Q.ON.BODY.1                 := ( 1.0, 0.0, 0.0 )
   Q.ON.BODY.2                 := ( 1.0, 0.0, 0.0 )
   CURVE.NAME                  := 'NONE'
   JOINT.NAME                  := 'NONE'
   FLEXIBLE.NODE.1             := '0'
   FLEXIBLE.NODE.2             := '0'
   ANGULAR.UNITS               := 'DEGREES'
   EXTNUM                      := '0'
   SAMPLE.RATE                 := '0.0'
   DIGITAL.FLAG                := 'FALSE'
   LINEAR.FLAG                 := 'FALSE'
UP
CREATE OUTPUT
```

```
    NAME                        := 'OUTPUT_FORCE'
    OUTPUT.NODE                 := 'VEL_FORCE'
    TYPE                        := 'Y.FORCE'
    BODY.1.NAME                 := 'CHASSIS'
    BODY.2.NAME                 := 'NONE'
    P.ON.BODY.1                 := ( 0.0, 0.0, 0.0 )
    P.ON.BODY.2                 := ( 0.0, 0.0, 0.0 )
    JOINT.NAME                  := 'NONE'
    FLEXIBLE.NODE.1             := '0'
    FLEXIBLE.NODE.2             := '0'
UP
CREATE SUMMER
    NAME                        := 'VELOCITY_DIFFERENCE'
    OUTPUT.NODE                 := 'VEL_DIFF'
    INPUT.NODE.1                := 'CHASSIS_VEL'
    INPUT.NODE.2                := 'VEL_REF'
    INPUT.NODE.3                := 'NONE'
    COEFFICIENT.1               := '-'
    COEFFICIENT.2               := '+'
    COEFFICIENT.3               := '+'
UP
UP
CREATE BODY
    NAME                        := 'CHASSIS'
    CENTER.OF.GRAVITY           := ( 1.200, -97.070, 40.280 )
    TYPE.ANGULAR.COORD          := 'BRYANT'
    ANGLE.1                     := '0.0'
    ANGLE.2                     := '0.0'
    ANGLE.3                     := '0.0'
    FIXED.TO.GROUND             := 'FALSE'
    MASS                        := '11.835'
    INERTIA.XXL                 := '41300.0'
    INERTIA.YYL                 := '13900.0'
    INERTIA.ZZL                 := '52300.0'
    INERTIA.XYL                 := '0.0'
    INERTIA.XZL                 := '0.0'
    INERTIA.YZL                 := '0.0'
    XG.FORCE                    := '0.0'
    YG.FORCE                    := '0.0'
    ZG.FORCE                    := '0.0'
    XL.TORQUE                   := '0.0'
    YL.TORQUE                   := '0.0'
    ZL.TORQUE                   := '0.0'
    CURVE.XGF                   := 'NONE'
    CURVE.YGF                   := 'NONE'
    CURVE.ZGF                   := 'NONE'
    CURVE.XLT                   := 'NONE'
    CURVE.YLT                   := 'NONE'
    CURVE.ZLT                   := 'NONE'
    SIGN.E0                     := 'POSITIVE'
    ANGULAR.UNITS               := 'DEGREES'
```

```
   FLEXIBLE                  := 'FALSE'
   SUPERELEMENT              := 'FALSE'
UP
CREATE BODY
   NAME                      := 'ARM.LFL'
   CENTER.OF.GRAVITY         := ( -21.5275, -37.78, 28.445 )
   TYPE.ANGULAR.COORD        := 'BRYANT'
   ANGLE.1                   := '0.0'
   ANGLE.2                   := '-13.84'
   ANGLE.3                   := '0.0'
   FIXED.TO.GROUND           := 'FALSE'
   MASS                      := '0.0935'
   INERTIA.XXL               := '1.0'
   INERTIA.YYL               := '1.0'
   INERTIA.ZZL               := '1.0'
   INERTIA.XYL               := '0.0'
   INERTIA.XZL               := '0.0'
   INERTIA.YZL               := '0.0'
   XG.FORCE                  := '0.0'
   YG.FORCE                  := '0.0'
   ZG.FORCE                  := '0.0'
   XL.TORQUE                 := '0.0'
   YL.TORQUE                 := '0.0'
   ZL.TORQUE                 := '0.0'
   CURVE.XGF                 := 'NONE'
   CURVE.YGF                 := 'NONE'
   CURVE.ZGF                 := 'NONE'
   CURVE.XLT                 := 'NONE'
   CURVE.YLT                 := 'NONE'
   CURVE.ZLT                 := 'NONE'
   SIGN.E0                   := 'POSITIVE'
   ANGULAR.UNITS             := 'DEGREES'
   FLEXIBLE                  := 'FALSE'
   SUPERELEMENT              := 'FALSE'
UP
CREATE BODY
   NAME                      := 'ARM.LFR'
   CENTER.OF.GRAVITY         := ( 21.5275, -37.78, 28.445 )
   TYPE.ANGULAR.COORD        := 'BRYANT'
   ANGLE.1                   := '0.0'
   ANGLE.2                   := '13.84'
   ANGLE.3                   := '0.0'
   FIXED.TO.GROUND           := 'FALSE'
   MASS                      := '0.0932'
   INERTIA.XXL               := '1.0'
   INERTIA.YYL               := '1.0'
   INERTIA.ZZL               := '1.0'
   INERTIA.XYL               := '0.0'
   INERTIA.XZL               := '0.0'
   INERTIA.YZL               := '0.0'
   XG.FORCE                  := '0.0'
```

```
    YG.FORCE                    := '0.0'
    ZG.FORCE                    := '0.0'
    XL.TORQUE                   := '0.0'
    YL.TORQUE                   := '0.0'
    ZL.TORQUE                   := '0.0'
    CURVE.XGF                   := 'NONE'
    CURVE.YGF                   := 'NONE'
    CURVE.ZGF                   := 'NONE'
    CURVE.XLT                   := 'NONE'
    CURVE.YLT                   := 'NONE'
    CURVE.ZLT                   := 'NONE'
    SIGN.E0                     := 'POSITIVE'
    ANGULAR.UNITS               := 'DEGREES'
    FLEXIBLE                    := 'FALSE'
    SUPERELEMENT                := 'FALSE'
UP
CREATE BODY
    NAME                        := 'ARM.LRL'
    CENTER.OF.GRAVITY           := ( -21.5275, -170.77, 28.445 )
    TYPE.ANGULAR.COORD          := 'BRYANT'
    ANGLE.1                     := '0.0'
    ANGLE.2                     := '-13.84'
    ANGLE.3                     := '0.0'
    FIXED.TO.GROUND             := 'FALSE'
    MASS                        := '0.0932'
    INERTIA.XXL                 := '1.0'
    INERTIA.YYL                 := '1.0'
    INERTIA.ZZL                 := '1.0'
    INERTIA.XYL                 := '0.0'
    INERTIA.XZL                 := '0.0'
    INERTIA.YZL                 := '0.0'
    XG.FORCE                    := '0.0'
    YG.FORCE                    := '0.0'
    ZG.FORCE                    := '0.0'
    XL.TORQUE                   := '0.0'
    YL.TORQUE                   := '0.0'
    ZL.TORQUE                   := '0.0'
    CURVE.XGF                   := 'NONE'
    CURVE.YGF                   := 'NONE'
    CURVE.ZGF                   := 'NONE'
    CURVE.XLT                   := 'NONE'
    CURVE.YLT                   := 'NONE'
    CURVE.ZLT                   := 'NONE'
    SIGN.E0                     := 'POSITIVE'
    ANGULAR.UNITS               := 'DEGREES'
    FLEXIBLE                    := 'FALSE'
    SUPERELEMENT                := 'FALSE'
UP
CREATE BODY
    NAME                        := 'ARM.LRR'
    CENTER.OF.GRAVITY           := ( 21.5275, -170.77, 28.445 )
```

```
    TYPE.ANGULAR.COORD      := 'BRYANT'
    ANGLE.1                 := '0.0'
    ANGLE.2                 := '13.84'
    ANGLE.3                 := '0.0'
    FIXED.TO.GROUND         := 'FALSE'
    MASS                    := '0.0932'
    INERTIA.XXL             := '1.0'
    INERTIA.YYL             := '1.0'
    INERTIA.ZZL             := '1.0'
    INERTIA.XYL             := '0.0'
    INERTIA.XZL             := '0.0'
    INERTIA.YZL             := '0.0'
    XG.FORCE                := '0.0'
    YG.FORCE                := '0.0'
    ZG.FORCE                := '0.0'
    XL.TORQUE               := '0.0'
    YL.TORQUE               := '0.0'
    ZL.TORQUE               := '0.0'
    CURVE.XGF               := 'NONE'
    CURVE.YGF               := 'NONE'
    CURVE.ZGF               := 'NONE'
    CURVE.XLT               := 'NONE'
    CURVE.YLT               := 'NONE'
    CURVE.ZLT               := 'NONE'
    SIGN.E0                 := 'POSITIVE'
    ANGULAR.UNITS           := 'DEGREES'
    FLEXIBLE                := 'FALSE'
    SUPERELEMENT            := 'FALSE'
UP
CREATE BODY
    NAME                    := 'ARM.UFL'
    CENTER.OF.GRAVITY       := ( -23.1765, -41.935, 39.3445 )
    TYPE.ANGULAR.COORD      := 'BRYANT'
    ANGLE.1                 := '12.557'
    ANGLE.2                 := '0.0'
    ANGLE.3                 := '-8.209'
    FIXED.TO.GROUND         := 'FALSE'
    MASS                    := '0.0311'
    INERTIA.XXL             := '1.0'
    INERTIA.YYL             := '1.0'
    INERTIA.ZZL             := '1.0'
    INERTIA.XYL             := '0.0'
    INERTIA.XZL             := '0.0'
    INERTIA.YZL             := '0.0'
    XG.FORCE                := '0.0'
    YG.FORCE                := '0.0'
    ZG.FORCE                := '0.0'
    XL.TORQUE               := '0.0'
    YL.TORQUE               := '0.0'
    ZL.TORQUE               := '0.0'
    CURVE.XGF               := 'NONE'
```

```
    CURVE.YGF                   := 'NONE'
    CURVE.ZGF                   := 'NONE'
    CURVE.XLT                   := 'NONE'
    CURVE.YLT                   := 'NONE'
    CURVE.ZLT                   := 'NONE'
    SIGN.E0                     := 'POSITIVE'
    ANGULAR.UNITS               := 'DEGREES'
    FLEXIBLE                    := 'FALSE'
    SUPERELEMENT                := 'FALSE'
UP
CREATE BODY
    NAME                        := 'ARM.UFR'
    CENTER.OF.GRAVITY           := ( 23.1765, -41.935, 39.3445 )
    TYPE.ANGULAR.COORD          := 'BRYANT'
    ANGLE.1                     := '12.557'
    ANGLE.2                     := '0.00'
    ANGLE.3                     := '8.209'
    FIXED.TO.GROUND             := 'FALSE'
    MASS                        := '0.0311'
    INERTIA.XXL                 := '1.0'
    INERTIA.YYL                 := '1.0'
    INERTIA.ZZL                 := '1.0'
    INERTIA.XYL                 := '0.0'
    INERTIA.XZL                 := '0.0'
    INERTIA.YZL                 := '0.0'
    XG.FORCE                    := '0.0'
    YG.FORCE                    := '0.0'
    ZG.FORCE                    := '0.0'
    XL.TORQUE                   := '0.0'
    YL.TORQUE                   := '0.0'
    ZL.TORQUE                   := '0.0'
    CURVE.XGF                   := 'NONE'
    CURVE.YGF                   := 'NONE'
    CURVE.ZGF                   := 'NONE'
    CURVE.XLT                   := 'NONE'
    CURVE.YLT                   := 'NONE'
    CURVE.ZLT                   := 'NONE'
    SIGN.E0                     := 'POSITIVE'
    ANGULAR.UNITS               := 'DEGREES'
    FLEXIBLE                    := 'FALSE'
    SUPERELEMENT                := 'FALSE'
UP
CREATE BODY
    NAME                        := 'ARM.URL'
    CENTER.OF.GRAVITY           := (-23.1825, -165.875, 39.4625 )
    TYPE.ANGULAR.COORD          := 'BRYANT'
    ANGLE.1                     := '0.0'
    ANGLE.2                     := '-2.21'
    ANGLE.3                     := '0.0'
    FIXED.TO.GROUND             := 'FALSE'
    MASS                        := '0.0311'
```

```
    INERTIA.XXL              := '1.0'
    INERTIA.YYL              := '1.0'
    INERTIA.ZZL              := '1.0'
    INERTIA.XYL              := '0.0'
    INERTIA.XZL              := '0.0'
    INERTIA.YZL              := '0.0'
    XG.FORCE                 := '0.0'
    YG.FORCE                 := '0.0'
    ZG.FORCE                 := '0.0'
    XL.TORQUE                := '0.0'
    YL.TORQUE                := '0.0'
    ZL.TORQUE                := '0.0'
    CURVE.XGF                := 'NONE'
    CURVE.YGF                := 'NONE'
    CURVE.ZGF                := 'NONE'
    CURVE.XLT                := 'NONE'
    CURVE.YLT                := 'NONE'
    CURVE.ZLT                := 'NONE'
    SIGN.E0                  := 'POSITIVE'
    ANGULAR.UNITS            := 'DEGREES'
    FLEXIBLE                 := 'FALSE'
    SUPERELEMENT             := 'FALSE'
UP
CREATE BODY
    NAME                     := 'ARM.URR'
    CENTER.OF.GRAVITY        := ( 23.1825, -165.875, 39.4625 )
    TYPE.ANGULAR.COORD       := 'BRYANT'
    ANGLE.1                  := '0.0'
    ANGLE.2                  := '2.21'
    ANGLE.3                  := '0.0'
    FIXED.TO.GROUND          := 'FALSE'
    MASS                     := '0.0311'
    INERTIA.XXL              := '1.0'
    INERTIA.YYL              := '1.0'
    INERTIA.ZZL              := '1.0'
    INERTIA.XYL              := '0.0'
    INERTIA.XZL              := '0.0'
    INERTIA.YZL              := '0.0'
    XG.FORCE                 := '0.0'
    YG.FORCE                 := '0.0'
    ZG.FORCE                 := '0.0'
    XL.TORQUE                := '0.0'
    YL.TORQUE                := '0.0'
    ZL.TORQUE                := '0.0'
    CURVE.XGF                := 'NONE'
    CURVE.YGF                := 'NONE'
    CURVE.ZGF                := 'NONE'
    CURVE.XLT                := 'NONE'
    CURVE.YLT                := 'NONE'
    CURVE.ZLT                := 'NONE'
    SIGN.E0                  := 'POSITIVE'
```

```
    ANGULAR.UNITS              := 'DEGREES'
    FLEXIBLE                   := 'FALSE'
    SUPERELEMENT               := 'FALSE'
UP
CREATE BODY
    NAME                       := 'WHEEL.FL'
    CENTER.OF.GRAVITY          := ( -35.815, -39.37, 29.735 )
    TYPE.ANGULAR.COORD         := 'BRYANT'
    ANGLE.1                    := '0.0'
    ANGLE.2                    := '0.0'
    ANGLE.3                    := '-0.246'
    FIXED.TO.GROUND            := 'FALSE'
    MASS                       := '0.5047'
    INERTIA.XXL                := '1.0'
    INERTIA.YYL                := '1.0'
    INERTIA.ZZL                := '1.0'
    INERTIA.XYL                := '0.0'
    INERTIA.XZL                := '0.0'
    INERTIA.YZL                := '0.0'
    XG.FORCE                   := '0.0'
    YG.FORCE                   := '0.0'
    ZG.FORCE                   := '0.0'
    XL.TORQUE                  := '0.0'
    YL.TORQUE                  := '0.0'
    ZL.TORQUE                  := '0.0'
    CURVE.XGF                  := 'NONE'
    CURVE.YGF                  := 'NONE'
    CURVE.ZGF                  := 'NONE'
    CURVE.XLT                  := 'NONE'
    CURVE.YLT                  := 'NONE'
    CURVE.ZLT                  := 'NONE'
    SIGN.E0                    := 'POSITIVE'
    ANGULAR.UNITS              := 'DEGREES'
    FLEXIBLE                   := 'FALSE'
    SUPERELEMENT               := 'FALSE'
UP
CREATE BODY
    NAME                       := 'WHEEL.FR'
    CENTER.OF.GRAVITY          := ( 35.815, -39.37, 29.735 )
    TYPE.ANGULAR.COORD         := 'BRYANT'
    ANGLE.1                    := '0.0'
    ANGLE.2                    := '0.0'
    ANGLE.3                    := '0.246'
    FIXED.TO.GROUND            := 'FALSE'
    MASS                       := '0.5047'
    INERTIA.XXL                := '1.0'
    INERTIA.YYL                := '1.0'
    INERTIA.ZZL                := '1.0'
    INERTIA.XYL                := '0.0'
    INERTIA.XZL                := '0.0'
    INERTIA.YZL                := '0.0'
```

```
    XG.FORCE                    := '0.0'
    YG.FORCE                    := '0.0'
    ZG.FORCE                    := '0.0'
    XL.TORQUE                   := '0.0'
    YL.TORQUE                   := '0.0'
    ZL.TORQUE                   := '0.0'
    CURVE.XGF                   := 'NONE'
    CURVE.YGF                   := 'NONE'
    CURVE.ZGF                   := 'NONE'
    CURVE.XLT                   := 'NONE'
    CURVE.YLT                   := 'NONE'
    CURVE.ZLT                   := 'NONE'
     IGN.E0                     := 'POSITIVE'
    ANGULAR.UNITS               := 'DEGREES'
    FLEXIBLE                    := 'FALSE'
    SUPERELEMENT                := 'FALSE'
UP
CREATE BODY
    NAME                        := 'WHEEL.RL'
    CENTER.OF.GRAVITY           := ( -35.815, -169.37, 29.735 )
    TYPE.ANGULAR.COORD          := 'BRYANT'
    ANGLE.1                     := '0.0'
    ANGLE.2                     := '0.0'
    ANGLE.3                     := '0.246'
    FIXED.TO.GROUND             := 'FALSE'
    MASS                        := '0.5046'
    INERTIA.XXL                 := '1.0'
    INERTIA.YYL                 := '1.0'
    INERTIA.ZZL                 := '1.0'
    INERTIA.XYL                 := '0.0'
    INERTIA.XZL                 := '0.0'
    INERTIA.YZL                 := '0.0'
    XG.FORCE                    := '0.0'
    YG.FORCE                    := '0.0'
    ZG.FORCE                    := '0.0'
    XL.TORQUE                   := '0.0'
    YL.TORQUE                   := '0.0'
    ZL.TORQUE                   := '0.0'
    CURVE.XGF                   := 'NONE'
    CURVE.YGF                   := 'NONE'
    CURVE.ZGF                   := 'NONE'
    CURVE.XLT                   := 'NONE'
    CURVE.YLT                   := 'NONE'
    CURVE.ZLT                   := 'NONE'
    SIGN.E0                     := 'POSITIVE'
    ANGULAR.UNITS               := 'DEGREES'
    FLEXIBLE                    := 'FALSE'
    SUPERELEMENT                := 'FALSE'
UP
CREATE BODY
    NAME                        := 'WHEEL.RR'
```

```
   CENTER.OF.GRAVITY          := ( 35.815, -169.37, 29.735 )
   TYPE.ANGULAR.COORD         := 'BRYANT'
   ANGLE.1                    := '0.0'
   ANGLE.2                    := '0.0'
   ANGLE.3                    := '-0.246'
   FIXED.TO.GROUND            := 'FALSE'
   MASS                       := '0.5046'
   INERTIA.XXL                := '1.0'
   INERTIA.YYL                := '1.0'
   INERTIA.ZZL                := '1.0'
   INERTIA.XYL                := '0.0'
   INERTIA.XZL                := '0.0'
   INERTIA.YZL                := '0.0'
   XG.FORCE                   := '0.0'
   YG.FORCE                   := '0.0'
   ZG.FORCE                   := '0.0'
   XL.TORQUE                  := '0.0'
   YL.TORQUE                  := '0.0'
   ZL.TORQUE                  := '0.0'
   CURVE.XGF                  := 'NONE'
   CURVE.YGF                  := 'NONE'
   CURVE.ZGF                  := 'NONE'
   CURVE.XLT                  := 'NONE'
   CURVE.YLT                  := 'NONE'
   CURVE.ZLT                  := 'NONE'
   SIGN.E0                    := 'POSITIVE'
   ANGULAR.UNITS              := 'DEGREES'
   FLEXIBLE                   := 'FALSE'
   SUPERELEMENT               := 'FALSE'
UP
CREATE INITIAL.CONDITION
   NAME                       := 'INIT.CHASSIS.ORIEN'
   BODY.1.NAME                := 'CHASSIS'
   BODY.2.NAME                := 'NONE'
   ELEMENT.NAME               := 'NONE'
   TYPE.INITIAL.COND          := 'ORIENTATION'
   INITIAL.VALUE              := '0.0'
   TIME.DERIVATIVE            := '0.0'
   OMEGA.Y                    := '0.0'
   OMEGA.Z                    := '0.0'
   P.ON.BODY.1                := ( 0.0, 0.0, 0.0 )
   P.ON.BODY.2                := ( 0.0, 0.0, 0.0 )
   EXTRA.COORD                := '0'
   ANGULAR.UNITS              := 'DEGREES'
UP
CREATE INITIAL.CONDITION
   NAME                       := 'INIT.CHASSIS.X'
   BODY.1.NAME                := 'CHASSIS'
   BODY.2.NAME                := 'NONE'
   ELEMENT.NAME               := 'NONE'
   TYPE.INITIAL.COND          := 'X'
```

```
    INITIAL.VALUE              := '0.0'
    TIME.DERIVATIVE            := '0.0'
    OMEGA.Y                    := '0.0'
    OMEGA.Z                    := '0.0'
    P.ON.BODY.1                := ( 0.0, 0.0, 0.0 )
    P.ON.BODY.2                := ( 0.0, 0.0, 0.0 )
    EXTRA.COORD                := '0'
    ANGULAR.UNITS              := 'DEGREES'
UP
CREATE INITIAL.CONDITION
    NAME                       := 'INIT.CHASSIS.Y'
    BODY.1.NAME                := 'CHASSIS'
    BODY.2.NAME                := 'NONE'
    ELEMENT.NAME               := 'NONE'
    TYPE.INITIAL.COND          := 'Y'
    INITIAL.VALUE              := '0.0'
    TIME.DERIVATIVE            := '176.00'
    OMEGA.Y                    := '0.0'
    OMEGA.Z                    := '0.0'
    P.ON.BODY.1                := ( 0.0, 0.0, 0.0 )
    P.ON.BODY.2                := ( 0.0, 0.0, 0.0 )
    EXTRA.COORD                := '0'
    ANGULAR.UNITS              := 'DEGREES'
UP
CREATE INITIAL.CONDITION
    NAME                       := 'INIT.CHASSIS.Z'
    BODY.1.NAME                := 'CHASSIS'
    BODY.2.NAME                := 'NONE'
    ELEMENT.NAME               := 'NONE'
    TYPE.INITIAL.COND          := 'Z'
    INITIAL.VALUE              := '0.0'
    TIME.DERIVATIVE            := '0.0'
    OMEGA.Y                    := '0.0'
    OMEGA.Z                    := '0.0'
    P.ON.BODY.1                := ( 0.0, 0.0, 0.0 )
    P.ON.BODY.2                := ( 0.0, 0.0, 0.0 )
    EXTRA.COORD                := '0'
    ANGULAR.UNITS              := 'DEGREES'
UP
CREATE INITIAL.CONDITION
    NAME                       := 'INIT.WHEEL.FL'
    BODY.1.NAME                := 'WHEEL.FL'
    BODY.2.NAME                := 'NONE'
    ELEMENT.NAME               := 'NONE'
    TYPE.INITIAL.COND          := 'Z'
    INITIAL.VALUE              := '0.0'
    TIME.DERIVATIVE            := '0.0'
    OMEGA.Y                    := '0.0'
    OMEGA.Z                    := '0.0'
    P.ON.BODY.1                := ( 0.0, 0.0, 0.0 )
    P.ON.BODY.2                := ( 0.0, 0.0, 0.0 )
```

```
    EXTRA.COORD                 := '0'
    ANGULAR.UNITS               := 'DEGREES'
UP
CREATE INITIAL.CONDITION
    NAME                        := 'INIT.WHEEL.FR'
    BODY.1.NAME                 := 'WHEEL.FR'
    BODY.2.NAME                 := 'NONE'
    ELEMENT.NAME                := 'NONE'
    TYPE.INITIAL.COND           := 'Z'
    INITIAL.VALUE               := '0.0'
    TIME.DERIVATIVE             := '0.0'
    OMEGA.Y                     := '0.0'
    OMEGA.Z                     := '0.0'
    P.ON.BODY.1                 := ( 0.0, 0.0, 0.0 )
    P.ON.BODY.2                 := ( 0.0, 0.0, 0.0 )
    EXTRA.COORD                 := '0'
    ANGULAR.UNITS               := 'DEGREES'
UP
CREATE INITIAL.CONDITION
    NAME                        := 'INIT.WHEEL.RR'
    BODY.1.NAME                 := 'WHEEL.RR'
    BODY.2.NAME                 := 'NONE'
    ELEMENT.NAME                := 'NONE'
    TYPE.INITIAL.COND           := 'Z'
    INITIAL.VALUE               := '0.0'
    TIME.DERIVATIVE             := '0.0'
    OMEGA.Y                     := '0.0'
    OMEGA.Z                     := '0.0'
    P.ON.BODY.1                 := ( 0.0, 0.0, 0.0 )
    P.ON.BODY.2                 := ( 0.0, 0.0, 0.0 )
    EXTRA.COORD                 := '0'
    ANGULAR.UNITS               := 'DEGREES'
UP
CREATE INITIAL.CONDITION
    NAME                        := 'INIT.WHEEL.RL'
    BODY.1.NAME                 := 'WHEEL.RL'
    BODY.2.NAME                 := 'NONE'
    ELEMENT.NAME                := 'NONE'
    TYPE.INITIAL.COND           := 'Z'
    INITIAL.VALUE               := '0.0'
    TIME.DERIVATIVE             := '0.0'
    OMEGA.Y                     := '0.0'
    OMEGA.Z                     := '0.0'
    P.ON.BODY.1                 := ( 0.0, 0.0, 0.0 )
    P.ON.BODY.2                 := ( 0.0, 0.0, 0.0 )
    EXTRA.COORD                 := '0'
    ANGULAR.UNITS               := 'DEGREES'
UP
CREATE POINT.OF.INTEREST
    NAME                        := 'U_DRIVER_SEAT'
    BODY.NAME                   := 'CHASSIS'
```

```
   P.ON.BODY                  := ( -27.815, -93.370, 26.380 )
   NODE                       := '0'
UP
CREATE POINT.OF.INTEREST
   NAME                       := 'CENTER_CARGO'
   BODY.NAME                  := 'CHASSIS'
   P.ON.BODY                  := ( 0.0, -155.370, 41.380 )
   NODE                       := '0'
UP
CREATE POINT.OF.INTEREST
   NAME                       := 'LOWER_LF'
   BODY.NAME                  := 'WHEEL.FL'
   P.ON.BODY                  := ( -30.965, -39.37, 31.235 )
   NODE                       := '0'
UP
CREATE ROAD
   NAME                       := 'ROAD'
   CURVE.NAME                 := '6IN_10MPH.CU'
   BUMP.RADIUS                := '0.0'
   BUMP.MODULUS               := '0.0'
   COHESIVENESS.COEFF         := '0.0'
   FRICTION.COEFF             := '0.0'
   EXPONENT                   := '0.0'
   DAMPING                    := '0.0'
   SHEAR.MODULUS              := '0.0'
   SHEAR.COHESIVENESS         := '0.0'
   FRICTION.ANGLE             := '0.0'
   UTILITY.1                  := '0.0'
   UTILITY.2                  := '0.0'
   UTILITY.3                  := '0.0'
   UTILITY.4                  := '0.0'
   ANGULAR.UNITS              := 'DEGREES'
UP
CREATE CURVE
   NAME                       := 'F_DAMP.CU'
   TYPE.DATA                  := 'PAIRED.XY'
   SLOPE.LEFT                 := '25'
   SLOPE.RIGHT                := '15'
   SCALE.X                    := '1.0'
   SCALE.Y                    := '1.0'
   START.X                    := '0.0'
   INCREMENT.X                := '0.0'
   INTERPOLATION              := 'LINEAR'
   CYCLIC                     := 'FALSE'
   DATA
     -13.35200000      -430.0000000
     -6.676000000      -212.0000000
     -2.356000000      -46.00000000
     0.0000000000E+00  0.0000000000E+00
      2.356000000       184.0000000
      6.676000000       400.0000000
```

```
      13.35200000        900.0000000
    ENDDATA
UP
CREATE CURVE
    NAME                    := 'R_DAMP.CU'
    TYPE.DATA               := 'PAIRED.XY'
    SLOPE.LEFT              := '25'
    SLOPE.RIGHT             := '15'
    SCALE.X                 := '1.0'
    SCALE.Y                 := '1.0'
    START.X                 := '0.0'
    INCREMENT.X             := '0.0'
    INTERPOLATION           := 'LINEAR'
    CYCLIC                  := 'FALSE'
    DATA
      -13.35200000      -576.0000000
      -6.676000000      -248.0000000
      -2.356000000      -62.00000000
       0.0000000000E+00  0.0000000000E+00
       2.356000000       228.0000000
       6.676000000       634.0000000
       13.35200000       1142.000000
    ENDDATA
UP
CREATE CURVE
    NAME                    := 'F_SPRING.CU'
    TYPE.DATA               := 'PAIRED.XY'
    SLOPE.LEFT              := '5000.0'
    SLOPE.RIGHT             := '1500.0'
    SCALE.X                 := '1.0'
    SCALE.Y                 := '1.0'
    START.X                 := '0.0'
    INCREMENT.X             := '0.0'
    INTERPOLATION           := 'LINEAR'
    CYCLIC                  := 'FALSE'
    DATA
      -5.240000000      -7000.000000
      -1.560000000      -1488.000000
      -1.559000000       1488.000000
    ENDDATA
UP
CREATE CURVE
    NAME                    := 'R_SPRING.CU'
    TYPE.DATA               := 'PAIRED.XY'
    SLOPE.LEFT              := '5000.0'
    SLOPE.RIGHT             := '1728.0'
    SCALE.X                 := '1.0'
    SCALE.Y                 := '1.0'
    START.X                 := '0.0'
    INCREMENT.X             := '0.0'
    INTERPOLATION           := 'LINEAR'
```

```
   CYCLIC                    := 'FALSE'
   DATA
     -4.350000000      -7516.800000
      -.5100000000      -881.2800000
     -.5090000000       881.2800000
   ENDDATA
UP
CREATE CURVE
   NAME                              := '6IN_10MPH.CU'
   TYPE.DATA                         := 'PAIRED.XY'
   SLOPE.LEFT                        := '0.0'
   SLOPE.RIGHT                       := '0.0'
   SCALE.X                           := '1.0'
   SCALE.Y                           := '1.0'
   START.X                           := '0.0'
   INCREMENT.X                       := '0.0'
   INTERPOLATION                     := 'LINEAR'
   CYCLIC                            := 'FALSE'
   DATA
   ENDDATA
UP
```

A.2 VEHDYN Vehicle Input File

```
m998_vd3
6 in bump test at 10mph with the m998 unloaded with bias ply
tires
1,2,2,0,0,0
5,0,0,0,0,0,2.54,11.12
-15.0,2.53,2.54,11.12,23.85
-5016,-633,633,2778,70800
5,0,0,0,0,0,1.16,10.10
-15.12,1.15,1.16,10.10,21.78
-6100,-406,406,3535,71928
9,0,0,0,0,0
-234,-31,-16,-6,0,6,16,31,234
-2000,-383,-177,-85,0,21,91,180,1500
9,0,0,0,0,0
-234,-31,-16,-6,0,6,16,31,234
-2000,-487,-278,-106,0,29,108,243,1000
0,0,0,2,0,0,1
5.7,-13.9
170,0,0,0
5545,41300,29.81,8.29,39.1,101.3,77.2,0.0
18.15,250,57.7,17.02,2,3600,1550,1
18.15,250,-72.3,17.22,2,4000,1225,1
1,1,1,0,0
2,2,2,0,0
```